AN INVESTIGATION OF VARIABLE-TIME INTERVAL "K-LIKE" GEOMAGNETIC INDICES

DEVIN J. DELLA-ROSE

1999

REPORT DOCUMENTATION PAGE			*Form Approved* *OMB No. 0704-0188*

1. AGENCY USE ONLY *(Leave blank)*	2. REPORT DATE 16.Dec.99	3. REPORT TYPE AND DATES COVERED DISSERTATION

4. TITLE AND SUBTITLE
AN INVESTIGATION OF VARIABLE-TIME INTERVAL "K-LIKE"
GEOMAGNETIC INDICES

5. FUNDING NUMBERS

6. AUTHOR(S)
MAJ DELLA-ROSE DEVIN J

7. PERFORMING ORGANIZATION NAME(S) AND ADDRESS(ES)
UTAH STATE UNIVERSITY

8. PERFORMING ORGANIZATION REPORT NUMBER

9. SPONSORING/MONITORING AGENCY NAME(S) AND ADDRESS(ES)
THE DEPARTMENT OF THE AIR FORCE
AFIT/CIA, BLDG 125
2950 P STREET
WPAFB OH 45433

10. SPONSORING/MONITORING AGENCY REPORT NUMBER
FY99-442

11. SUPPLEMENTARY NOTES

12a. DISTRIBUTION AVAILABILITY STATEMENT
Unlimited distribution
In Accordance With AFI 35-205/AFIT Sup 1

12b. DISTRIBUTION CODE

13. ABSTRACT *(Maximum 200 words)*

14. SUBJECT TERMS

15. NUMBER OF PAGES
119

16. PRICE CODE

17. SECURITY CLASSIFICATION OF REPORT	18. SECURITY CLASSIFICATION OF THIS PAGE	19. SECURITY CLASSIFICATION OF ABSTRACT	20. LIMITATION OF ABSTRACT

AN INVESTIGATION OF VARIABLE-TIME INTERVAL

"*K*-LIKE" GEOMAGNETIC INDICES

by

Devin J. Della-Rose

A dissertation submitted in partial fulfillment
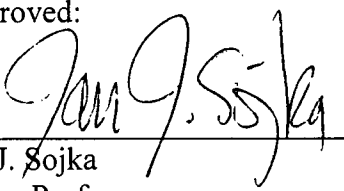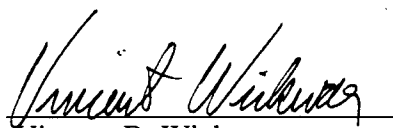of the requirements for the degree
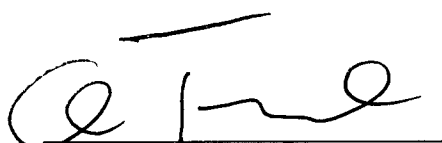
of

DOCTOR OF PHILOSOPHY
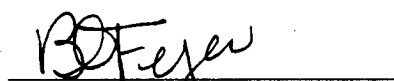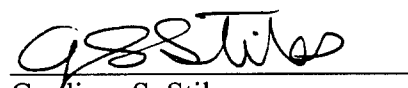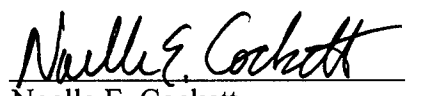
in

Physics

Approved:

_____
Jan J. Sojka
Major Professor

_____
Vincent B. Wickwar
Committee Member

_____
Charles G. Torre
Committee Member

_____
Bela G. Fejer
Committee Member

_____
Gardiner S. Stiles
Committee Member

_____
Noelle E. Cockett
Interim Dean of Graduate Studies

UTAH STATE UNIVERSITY
Logan, Utah

1999

20000112 054

ABSTRACT

An Investigation of Variable Time Interval

"*K*-like" Geomagnetic Indices

by

Devin J. Della-Rose, Doctor of Philosophy

Utah State University

Major Professor: Dr. Jan J. Sojka
Department: Physics

The 3-hour planetary K index derivative, Kp, is designed to measure irregular fluctuations in the Earth's magnetic field due to currents in the magnetosphere-ionosphere system. The index is widely used to drive empirical models of auroral particle precipitation, high-latitude convection patterns, thermospheric composition, and neutral winds. The 3-hour time interval of Kp makes it suitable for use as a parameter in thermospheric models, since the neutral atmosphere changes slowly. However, ionospheric time constants can be quite short, and this makes the 3-hour interval too coarse for accurate modeling.

My research examined the feasibility of improving ionospheric modeling via use of a "*K*-like" index with a variable time interval. We first created an algorithm to create such indices (following the same definitions as used in the traditional 3-hour index), then applied the code to the 1990-1992 raw data set from the Fredericksburg, Virginia, magnetometer. To validate our code, we processed the data using a 3-hour interval, then

compared the results of our routine against the official 3-hour indices computed at Fredericksburg. Our code was 95% accurate for the 1990-1992 period. We then reprocessed the data for several different time intervals ranging from 15 minutes up to 24 hours; we referred to the resulting indices as "*JD*" indices. The average *JD* index changed significantly as a function of time interval. However, using a simple normalization technique, we were able to produce variable time *JD* indices with frequency distributions quite similar to the traditional Fredericksburg 3-hour *K* index; the best agreement was achieved with the normalized 15-minute *JD* index.

This normalization procedure enabled us to perform an ionospheric sensitivity study using the Utah State University (USU) Time-Dependent Ionospheric Model (TDIM). We used our normalized 15-minute Fredericksburg *JD* index as a proxy for a planetary index time series, then studied the high-latitude NmF2 response. For winter solstice, solar maximum, geomagnetic storm conditions, use of our *JD* index produced NmF2 variations at about the 20% level (versus NmF2 values produced by driving TDIM with the traditional 3-hour index). However, in most cases, changing the IMF gave NmF2 variations 2-3 times larger.

(132 pages)

DEDICATION

This work is dedicated to my parents, Eugene and Monema.

ACKNOWLEDGMENTS

Finally, I have my family to thank. Dale is the best partner for life I could have, and has shared this whole experience with me through the past five years—even when I did not know if the Air Force would send me here at all. Her two great sons, Brad and Neal, are a special part of my life, and I am happy to call them my "kids" (HA!). We have had some great times together, and I am looking forward to many, many more.

Devin J. Della-Rose

CONTENTS

LIST OF TABLES

LIST OF FIGURES

CHAPTER 1

INTRODUCTION

Over the past century, scientists interested in energy input and dissipation in near-Earth space have remotely sensed magnetic fluctuations caused by changes in magnetosphere-ionosphere current systems. Raw measurements were synthesized into magnetic "indices" to describe the magnetosphere-ionosphere (M-I) disturbance level (as described in chapter 3). The "modern era" of indices is over half a century old, and one of the most widely used modern indices is the 3-hour station K index (Bartels et al., 1939). The planetary version of this index, Kp, is used as a measure of geomagnetic activity for ionospheric studies (e.g., Sojka, 1989; Sojka and Schunk, 1997). Specifically, it is the index used to determine the geomagnetic dependence of statistical auroral oval patterns (Hardy et al., 1987) as well as convection electric field patterns (Heppner and Maynard, 1987). Its quasi anti-logarithm,[1] the Ap index, is similarly used in statistical models of the neutral atmosphere (Hedin, 1987) and neutral wind (Hedin et al., 1991).

The magnetosphere drives high- and mid-latitude ionospheric phenomena on time scales varying from seconds to days. Associated with these phenomena are changes in the M-I currents and hence ground-based magnetic field observations. Energy is deposited in the ionosphere-thermosphere system, causing changes in the thermospheric composition, temperature, and consequently the recombination rates. Particle precipitation in the auroral zone both deposits energy into the ionosphere-thermosphere

---

[1] A perfect logarithmic conversion implies the ratio of class boundaries is a constant; however, the range-to-K index conversion departs from this rule for index values 4 and above (see Table 1), and so becomes a "quasi" logarithmic conversion.

system and provides an ionization source. At night this auroral ionization source dominates.

The *E*-region plasma has short chemical time constants (on the order of seconds). At the *F*-region peak and above, E×B drifts convect ionospheric plasma around the high-latitude region. Figure 1 shows an idealization of this convection, along with the corresponding electric field directions; the real-world motion is usually much more complex. *F*-region time constants are on the order of minutes up to 1-2 hours.

The thermosphere in general has even longer time constants on the order of tens of minutes up to hours. All three regions are coupled and interact with these dramatically different time constants. The M-I current systems have variability on all these time scales due to the current generator (magnetospheric) dynamics. All these time constants are shorter than the standard 3-hour magnetic *K* index time interval, with the exception of the thermosphere, whose constants are comparable.

On the other hand, the ionosphere is driven at the time scales of the entire solar wind-magnetosphere-ionosphere system. This introduces characteristic time scales that range from tens of minutes (e.g., pseudo breakups) to 1-3 hours (e.g., substorms) to days (e.g., major magnetic storms). Compared to the 3-hour window for the *Kp* index, the major storms are resolvable. Not so, however, for substorms and other high-frequency space weather events. From a climatological perspective the 3-hour *Kp* index would reasonably be viewed as giving the integrated—but heavily averaged—energy input into the magnetosphere-ionosphere-thermosphere system. Hence statistical models of conductivity, auroral precipitation, electric fields, etc., do justice to the storm "climatology." An example of such a statistical model for auroral precipitation is shown
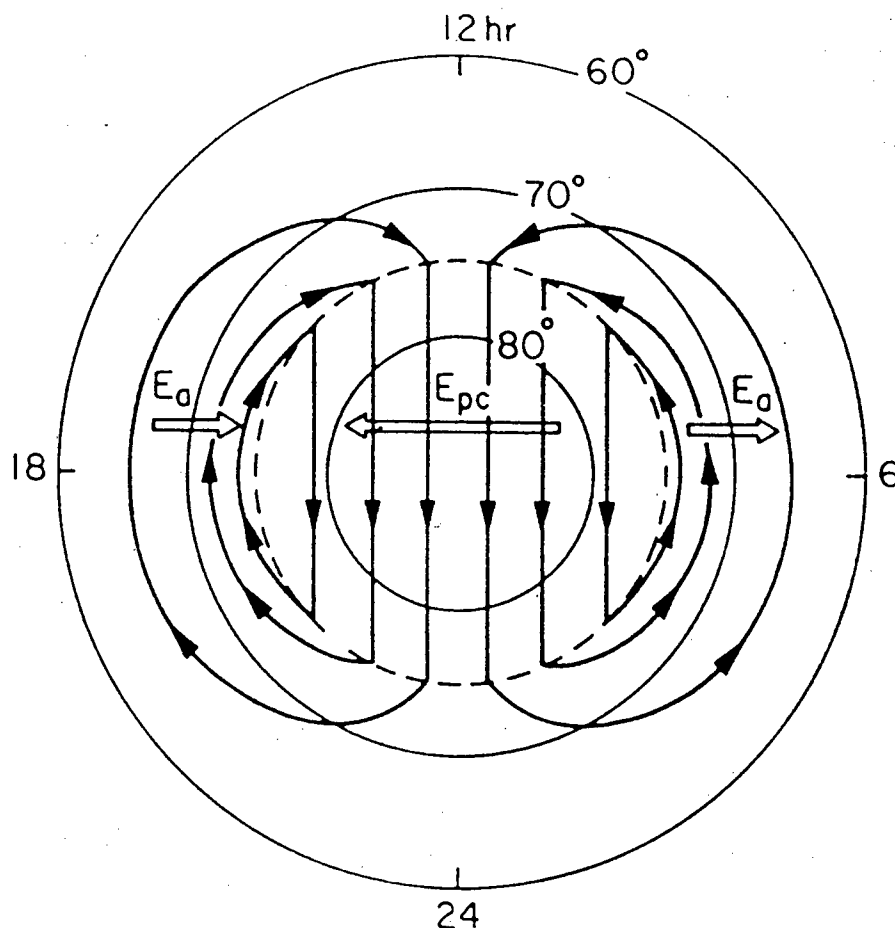
Fig. 1. Idealized high-latitude F-region E×B plasma convection pattern. The coordinate system shown is magnetic local time (hours) versus geomagnetic latitude (60 to 90 degrees). The arrowed trajectories are the E×B plasma paths (B is into the page in the northern geographic hemisphere). The electric fields mapped down from the magnetosphere are also shown as E_{pc} (polar cap) and E_a (auroral zone). Note the antisunward convection over the polar cap, and the sunward return flow equatorward of the cap. The dashed line in the figure marks the division between sunward and antisunward flow and is called the convection reversal (taken from Kelley, 1989).

in Figure 2. Unfortunately, each storm is different in its impact on the ionosphere, with only crude morphologies—such as density excursions above or below the norm—being understood. Because the physical processes occur on shorter time scales than 3 hours, and since space weather effects are not simply a linear superposition of individual energy contributions, our ability to model storms using a 3-hour geomagnetic index falls short.

Other higher-time resolution geomagnetic indices have been developed to monitor specific current systems. The auroral electrojet, or AE index (Davis and Sugiura, 1966), employs a network of auroral-latitude stations to measure the resultant fluctuation in both the eastward and westward electrojets (see chapter 2 for more details on these current systems). The index is computed every 2.5 minutes, and is also available in hourly averages. Disturbances in the equatorial ring current (again, see chapter 2 for details) are measured by the disturbance storm time, or Dst, index (Sugiura, 1964). Data from a nominal set of four equatorial magnetometers are taken to form this index; Dst is computed once an hour. More recently, the PC index has been proposed by Vennerstrøm (1991). As described in Kivelson and Russell (1995), this index is designed to measure the strength of the sunward polar cap sheet current, and thus provides a measure of the penetration of the solar-wind electric field into the magnetosphere.

All three of these indices, however, have their own shortcomings. Rostoker (1972) discusses some of the problems with AE and Dst. The AE index does not use statistical weighting factors among the stations, and so pronounced dependencies are present in the index with respect to universal time, season, and solar cycle. With only four stations, the Dst network is not optimized to quantitatively describe the strength of the equatorial ring current, especially since the current is often asymmetric in character. Ballatore and

Hardy Energy Flux for Kp=3
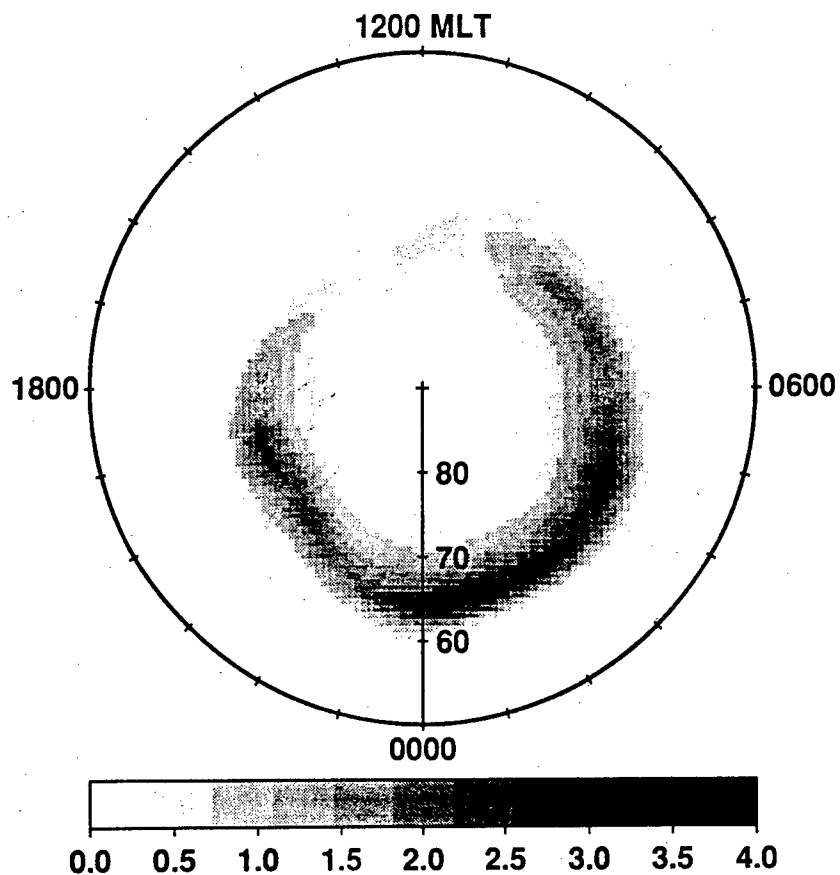
Fig. 2. Sample plot from the Hardy et al. (1987) empirical model for auroral energy flux. This plot (same coordinate system as Figure 1, except magnetic latitude begins at 50 degrees) shows the downward energy flux for $Kp = 3$. The units are [erg/cm^2 sec], as reflected on the gray scale at the bottom of the plot.

Lanzerotti (1998) have suggested that the *PC* index is not indisputably better than *AE* in monitoring the interplanetary activity coupling with the M-I system. Finally, and perhaps most importantly, there is the issue of availability. The *PC* index is still in the research and analysis phase. The official *AE* and *Dst* indices are not available until months after the fact, although the World Data Center-C2 for geomagnetism (Kyoto, Japan) does offer a near-real time version of *Dst* on the internet. Therefore, most space weather modeling efforts, discussed next, have focused on "*K*-like" indices, which are both officially accepted and widely available in real (or near-real) time.

The physical models of both the thermosphere and ionosphere are designed to respond at their appropriate time scales. However, a statistical input driven by a 3-hour magnetic index does not produce realistic inputs. Three hours would typically span the evolution of a substorm including wedge current formation, reorganization of high-latitude convection, etc. To date it has been difficult to simulate, or even study, the ionospheric responses to more realistic, shorter time inputs. Sojka and Schunk (1983) used an artificial *Kp* index to simulate a substorm in the Utah State University (USU) Time-Dependent Ionospheric Model (TDIM). Similarly, Fuller-Rowell et al. (1994, 1996) studied the thermospheric response to such storms. More recently, Schunk et al. (1997) and Sojka et al. (1998) and have tried to bypass the statistical drivers by interfacing the output of first-principles magnetohydrodynamic (MHD) models with the TDIM. These studies have found an extremely rich set of ionospheric responses on time scales significantly shorter than 3 hours. However, longer time constants have also been identified. Overall, the difficulty of realistically obtaining electric fields and auroral precipitation on faster time scales is the major shortcoming.

One of the recent efforts of the space weather community is to find better near real-time indices of geomagnetic activity to overcome this shortcoming. Is it reasonable to consider higher time resolution Kp (ap) indices as a possible solution? If so, is it then true that such higher time resolution indices are good proxies for the temporal behavior of ionospheric drivers?

Our investigation marks the first serious effort to address this issue. We start in chapter 2 by giving some background material regarding the science of geomagnetism. Chapter 3 then covers the history of "K-like" magnetic indices. In chapter 4 we establish our method of altering the traditional 3-hour station K index into a variable time interval index, then compare our new indices against the 3-hour K index in chapter 5. Finally, we examine the effect of using variable time interval indices to drive space weather forecast models used to calculate high-latitude electron densities. The description and results of this sensitivity study are presented in chapter 6. Our conclusions are summarized, and recommendations for further work discussed, in chapter 7.

CHAPTER 2

FUNDAMENTALS OF GEOMAGNETISM

2.1. Introduction

Research in geomagnetic indices naturally requires a certain appreciation for the fundamental physics of the Earth's magnetic field. In this regard there are scores of wonderful references; two primary works used in my research are Campbell (1997) and a four-volume set entitled Geomagnetism (Jacobs, 1989). This chapter is meant to provide enough background to support the material presented in the remainder of the dissertation. It will involve coordinate systems used to describe the field, basic data related to the internal magnetic field of the Earth, external field sources, which cause both periodic and aperiodic fluctuations in the Earth's field, and finally a brief look at the instruments used to measure such variations.

2.2. Coordinate systems

One of the primary coordinate systems used in geomagnetism is shown in Figure 3. The axes of this system are aligned with the Earth's *geographic* axes. The positive X-axis points to geographic (true) north, the positive Y-axis points east, and the Z-axis is positive downward. As shown, the total magnetic field vector is labeled "F", the horizontal (X-Y plane) component is "H", and "D" is the declination angle measured clockwise from the X-axis to the "H" vector ("D" is negative if "H" is westward of true north). This coordinate system is often referred to as the "XYZ" system.

In the derivation of "*K*-like" geomagnetic indices, it is customary to express the declination "D" in dimensions of magnetic induction instead of an angle. This

F: total field
H: horizontal component
X: northward component
Y: eastward component
Z: vertical component
D: declination
I: inclination
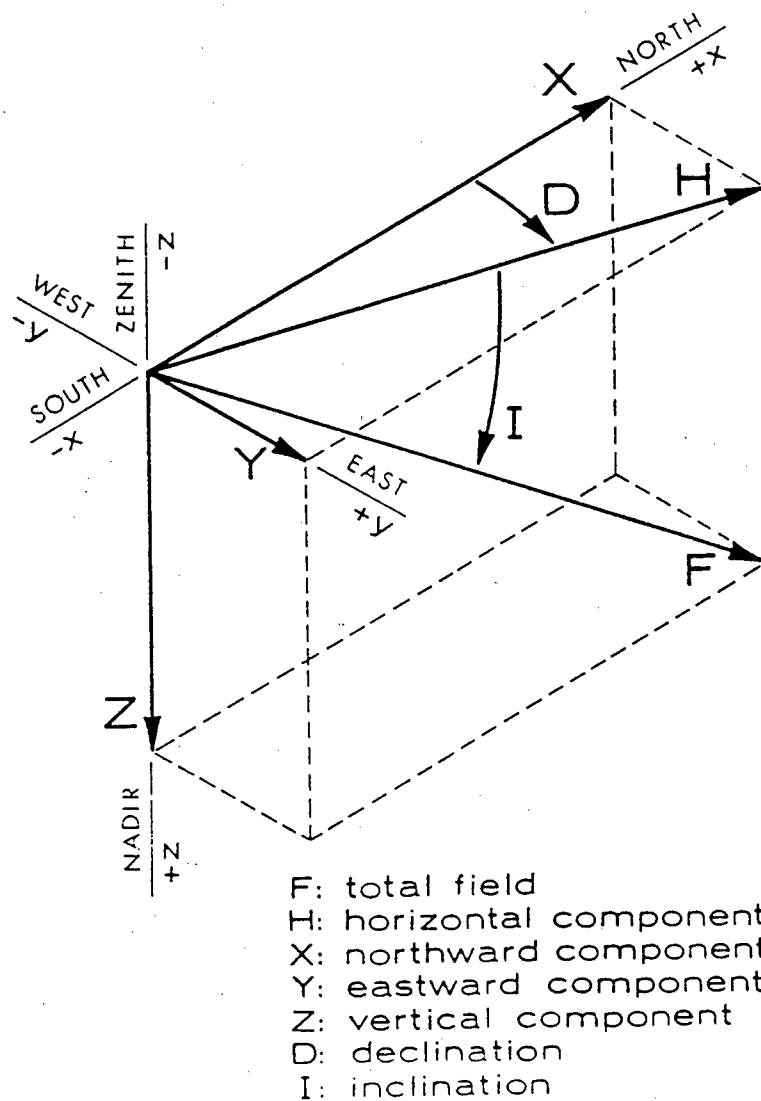
Fig. 3. Definition and sign convention for the magnetic elements. Directions shown (north, south, east, west) are geographic, *not* geomagnetic (taken from Knecht and Shuman, 1985).

transformation is accomplished via a rotation of the "XYZ" system as follows. The X-axis (from Figure 3) is rotated into alignment with the direction of the *baseline* "H" vector, i.e., the horizontal projection of the Earth's field determined by *internal* sources (see discussion below). We label this new axis as the X'-axis. We also label the angle of rotation between true north and X' as "D_{mean}," which is the declination angle between true north and the baseline "H" vector. Thus the *total* "H" vector at any moment—which is the sum of the baseline value *plus* the field due to external sources—is resolved into two orthogonal components in this new coordinate system. One component is along the X'-axis; the other component orthogonal to X' is labeled as D'. Thus D' now has the dimensions of magnetic induction (the same as "H"). The formula for D' is given by Campbell (1997):

$$D' = H \sin(D - D_{mean}) \tag{1}$$

where H is the magnitude of the total "H" vector, and D is the declination of H (again measured from true north). Note that D' has the same units as H. The relationship between this system and the "XYZ" system, as well as a pictorial description of equation (1), is shown in Figure 4. As we will see in chapter 4, equation (1) is used in the computation of the geomagnetic K index.

2.3. Internal field sources

The Earth's internal magnetic field consists of dipole-like and non-dipole-like sources. The dipole-like component is due to fluid motion of the Earth's core. In a completely oversimplified fashion, the resulting magnetic field can be thought of as a giant "bar magnet" inside the Earth, with the *south* pole of the magnet in the *northern* geographic
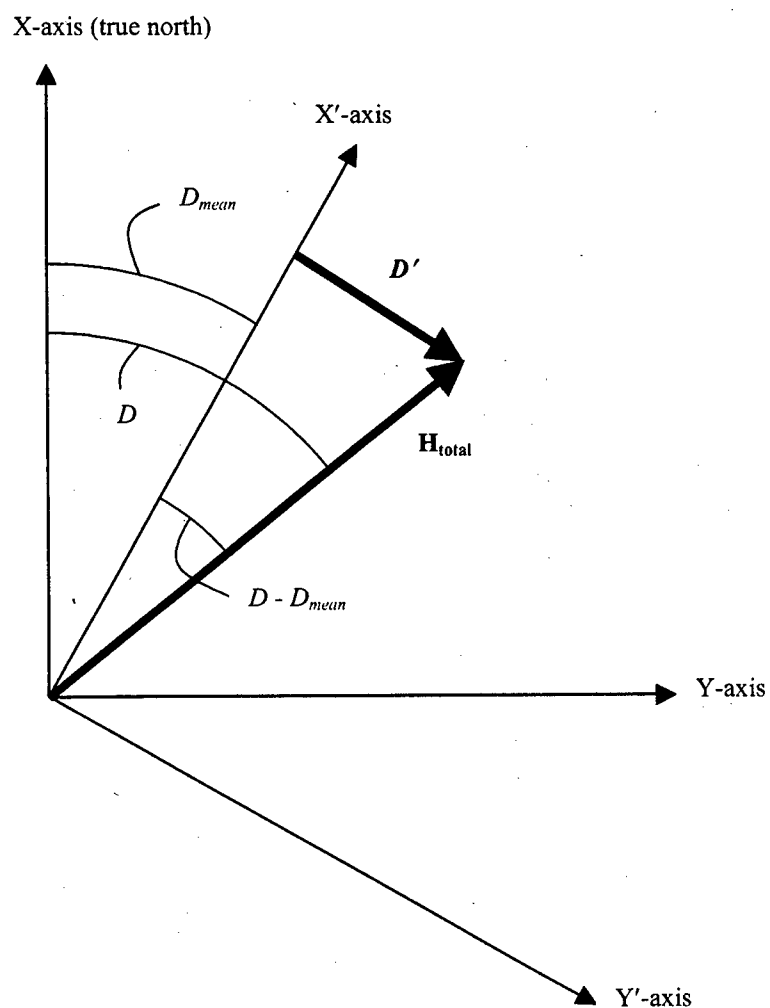
Fig. 4. Relationship between D (an angle) and D' (dimensions of magnetic induction). The X-Y plane from Figure 3 is rotated so that X aligns with magnetic north (due to the main field). The D' component of H_{total} is then perpendicular to the X' axis.

hemisphere. In reality, the center of the "bar magnet" is displaced from the center of the Earth (generally toward India). Many other factors, such as magnetic materials in the Earth, further complicate the real-life situation. These are the non-dipole-like components; I will not attempt to elaborate further on such effects. At the Earth's surface, the average strength of the magnetic field is about 0.5 Gauss (1 Gauss = 10^{-4} Tesla). Again assuming the field to be a perfect dipole, the magnitude of the field decreases as r^{-3} with the distance from the Earth's center. Thus, at ionospheric heights of about 100 km, the dipole field strength has decreased to about 0.47 Gauss. A more realistic field model is achieved through a spherical harmonic analysis (SHA) of actual field measurements. One popular model using this approach is the International Geomagnetic Reference Field (IGRF) model. The coefficients for this model are updated about every 5 years.

Internal field sources are never constant. In fact, paleomagnetic studies have revealed that the main field polarity reverses about once every million years. In fact, the magnitude of the Earth's magnetic dipole moment, $|\mathbf{M}|$, is currently decreasing at a rate which, if continued, will cause $\mathbf{M}$ to pass through *zero* magnitude in about the year 3737 AD (lecture given by Dr. Robert McPherron, 1995). Slow temporal changes in the internal field sources are called *secular variations*.

2.4. External field sources

The wide variety of current systems in the space environment serves as external magnetic field sources which, by the principle of superposition, add to the magnetic field created by internal sources. This section will describe many of these external current systems, starting with the ones farthest from the Earth (several Earth radii (R_E) away),

then move inward and describe ionospheric current systems (about 100 kilometers above the Earth). Most of these current systems can be detected from the ground via their magnetic signatures. The most appropriate units to describe these signatures is the nanotesla (10^{-9} Tesla). One nanotesla (abbreviated as nT) is also referred to as a *gamma*.

The interaction between the ionized solar wind stream and the Earth's magnetic field compresses the Earth's field on the sunward side, and stretches it out into a long tail on the antisunward side, as shown in Figure 5. The magnetic "cavity" formed by this interaction is called the Earth's magnetosphere. The sunward compression can be viewed in terms of a current sheet—as suggested by Chapman and Ferraro in 1930—created because the Lorentz force has opposite sign for ions and electrons. This current sheet flows from the dawn side of the Earth to the dusk side, as shown in Figure 6. The magnetic field associated with this current sheet tends to enhance the Earth's magnetic field Earthward of the sheet, and cancel it sunward of the sheet. Given the presence of the Chapman-Ferraro current sheet, the nominal distance to the "nose" of the magneto-sphere—often called the "standoff" distance—is about 10 R_E. This corresponds to about a 25 nT increase in the magnetic field "H" component at the Earth's geomagnetic equator (Campbell, 1997).

Another important current system is the so-called ring current, which exists over a height range of 4 to 6 R_E, measured from the center of the Earth. This altitude range places the ring current coincident with the outer Van Allen radiation belt. The radial gradient in the Earth's magnetic field (directed inward) causes energetic protons to drift westward, and energetic electrons to drift eastward (the particles also "mirror" between the magnetic north and south poles as they drift). The net result is a westward current as
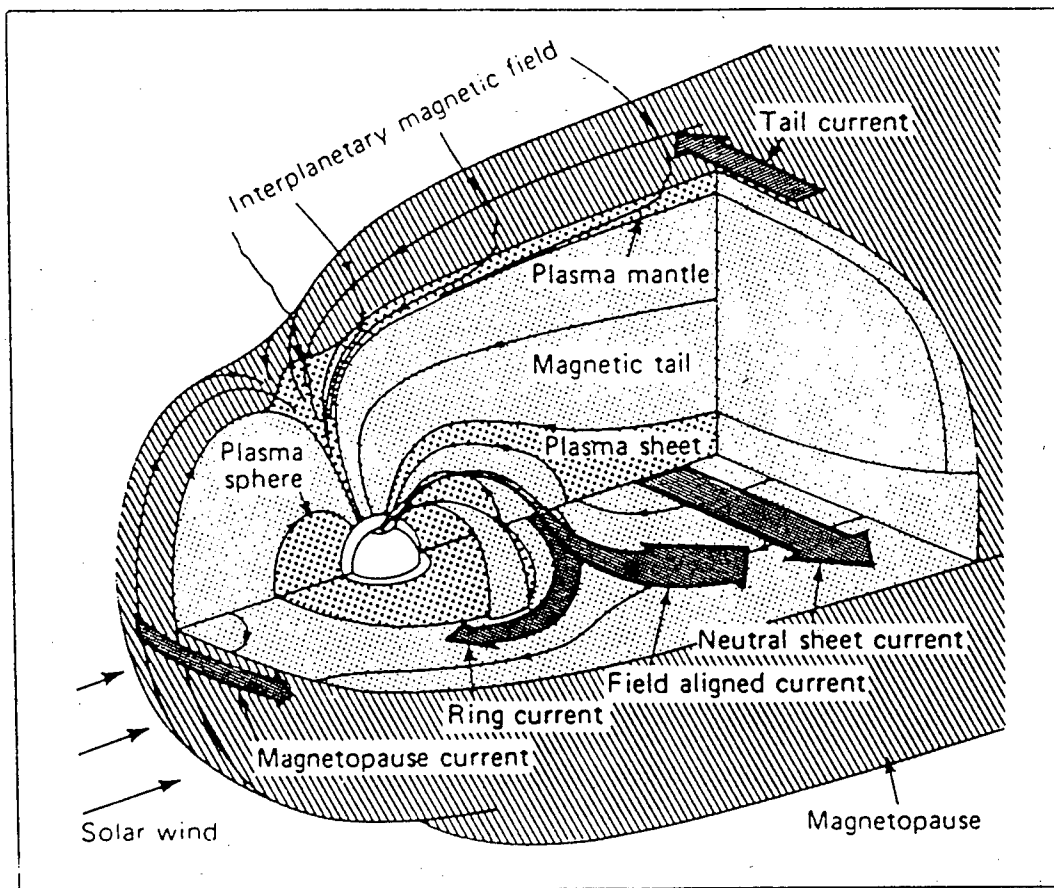
Fig. 5. The Earth's magnetic cavity, showing large-scale morphology and current systems (taken from Hargreaves, 1992).
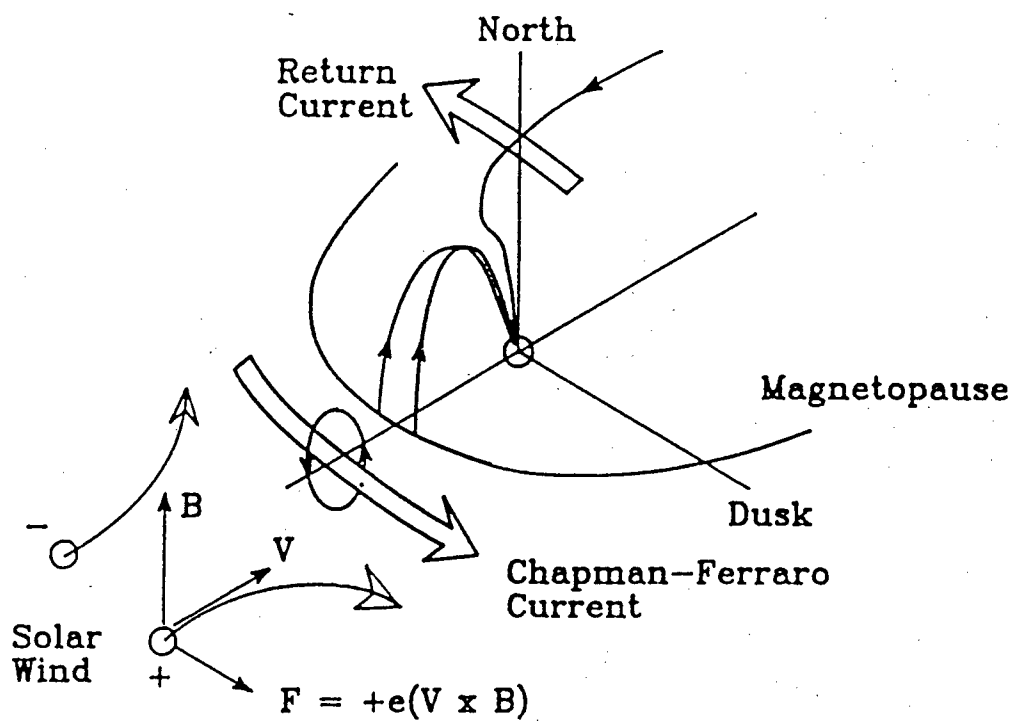
Fig. 6. The Chapman-Ferraro current system. The Lorentz force separates solar wind charges in the Earth's magnetic field to create this "eastward" current. Notice the return current closure above the Earth's (south) magnetic pole (taken from McPherron, 1991).

shown in Figure 7. The magnetic field due to this current is directed from north to south at the Earth's surface—which is opposite the direction of the internal field—and thus results in a depression of the "H" component at low latitudes. The magnitude of this depression is typically less than 50 nT, but can be over 1000 nT during magnetic storms, i.e., when the ring current becomes "energized." Measurement of the magnetic variations caused by changes in ring current strength form the basis of the Dst index, as discussed in chapter 1.

The ionosphere supports several current systems; some are low latitude, others flow at high latitudes. Most ionospheric current systems—at any latitude—flow in the E-region (between about 90 and 150 km) because, at these heights, ions and electrons are controlled by different forcing mechanisms, and so flow in different directions. This results in current flow.

We shall treat the high-latitude currents first, starting with the auroral electrojets. Particle precipitation into the auroral zone enhances the electron density—and thus conductivity—at E-region heights. This increased conductivity supports a strong anti-sunward Hall current carried by the electrons; similar currents flow in both hemispheres. On the dawn side this current flows westward, and is called the westward auroral electrojet; on the dusk side the electrojet flows eastward. This current system is illustrated in Figure 8. The magnetic field due to these electrojets is easily detected from the ground. The westward jet magnetic field points south at the surface, and so subtracts from the main field "H" component. Of course, this effect is most pronounced directly underneath the jet. However, the field due to the eastward jet points north at the surface and adds to the main field "H" component. During magnetic substorms, these perturb-
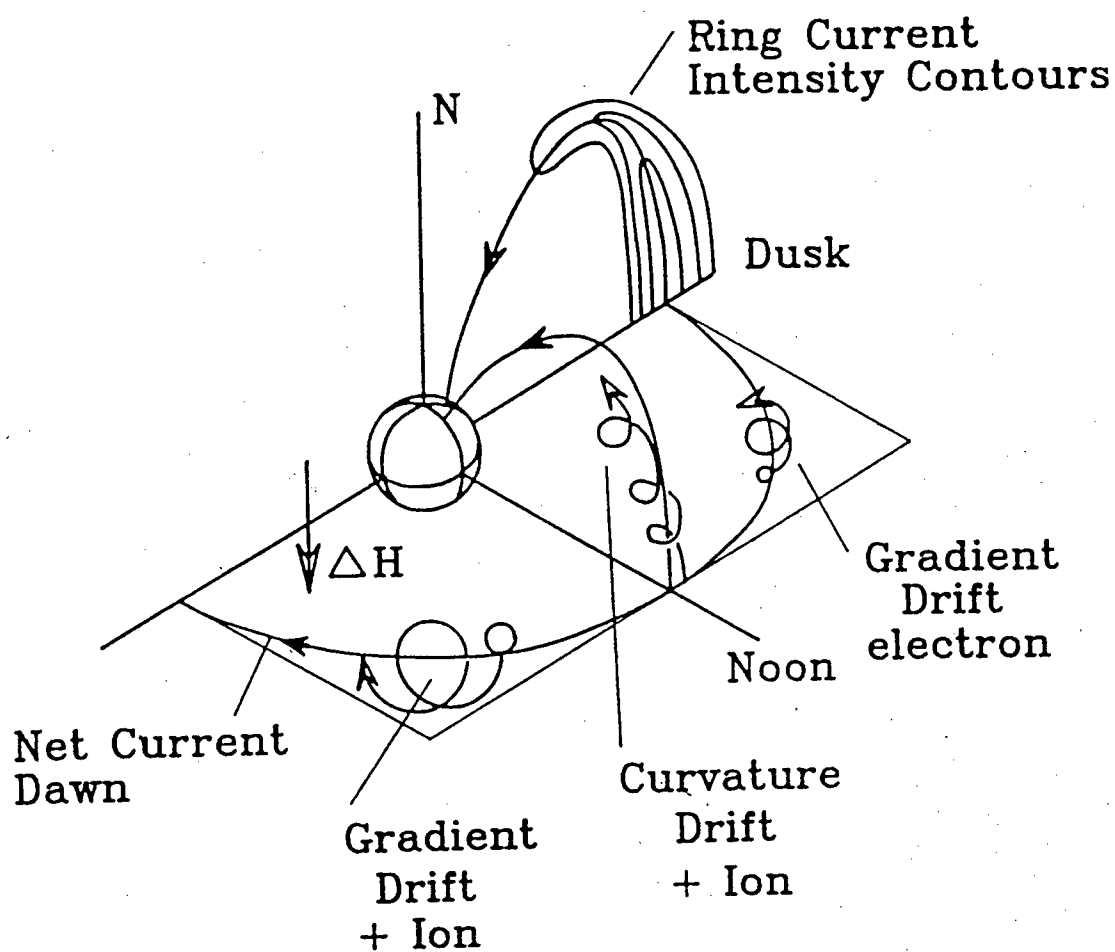
Fig. 7. The magnetospheric ring current system. This "westward" current is produced by gradient and curvature drift of energetic particles. Contours of constant current form nested toroids around the Earth (taken from McPherron, 1991).
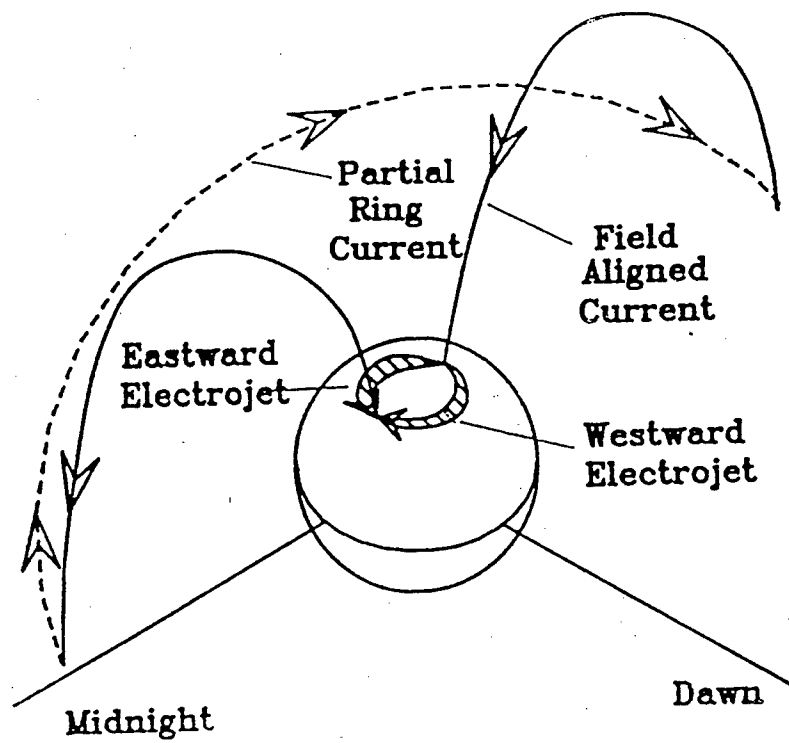
Fig. 8. The auroral electrojets. Both the eastward and westward electrojet currents flow antisunward in the high conductivity auroral channels in the *E*-region (taken from McPherron, 1991).

ations can be more than 10^3 nT at the surface. As mentioned in the previous chapter, measurement of electrojet magnetic fields is the basis of the *AE* magnetic index. These fields also play a major role in determining the magnetic *K* index, as explained in the next chapter.

E-region densities and conductivities are typically lower in the polar cap than in the auroral zone, but electrons still carry a Hall current in a generally sunward direction. To get an idea of the strength of the corresponding magnetic field, assume a uniform current sheet with a surface current density of about 0.1 amp/meter (Kamide and Akasofu, 1981). This leads to a surface magnetic field of about 60 nT. The polar cap (*PC*) magnetic index is designed to monitor changes in this current system.

Horizontal convection currents as described so far do not explain the entire high-latitude picture, because horizontal conductivity gradients make it impossible for such currents to close entirely in the ionosphere. This fact, together with the knowledge that conductivity is large along magnetic field lines, implies that current closure is a three-dimensional process involving horizontal currents as well as field-aligned currents flowing between the ionosphere and magnetosphere. The idea of field-aligned currents was first suggested by the Norwegian physicist Kristian Birkeland in 1908. The existence of such currents was finally confirmed in the early 1970s using satellite magnetometers. The reason for this long time lag is that one cannot uniquely derive a three-dimensional current system from ground-based measurements alone (Hargreaves, 1992). As a result, there can be no ground-based magnetic indices of field-aligned current activity.

The preceding descriptions of high-latitude current systems are idealized; in reality, the dynamic interaction of the interplanetary magnetic field (IMF) with the Earth's magnetic field alters the morphology of these currents. However, for the purpose of describing magnetic variations and their relationship to magnetic activity indices, the idealized current description is often a useful tool.

Now we describe mid- and low-latitude current systems, beginning with the solar quiet, or *Sq*, current. Knowledge of this current system is crucial in deriving the magnetic *K* index (as described in chapter 3). As the name implies, this current system is driven by the sun (more on this in a moment), and its characteristics are defined during geomagnetically quiet periods. The process responsible for *Sq* currents is the thermospheric (neutral) winds that push the conducting ionosphere across the Earth's magnetic field. This produces an electromotive force via Faraday's Law, and the result is the current system illustrated in Figure 9. Panel (a) of this figure shows the *Sq* system during equinox. On the dayside, differential solar heating produces high pressure at low latitudes. Thermospheric winds in both hemispheres blow generally poleward in response to the resulting pressure gradient. This sets up a two-cell *Sq* current system in the dayside *E*-region. At night the winds blow equatorward, reversing the current flow directions in the nighttime cells. However, current magnitudes are much smaller because nighttime ionospheric densities are reduced by one to two orders of magnitude.

This entire pattern is fixed to the sun and the Earth rotates underneath it. Now the Earth is also a conductor, so the rotation induces a secondary *Sq* system underground. This secondary current system is shown in Figure 9(b), and is only about one-third the strength of the ionospheric *Sq* current. The ground-based magnetic signature of *Sq* is a
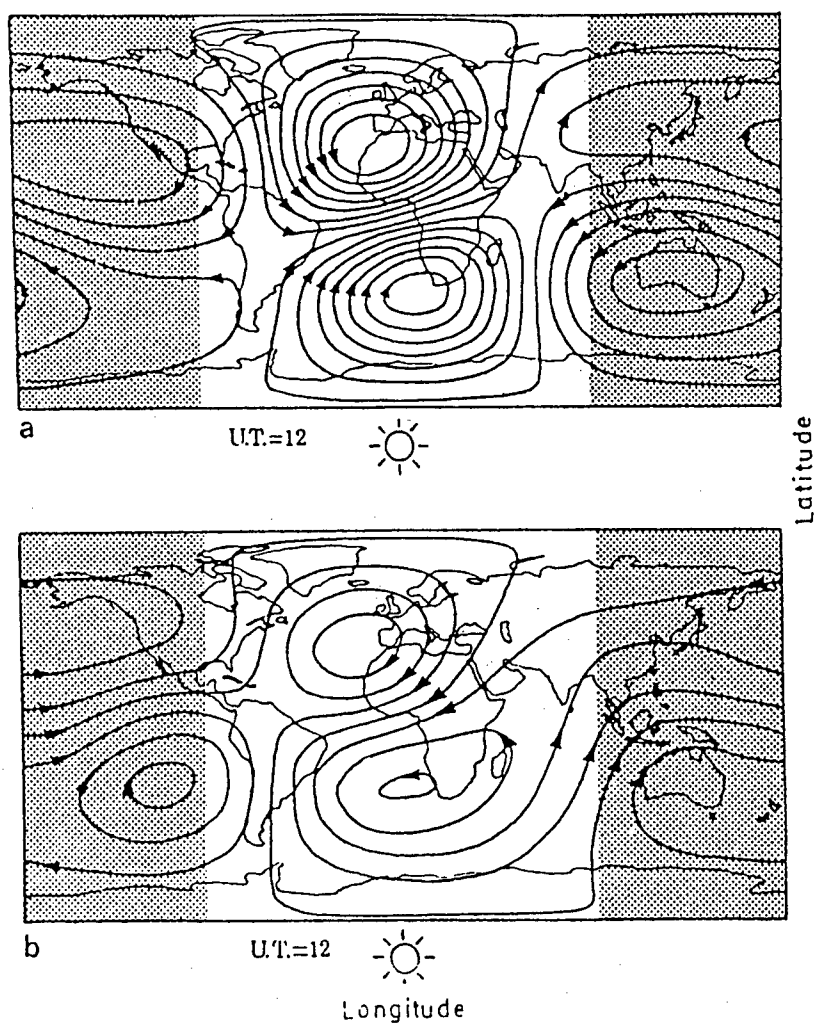
Fig. 9. Streamlines of ionospheric *Sq* current during equinox (1957-1960) at 1200 UT. Panel (a) shows the ionospheric (primary) component, while panel (b) illustrates the secondary current induced in the Earth (caused by the temporal variation of the primary current). Twenty kiloamperes flow between any pair of streamlines (taken from Volland, 1984).

superposition of the external and internal *Sq*-produced fields, and is a function of local time, latitude, longitude, season, and solar cycle. The diurnal and latitudinal dependencies are illustrated in Figure 10; typical diurnal *Sq* amplitudes are less than 50 nanoteslas. The seasonal effects are shown in Figure 11 for the "H" component at Fredericksburg, Virginia. The solar cycle influence on *Sq* has been described in Campbell and Matsushita (1982). They found that mid-latitude, solar cycle maximum *Sq* currents are 1.6-3.0 times larger than those during solar cycle minimum, with the larger ratio occurring in mid-November, and the smaller ratio occurring near the June solstice. Finally, lunar tidal effects modify the *Sq* system; however, the effect is rather small— only a few nanoteslas in most cases. Still, quiet-day magnetic signatures do reflect the moon's presence.

Another low-latitude current system is the equatorial electrojet. This jet is about 500 kilometers wide, and extends from about 90 to 120 kilometers above the ground. Ideally, the current flows parallel to—and centered on—the magnetic equator. The near-horizontal magnetic field in this region increases the *E*-region conductivity in the east-west direction (called the *Cowling* conductivity), setting up an electron current along that axis. Generally, the current flows eastward in the day and westward at night, though there can be reversals from this scenario. Magnetic deflections at the ground due to this electrojet can be as large as 150 nT, but the effect falls off rapidly with latitude, as shown in Figure 12. Thus the equatorial electrojet is not a significant factor in mid- to high-latitude magnetic indices.

2.5. Magnetometers

Various instruments have been used over the past century to measure variations in the
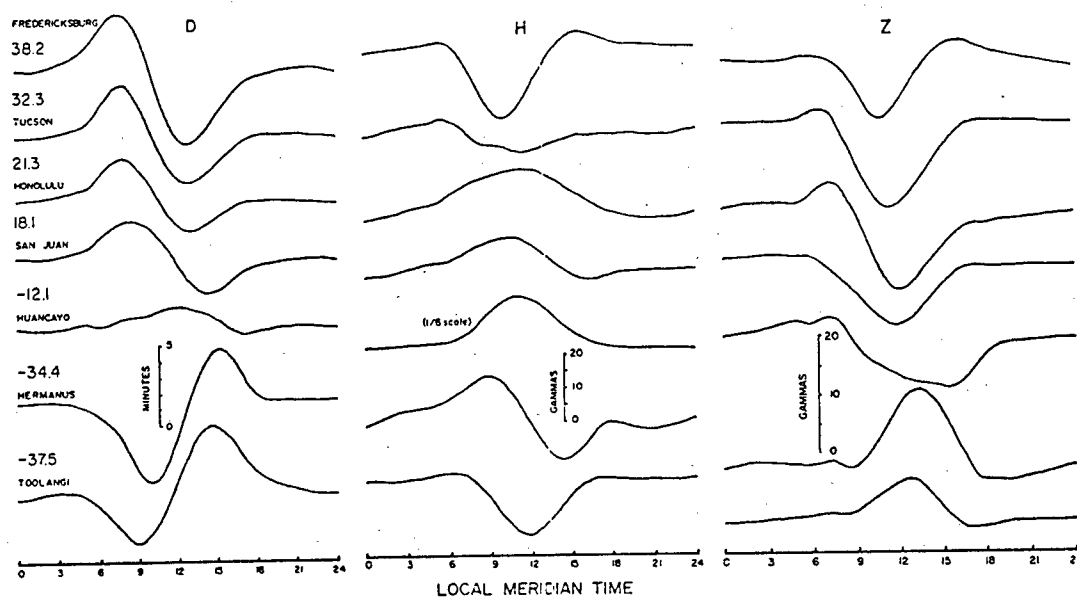
Fig. 10. Daily variation of H, D, and Z magnetic components for averaged quiet days of March 1965. Representative observatories (names to left) at mid- and low-geographic latitudes (values below the names) are selected to illustrate the pattern change of daily component variations between hemispheres. Note the 1/6-amplitude scale for Huancayo (taken from Campbell, 1997).
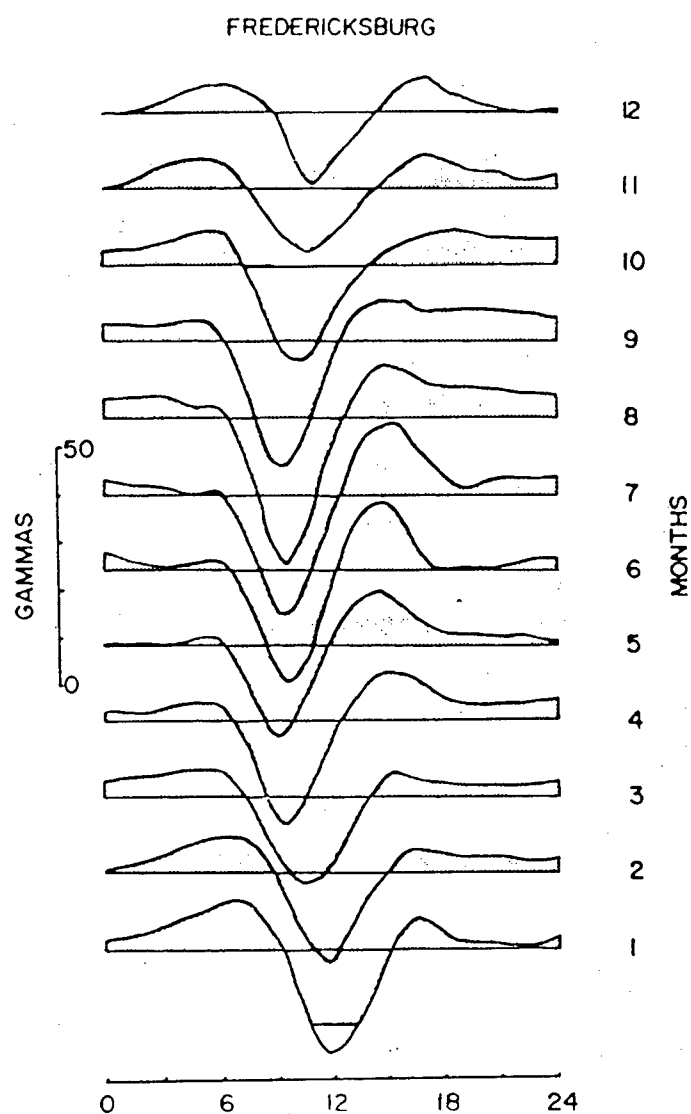
Fig. 11. Average daily variation of the *Sq* "H" component at Fredericksburg for each month of the year (the bottom plot is January; the top plot is December). Note the annual amplitude change and the seasonal summertime shift to earlier times of maximum amplitude (taken from Campbell, 1997).
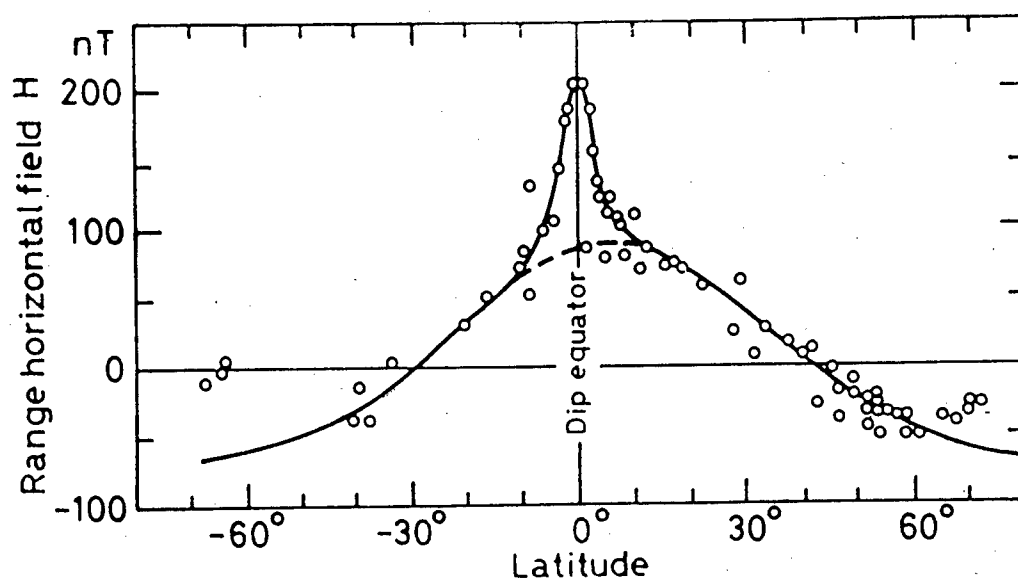
Fig. 12. Latitude profile of the daily range of the horizontal field *H* during 1958, showing the region of the equatorial electrojet superimposed on the worldwide *Sq* variation. Note that equatorial electrojet *enhancements* to *Sq* exist only within about 10 degrees of the dip equator (taken from Rastogi, 1989).

Earth's magnetic field. Descriptions of such instruments are contained in references

such as Kivelson and Russell (1995) and Campbell (1997). I will briefly

discuss the main features of one modern-day instrument, the fluxgate magnetometer.

Most modern observatories and satellites use fluxgate magnetometers. Figure 13 shows

a schematic of this instrument. The primary winding contains a highly permeable

ferromagnetic core, which is driven through continuous hysteresis cycles by a high-

frequency alternating current in the winding. The "natural" magnetic field external to the

instrument causes an asymmetry in the hysteresis cycle, which is detected in the output

signal of a secondary winding (surrounding the primary). The amplitude and phase of all

even harmonics in the output signal are proportional to the magnitude of the field along

the axis of the winding. To resolve the full three-dimensional external magnetic field,

three independent, orthogonal windings are used.
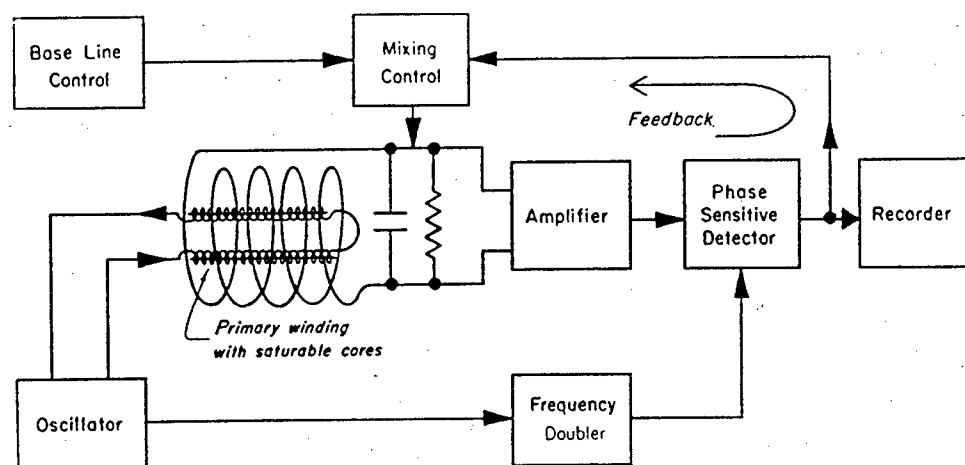
Fig. 13. Fluxgate magnetometer for directional (vector) geomagnetic field measurements
(taken from Campbell, 1997).

CHAPTER 3

HISTORY OF THE "K-LIKE" MAGNETIC INDICES

3.1. Introduction

Indices based on geomagnetic variations have been calculated since 1885. Mayaud (1980) and Menvielle and Berthelier (1991) give excellent histories of geomagnetic indices from the early years up to the present. Therefore, I will only note the highlights of the "early" indices, then concentrate on the "modern" era of geomagnetic indices, which began in 1939. Unless otherwise stated, all material in this chapter comes from the two references listed above.

3.2. Early indices

The first index was the daily range, calculated from 1885-1963 at the Greenwich Observatory. It was defined as the difference between the highest and lowest value recorded on one selected geomagnetic component at a given station, and as the name implies, had an integration time of 24 hours. Use of the daily range was discontinued for several obvious reasons: (1) The index did not subtract out the Sq variations, and so did not become "zero" even on the quietest days, (2) the statistical time variation of the daily range was therefore mainly due to Sq variations, and (3) the integration time of the daily range was too long (compared with the time constants of many of the phenomena responsible for the irregular geomagnetic variations).

The first attempt at describing irregular variations was contained in the "C" (for character) index. This index was calculated for the years 1884-1975 by various observatories. For each Greenwich day, an observer would subjectively remove the Sq

variations from the magnetometer trace, then assign a number 0, 1, or 2 to describe the disturbance level for the day. The daily numbers for all observatories in the "*C*" network were then averaged to produce the international character "*Ci*", which was the first attempt at a planetary index. The "*C/Ci*" indices were definitely an improvement over the crude daily range, but still suffered from defects such as the 24-hour integration time, as well as lack of standardization and objectivity among the "*C*" observatories.

3.3. Modern day indices

The transition to "modern day" indices occurred around the start of World War II, and from this time to the present, considerable effort has been made to correct the shortfalls (relative to the goal of measuring irregular geomagnetic variations) of previous indices. In 1938 Dr. J. Bartels began computing the well-known *K* index at Niemegk Observatory in Germany (the letter "*K*" comes from the German word *Kennziffer*, which means character). His method (Bartels et al., 1939) was officially adopted the next year, and has been in use ever since. The *K* index is different from previous indices in several ways. First, the index is computed once every 3 hours (still based on the Greenwich day), beginning at zero hours universal time (UT). Bartels felt that 3 hours would "strike a balance between the required precision and the necessary economy" required of a geomagnetic index. Bartels (1940, p. 28) also wrote that 3-hour intervals "seem to be long enough to give correct indications for such details as bays and other perturbations of only one hour or two in duration. At the same time, it is short enough not to affect too much of the day in cases where two successive intervals might be affected by a disturbance, such as the bay, occurring centered on their common point."

Next, specific procedures were developed for removal of Sq from the magnetometer trace, such as those outlined in Mayaud (1967). Finally, the K index is not simply the largest deviation measured from the magnetometer trace, but rather is an integer between zero and nine obtained from the range via a quasi-log conversion. Table 1 shows the conversion chart used by Dr. Bartels at the Niemegk Observatory. The limits of the classes follow a quasi-logarithmic scale in order to separate the lower levels of activity as well as the higher ones, so that the resulting indices will allow study of either magnetically quiet or stormy periods.

Now we look at an example of how the K index is computed. Figure 14 shows a sample H component magnetometer trace (solid line) and the station Sq trace (dashed line) versus universal time. Several 3-hour integration windows are highlighted in

Table 1
K index class limits at Niemegk Observatory

Range, nT	K value
0 – 4	0
5 – 9	1
10 – 19	2
20 – 39	3
40 – 69	4
70 – 119	5
120 – 199	6
200 – 329	7
330 – 499	8
500+	9
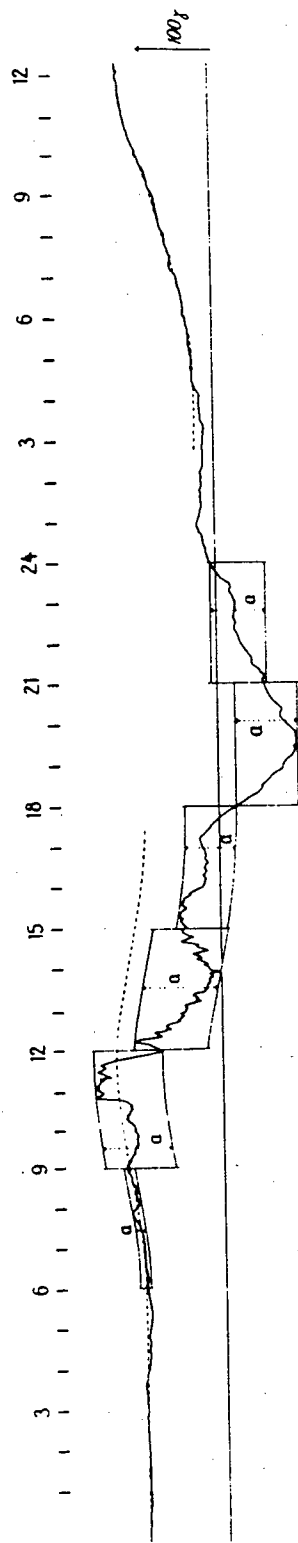
Fig. 14. A record of the *H* component at Guam, a low-latitude station. For some of the 3-hour intervals the range *a* corresponding to the definition of the *K* index (i.e., difference between the extreme of the variation within the interval after elimination of *Sq*) is indicated (after Mayaud, 1967). This figure also illustrates the process of eliminating *Sq* when scaling the *K* indices. Assuming the *Sq* from 6 to 18 hours may be estimated to be the dashed line, one draws (within each 3-hour interval) two parallel "copies" of the *Sq* curve. The upper one passes through the observed (raw) data maximum; the other passes through the data minimum. The vertical distance between these two *Sq* traces then corresponds to the range of the irregular magnetic variation for the given 3-hour period. One would then consult a range-to-*K* conversion table (such as Table 1) to compute the *K* index (taken from Mayaud, 1980).

the figure. In any one of these windows, the K index is derived by "sliding" the Sq trace up until it touches the maximum value of the magnetometer trace in the 3-hour window. The position of the Sq curve is recorded, and then it is moved down until it intersects the minimum value of the magnetometer trace. The result is two parallel "copies" of the Sq curve. The 3-hour range value for the H component is then the vertical "distance" (in nanoteslas) between these two Sq traces. The procedure is repeated for the D trace. Finally, the largest range value between H and D for a given 3-hour period is determined, and this value is then converted to the K index (using Table 1).

Before discussing the planetary version of the K index, I need to mention two points. First, the literature stresses that the K index should be regarded as a *code*, not a *number* that can be arithmetically averaged with other K values. This results from the fact that the station K index is arranged on a nearly logarithmic scale. However, as we will see, this caveat is ignored when computing the planetary index Kp. Second, the recipe given above for computing the station K index reveals something about the physical meaning of the index. Calculation of the index focuses only on magnetic variations due to alternating currents (AC) in the magnetosphere. Direct current (DC) energy deposition— which would tend to displace the *entire* magnetic field trace—is not detected by the K index. In the literature, this fact is acknowledged by noting "the typical time scale of the observed variations must be less than the 3-hour length of the interval used in measuring the range leading to the K index" (Menvielle and Berthelier, 1991, p. 422).

Dr. Bartels introduced the idea of using a network of stations to derive a planetary index of geomagnetic activity in the same paper that he defined the station K index. He

recognized that K indices from different stations had to be "standardized" before they could be combined into a planetary index. In other words, each K index value on the 0-9 scale must represent the same geophysical condition regardless of where the observatory is located on the globe. Bartels assumed this condition would be realized if the frequency distribution of K values was the same at every station. How then does one "adjust" things to make the frequency distributions equal at all stations? Bartels handled the latitudinal (geomagnetic) and local time/seasonal corrections separately.

Historically, the latitudinal correction was accounted for first. It was observed that stations nearer the geomagnetic equator, being farther removed from auroral current systems, experienced smaller magnetic deflections for a given level of geomagnetic disturbance. The solution was to adjust (in a proportional fashion) the Niemegk K scale (see Table 1) so that the K index frequency distributions would be equal at all stations. Thus, for example, the lower limit of $K=9$ might be 250 nT at an equatorial station, but remains 500 nT at a mid-latitude station (which is closer to the auroral currents). The factors of proportionality were derived empirically for each station. However, it was later shown that the "goal of proportional grids leading to similar significance of K values is achieved only in the subauroral regions, where the geomagnetic perturbations have similar local time and seasonal variations and where the distribution of K indices is lognormal" (Menvielle and Berthelier, 1991, p. 421). Mayaud later refined the process of determining proportionality factors by plotting irregular activity amplitudes versus corrected geomagnetic latitude for a nine-year sample of K indices from a chain of European stations.

The first planetary version of the K index was computed in 1938 based on an eight-station network using K scales with latitudinal corrections as described above. The procedure was the same as the C/Ci scheme, i.e., a simple arithmetic average of station K values. However, after a few months it was apparent that "such a crude definition of worldwide activity by the average of the existing K indices was not satisfactory" (Menvielle and Berthelier, 1991, p. 423). This led to the need for local time/seasonal corrections to the station K indices.

The philosophy for local time/seasonal corrections was identical to that of the latitude corrections—the same K values would have the same meaning provided their frequency distribution was the same. This standardization process is more involved than the one for latitude corrections, and I will not repeat it here. The modern process for these corrections is described fully by Bartels (1949, 1951). With this in mind, we are now in a position to discuss the modern Kp station network and calculation procedure.

The Kp network originally consisted of eight stations. The modern-day network has 13 stations as listed in Table 2 and Figure 15. The Kp calculation procedure is as follows. For a given 3-hour period, each station in the network calculates a 3-hour K index (using a latitude-corrected conversion table). Each station K is then converted into the so-called Ks ("s" for standardized) using the local time / season conversion table. Then the Ks values for Brorfelde and Lovö are averaged together (arithmetically), as are the Ks values for Eyrewell and Canberra. Thus the divisor for the final averaging process is 11, not 13.

Now the Ks—and the final Kp—are not simply integers from zero to nine. Instead the integer codes are further subdivided in a manner easiest explained with an example: the

Table 2
The present-day *Kp* network

Observatory	Corrected Geomagnetic Latitude	Derivation Method
Northern Hemisphere		
Meanook (MEA)	62.5°	AS (1994)
Sitka (SIT)	60.0°	USGS (1989)
Lerwick (LER)	58.9°	AS (1991)
Ottawa (OTT)	58.9°	AS (1994)
Lovö (LOV)	56.5°	FMI (1996)
Eskdalemuir (ESK)	54.3°	AS (1991)
Brorfelde (BJE)	52.7°	FMI (1993)
Fredericksburg (FRD)	51.8°	USGS (1997)
Wingst (WNG)	50.9°	FMI (1996)
Hartland (HAD)	50.0°	AS (1991)
Niemegk (NGK)	48.8°	FMI (1997)
Southern Hemisphere		
Eyrewell (EYR)	50.2°	LRNS (1996)
Canberra (CAN)	45.2°	Hand Scaling
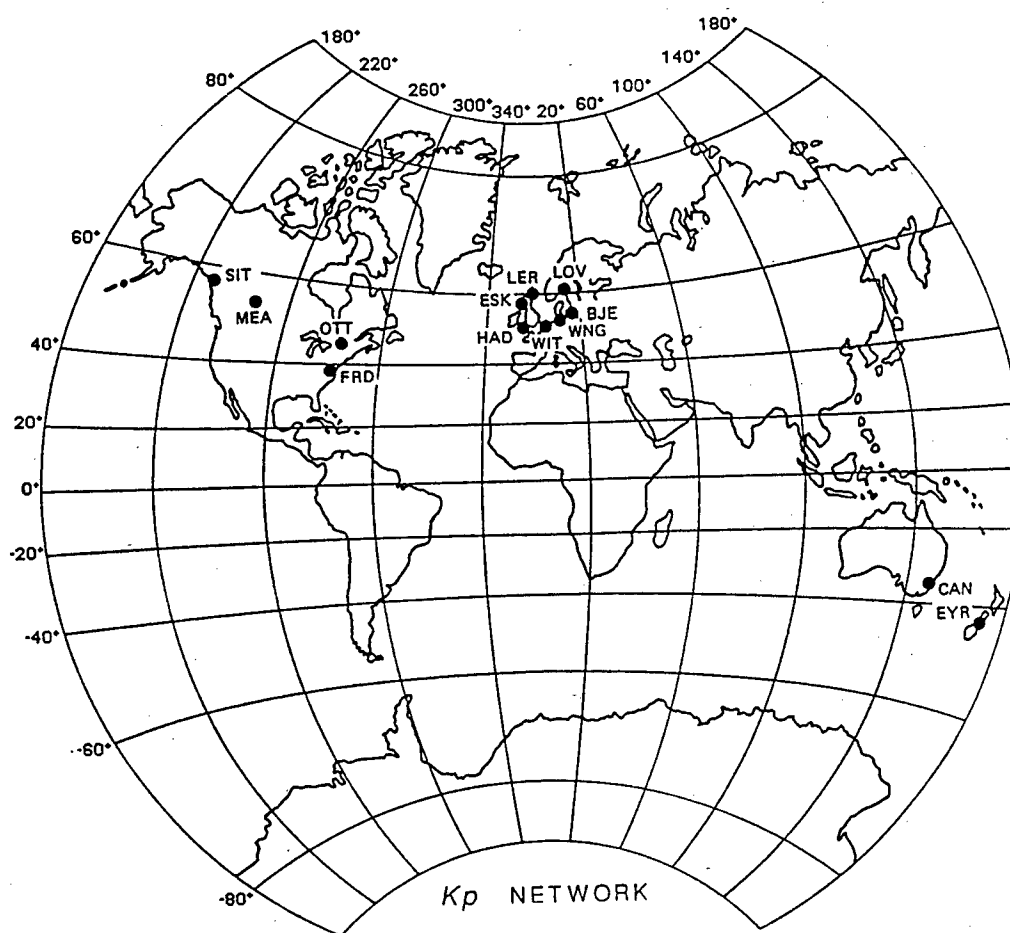
Fig. 15. The *Kp* network in 1988. In the present-day network, Witteveen (WIT) has been replaced by Niemegk (taken from Menvielle and Berthelier, 1991).

interval from 1.5 to 2.5 (surrounding $K = 2$) is divided equally into thirds and designated by 2- (for the lowest third), 2o (the middle third), and 2+ (the upper third). Each integer from zero to nine is divided this way except for the designators 0- and 9+, which are not used. Thus the entire scale ranges from 0o up to 9o (a total of 28 separate designators).

In the $Ks \rightarrow Kp$ averaging process, each designator is assigned to an integer; 0o is assigned to the number zero, up to 9o, which is assigned to 27. These designations are called "$3Ks$". The 11 "$3Ks$" values (for a given 3-hour period) are then arithmetically averaged into what is called "$3Kp$" (recall the previous note in this chapter regarding averaging of K codes). This value is then transferred back to Kp which, like Ks, uses the -/o/+ designation. Kp can then be converted back to a "range" type index in a manner opposite to the original quasi-log conversion. This index is called ap ("a" for amplitude). Table 3 shows the conversion scale from Kp to ap. Note that a given value of ap represents half the actual magnetic variation in nanoteslas. Finally, the eight ap values for a given UT day are averaged together to form the daily planetary amplitude index, or Ap. This entire process is represented in Figure 16.

Prior to 1970, all K index computations—both station and planetary—were done by hand. However, starting in 1970, the $K \rightarrow Kp$ process was computerized. The code was developed and run at the Institute for Geophysics, University of Göettingen, Germany. Then on 1 January 1997, the official site for Kp generation moved from Göettingen to Niemegk (Adolf Schmidt Observatory).

Table 3
Conversion from *Kp* to *ap* (taken from Menvielle and Berthelier, 1991)

Kp	*ap*	*kp*	*ap*
0o	0	5—	39
0+	2	5o	48
1—	3	5+	56
1o	4	6—	67
1+	5	6o	80
2—	6	6+	94
2o	7	7—	111
2+	9	7o	132
3—	12	7+	154
3o	15	8—	179
3+	18	8o	207
4—	22	8+	236
4o	27	9—	300
4+	32	9o	400

Values of *ap* are expressed in units of 2 nT. For instance, *ap* = 12 corresponds to 24-nT variation.
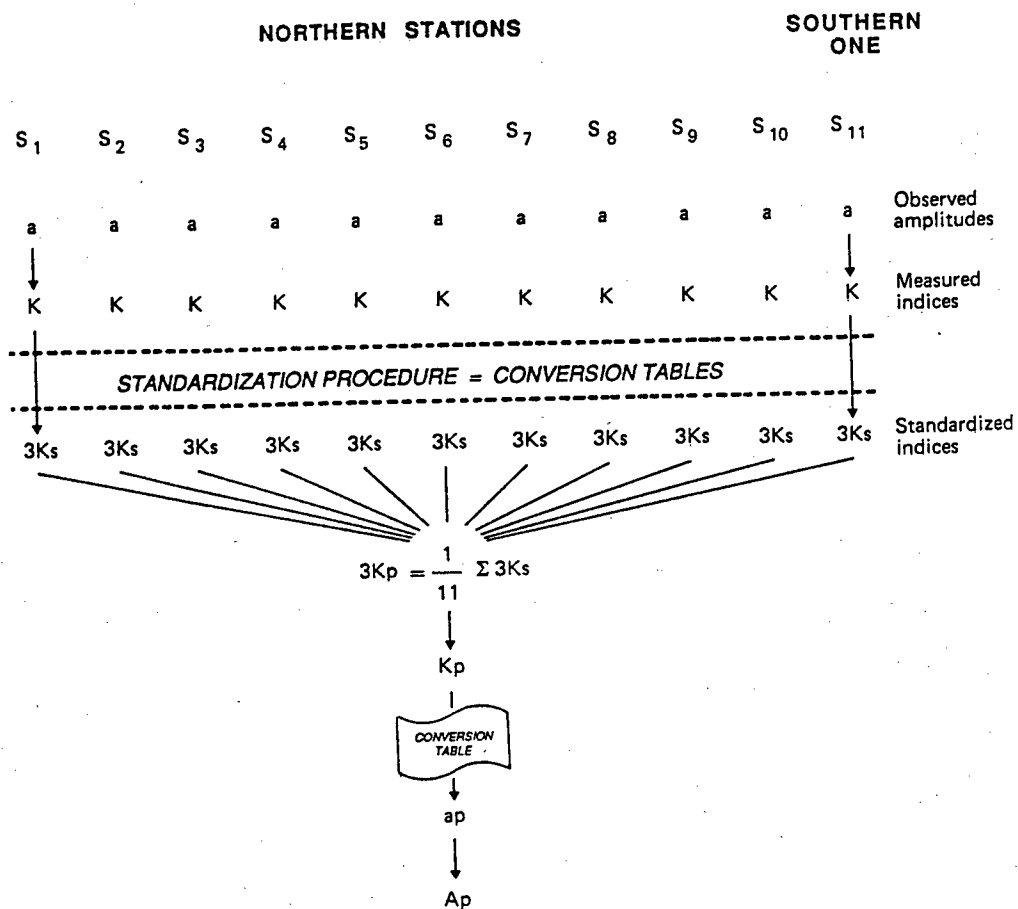
Fig. 16. Derivation scheme of the 3-hour *Kp* and *ap* indices. *Ap* is the daily mean value of *ap*; both are expressed in units of 2 nT (taken from Menvielle and Berthelier, 1991).

3.4. Computerization of the *K* indices

More recently, computerization of the station *K* indices has occurred. Over the past two decades, many different *K* index codes have been written, and in 1991, the International Association of Geomagnetism and Aeronomy (IAGA) acknowledged the following *K* index methods (private communication with Dr. Robert McPherron, 1997):

1. "USGS": the method developed by the United States Geological Survey (USGS) is described in Wilson (Journal of Geomagnetism and Geoelectricity, **39**, 97, 1987).

2. "AS": the Adaptive Smoothing method is described in Jankowski, et al. (Annales Geophysicae, **6**, 589, 1988) and in Novozynski et al. (Geophysics Journal International, **104**, 85, 1991).

3. "FMI": the method developed by the Finnish Meteorological Institute is described in Sucksdorff et al. (Geophysical Transactions, **36**, 344, 1991).

4. "LRNS": the Linear-phase Robust Non-Linear Smoothing method is described in Hattingh et al. (Annales Geophysicae, **6**, 611, 1988) and in Hattingh et al. (Geophysics Journal International, **99**, 533, 1989).

5. "HS": the Hand Scaling traditional derivation process remains the basic reference and a still accepted method, following the rules described in the "Atlas des Indices *K*" by Mayaud (IAGA Bulletin no. 21, 113 pp., 1967).

Twelve of the 13 *Kp* network stations now generate their *K* indices via computer (private communication with Dr. Hans-Joachim Linthe, 1998). Table 2 lists the current method used at each *Kp* network station (acronyms for the *K* derivation method refer to the list above, and years shown in parentheses indicate when computerization replaced hand-scaling).

3.5. Department of Defense *K*-like indices

Finally, the U. S. Air Force Air Weather Service (AWS) has, for many years, computed an approximate *Kp*. Initially, a six-station network was used to produce a

crude index; only the Boulder magnetometer removed the *Sq* current contribution from the raw data. In 1992, Schroeder and Cliffswallow documented their efforts to modernize the Air Force index. Significant differences between the official *Kp* and the revised Air Force index include:

1. Different network stations. The Air Force network (in 1992) is shown in Table 4.

2. The *Sq* currents are accounted for differently in the Air Force index.

3. The Air Force index does not include the $K \rightarrow Ks$ conversion, i.e., no seasonal/local time corrections are made.

4. Whereas the official *Kp* is computed eight times each UT day (beginning at 0000 UT), the Air Force index is derived once every UT hour. For the UT hours 0100, 0400, 0700, etc., the Air Force calculation uses only the past hours' data (remember every official *K* index calculation uses three hours of data). For the UT hours 0200, 0500, 0800, etc., the past two hours' data are used in the Air Force index.

5. Unlike the official index, the Air Force station *K* indices are converted to a linear scale prior to computing the planetary index.

6. Air Force personnel manually remove bad data each hour prior to index computation.

Cliffswallow (1993) showed that, for the period 17 June 1992 through 15 June 1993, the Air Force "*Kp*" values were within ±1 unit of the official *Kp* 96.1% of the time. Within the last four years, the Air Force index software has been rewritten; however, I do not know whether their algorithms have changed.

Table 4
The U. S. Air Force "*Kp*" network in 1992 (taken from Schroeder and Cliffswallow, 1992)

Observatory	Corrected Geomagnetic Latitude
Meanook	62.5°
Glenlea	60.3°
Sitka	60.0°
Ottawa	58.9°
Saint Johns	57.4°
Newport	55.0°
Fredericksburg	51.8°
Boulder	49.3°
Fresno	43.1°

CHAPTER 4

OUR GEOMAGNETIC INDEX ALGORITHM

4.1. Introduction

As stated in the introduction, this research aims to examine the viability of "*K*-like" geomagnetic indices. Such research obviously requires a reliable computer program to compute these indices. The meaning of "reliability" in this context will be discussed later; however, one can easily see that the quality of the science done in our research hinges upon the quality of our geomagnetic index generating "tool."

The first task was to decide whether to use one of the IAGA-approved codes, or to create our own software. We chose the latter for two reasons. First, creating my own code from scratch would help give me a thorough understanding of how raw magnetometer data are processed into a geomagnetic index. Second, modification of a geomagnetic index code (to produce variations of the standard 3-hour station *K* index) can be done more quickly and confidently using a program with which one is intimately familiar (as opposed to code written by others).

The method used in our program is the same one used to derive the official *K* index; references include Bartels et al. (1939), Bartels (1957), and Mayaud (1967). Following is a brief summary of how we implemented this method in our code:

a. Ingest and "clean" raw magnetometer "H" and "D" component data.

b. Derive the "H" and "D" *Sq* trace from the raw data.

c. Derive the irregular variation (range) for the given time interval.

d. Apply "range-to-index" quasi-log conversion for the given time interval.

The next few sections describe these steps in detail.

4.2. Raw data ingest and cleaning

The first step is, of course, to ingest the raw magnetometer "H" and "D" component data (recall that the "Z" component is not used in determining K-like indices). We chose to work with data gathered at the Fredericksburg, Virginia magnetometer. This is a mid-latitude station and a participating station in both the Adolf Schmidt and U. S. Air Force Kp networks. The data we used covered the period 1990-1992 (three years), and were extracted from a CD-ROM disk courtesy of Mr. Don Herzog, United States Geological Survey (USGS). This 3-year period, which includes some of the most active years in solar cycle 22, offered an excellent mix of geomagnetic activity levels for study. The data are spaced at 1-minute intervals, giving a total of 1,578,240 data points in our 3-year sample. However, as will be discussed later, missing data accounted for 32,400 points of this total.

The USGS did quality check the data prior to storage on the CD-ROM; however, since all our processing is automated, we decided to perform two further "cleaning" procedures on the raw data prior to use. The first of these eliminated any large, short-term (widths of 10 minutes or less) "spikes" in the data; we deemed such features as unphysical. Second, we smoothed the data with a first-order, three-point Gaussian technique as described in Thompson (1993). Figure 17 illustrates this smoothing process for the "H" magnetic component at Fredericksburg on 13 June 1990. Panel (a) shows the raw data from the instrument, and panel (b) depicts the same data after smoothing.

4.3. Sq derivation

Determination of the solar quiet day (Sq) curves for the Fredericksburg data was, by far, the most complicated part of creating our index "tool." Miscalculation of these
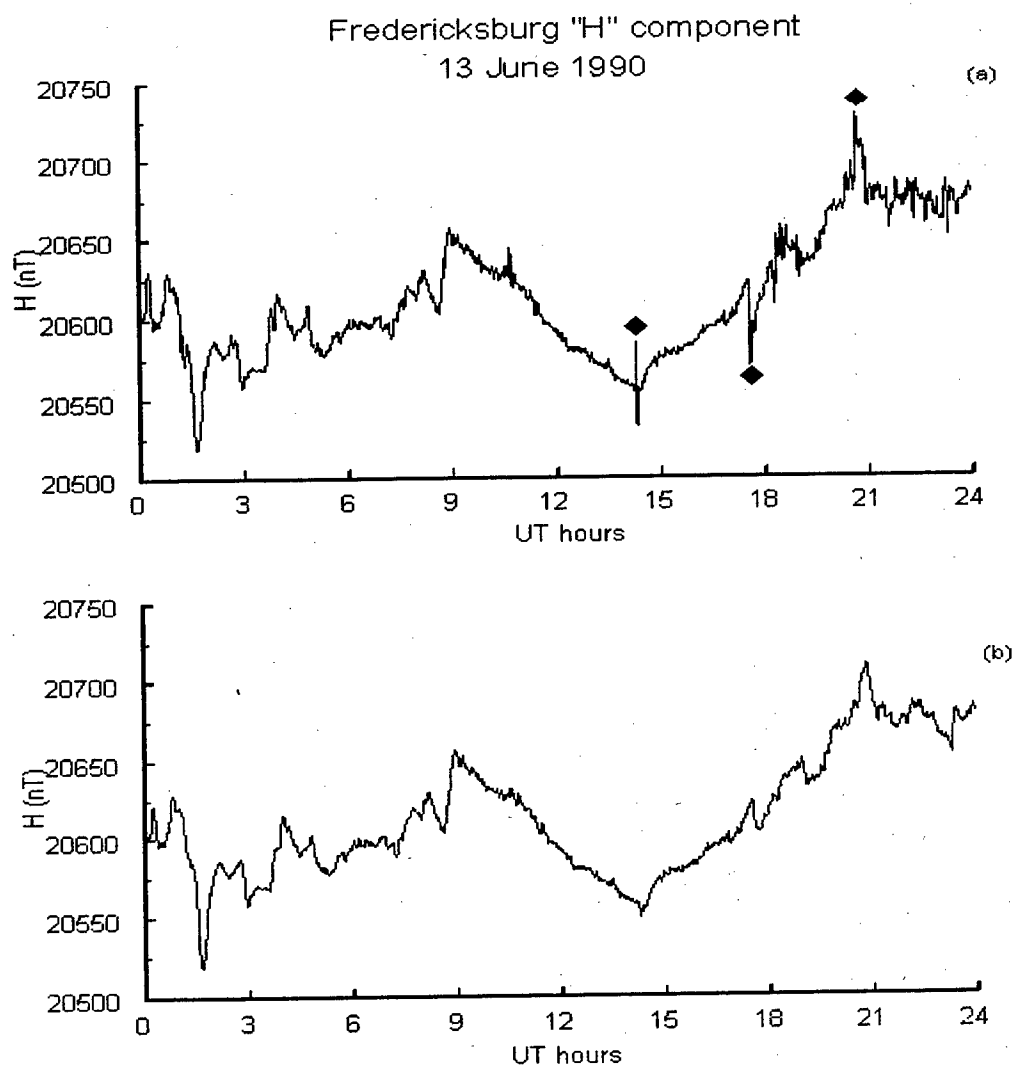
Fig. 17. Illustration of our raw-data smoothing process for the Fredericksburg "H" component on 13 July 1990. Panel (a) shows the raw (unsmoothed data). The three diamond shapes correspond to some of the physically suspect data "spikes" removed by our smoothing algorithm. The resulting curve is given in panel (b).

curves would result in faulty indices—and thus flawed science in all that followed.

The K index method references listed earlier contain discussions of Sq; however, the Mayaud paper gives the most specific set of rules for distinguishing the "non-K" variations from the K variations. For the purposes of our work, we adopted Mayaud's guidance to smooth the quiet parts of the magnetic record, retaining the "simplest and least speculative" curve that corresponds to a possible Sq variation. In this spirit we manually derived the Fredericksburg 1990-1992 Sq curves. However, we did not create distinct curves for each of the 1,096 days in our data set. Instead we attempted to create a set of "H" and "D" Sq curves for each calendar month—12 sets in all. We then assumed that the set for a given calendar month would be valid for every day in that month, and for each of the 3 years. For example, we used our January Sq set for each day of January 1990, 1991, and 1992. This assumption is valid because the changes in the shape and amplitude of the daily Sq curve throughout a given month—or even in a given month through three successive years—are too small to significantly affect the geomagnetic index calculations. This is especially true during geomagnetic storms, since the width of the range interval grows almost exponentially as K increases (see Table 1). Quantitative validation of this assumption is addressed later when we discuss comparisons with the Campbell et al. (1989) Sq set. The detailed procedure we used to derive our Sq set is described in the following paragraphs.

For each month of Fredericksburg data in our 3-year sample, we examined the official K index records, searching for the "quietest day" in each month (36 "quietest days" in all). Our criteria for "quietest day" was to choose the day with the smallest value of "equivalent daily amplitude," or A_K. The A_K is derived from the eight 3-hour K

values for the day in the following manner. First, each K value for the day is converted back to a linear scale, i.e., the inverse of the process used to determine the K values. These linear-scale values are called "equivalent amplitudes"; for a given K value, the equivalent amplitude is the mid-class value of the corresponding range class. Table 5 shows the $K \rightarrow A_K$ conversion applicable to subauroral observatories. The A_K is then figured as the arithmetic average of the eight "equivalent amplitudes" for that day.

However, finding the minimum A_K in a particular month was not always enough to uniquely specify the "quietest day." On several occasions in our three-year data sample, the minimum A_K occurred on more than one day in the same month. In such cases, we manually examined each of the "minimum A_K" days for the month concerned, and picked the one with the most "uniform" level of activity throughout the day. For example, a day with a K index value of one in all eight 3-hour periods was preferable to a day with $K=0$ for six periods and $K=3$ for the other two intervals.

Table 5
K-to-A_K conversion scale valid for subauroral observatories (taken from Menvielle and Berthelier, 1991)

K Index Value	a (K), nT
0	2.5
1	7.5
2	15
3	30
4	55
5	95
6	160
7	275
8	415
9	666

Amplitude in nanoteslas.

At this point we still had two further problems to resolve in choosing the quietest day in each month. The first problem involved missing data. Five of the 36 quietest days initially picked had one or more missing data periods. Now, according to Mayaud's rules, the Sq should be the "least speculative" curve; thus we did not attempt interpolation and/or extrapolation to replace the missing data. Instead we identified five replacement days. For a given month requiring a replacement, we looked at all the remaining days in that month for 1990, 1991, and 1992, and chose the day with the next lowest A_K, regardless of which year it occurred. For example, 6 December 1991, was replaced with 19 December 1990. The validity of this substitution is shown later when we discuss comparisons with the Campbell et al. (1989) Sq set.

The second problem was that the months of August and November 1991 were so active that no suitable days in those months could be used for Sq. So, using the same procedure as for missing data, 3 August 1992 was picked as the August 1991 "proxy," and 14 November 1990 was chosen as the November 1991 substitute.

Thus we finally had 36 "Sq-type" days identified from the Fredericksburg 1990-1992 data (three days from January, three from February, etc). A list of these days, and the corresponding A_K values are shown in Table 6. The final Sq curves for each month—one for the "H" component, and one for "D"—were obtained by averaging the three raw magnetometer curves for that month (for each component). The result was a set of 12 "H" component Sq curves (one per month), plus a corresponding set for "D".

Smoothing of data was an important part of obtaining these Sq curves. As stated at the start of this section, Mayaud (1967) discusses smoothing of the quiet portions of the magnetic record in determining Sq for the day. His rules for smoothing are complex and

Table 6
Fredericksburg 1990-1992 Sq days and corresponding A_K values

Date	A_K	Date	A_K	Date	A_K
27 Jan 1990	2	14 May 1990	2	2 Sept 1990	0
7 Jan 1991	1	16 May 1990	2	23 Sept 1991	2
23 Jan 1992	3	16 May 1992	4	1 Sept 1992	2
16 Feb 1991	3	17 Jun 1990	2	18 Oct 1990	2
17 Feb 1991	2	16 Jun 1991	4	16 Oct 1991	3
18 Feb 1991	2	2 Jun 1992	4	24 Oct 1992	2
17 Mar 1990	2	1 Jul 1990	4	5 Nov 1990	0
29 Mar 1991	2	5 Jul 1991	5	14 Nov 1992	0
14 Mar 1992	3	11 Jul 1992	3	29 Nov 1992	3
20 Apr 1991	3	5 Aug 1990	4	11 Dec 1990	1
11 Apr 1992	1	2 Aug 1992	3	19 Dec 1990	2
12 Apr 1992	3	3 Aug 1992	3	26 Dec 1992	3

vary according to factors such as geomagnetic activity level. For the purposes of our work it was impractical to carry out our Sq analysis to this level of detail; however, in the sense that Sq should not contain high-frequency fluctuations, we decided to perform smoothing of both the raw data (for our 36 Sq days) and the averaged Sq curves (12 curves apiece for "H" and "D"). Figures 18-20 illustrate the entire Sq derivation process for the September "H" component. Figure 18 shows the raw data for the three September Sq days (see Table 6), and Figure 19 shows the same three days after smoothing. Figure 20 gives the final (smoothed) September Sq "H" curve. The September "D" curve—as well as the curves for the other 11 months of the year—are derived in the same fashion. Next we wanted to test the temporal "coherence" (both time of day and seasonal) of
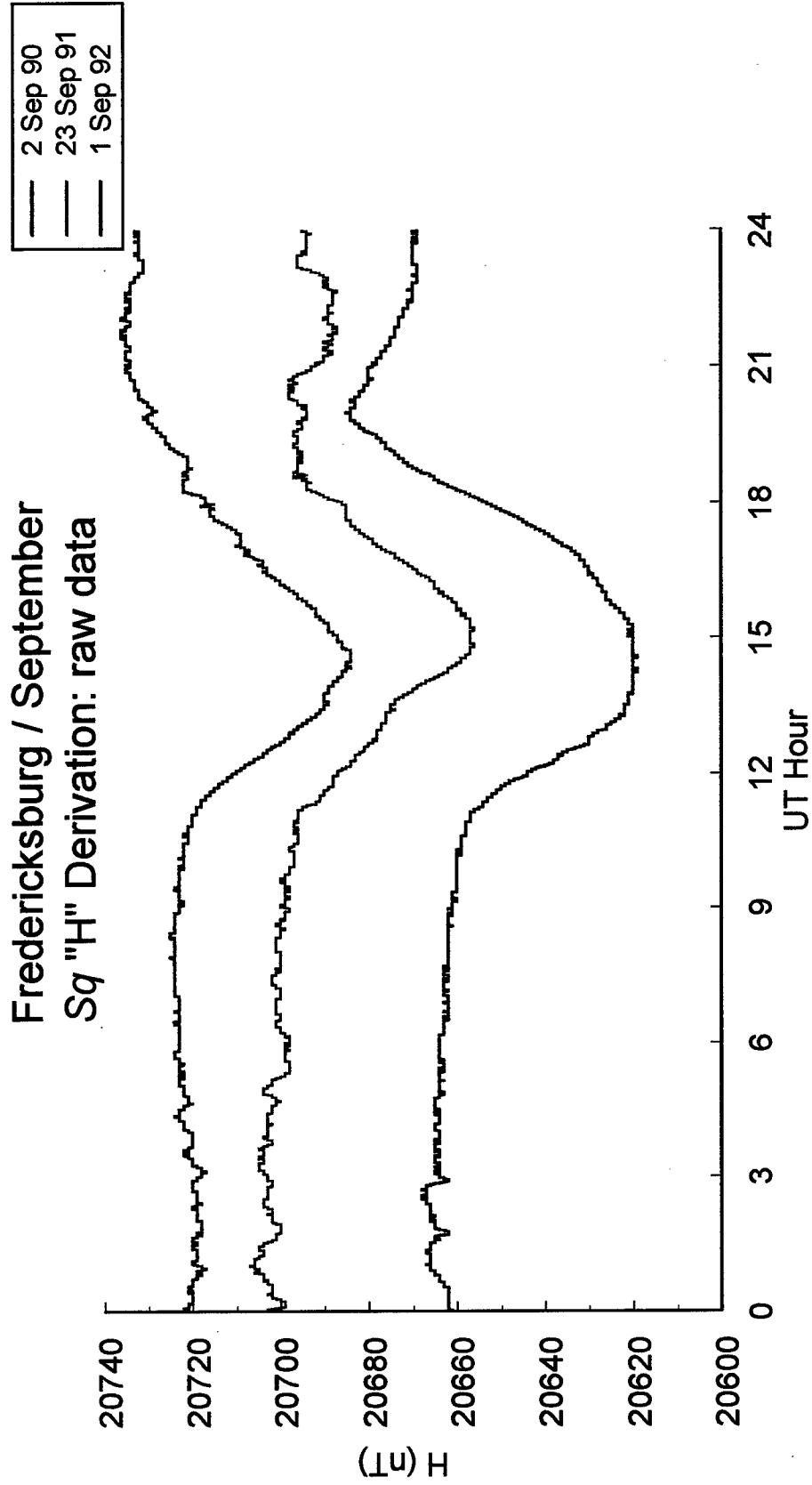
Fig. 18. Illustration of our *Sq* derivation for the September "H" component, showing the three raw-data curves for our September quiet day selections (see Table 6).
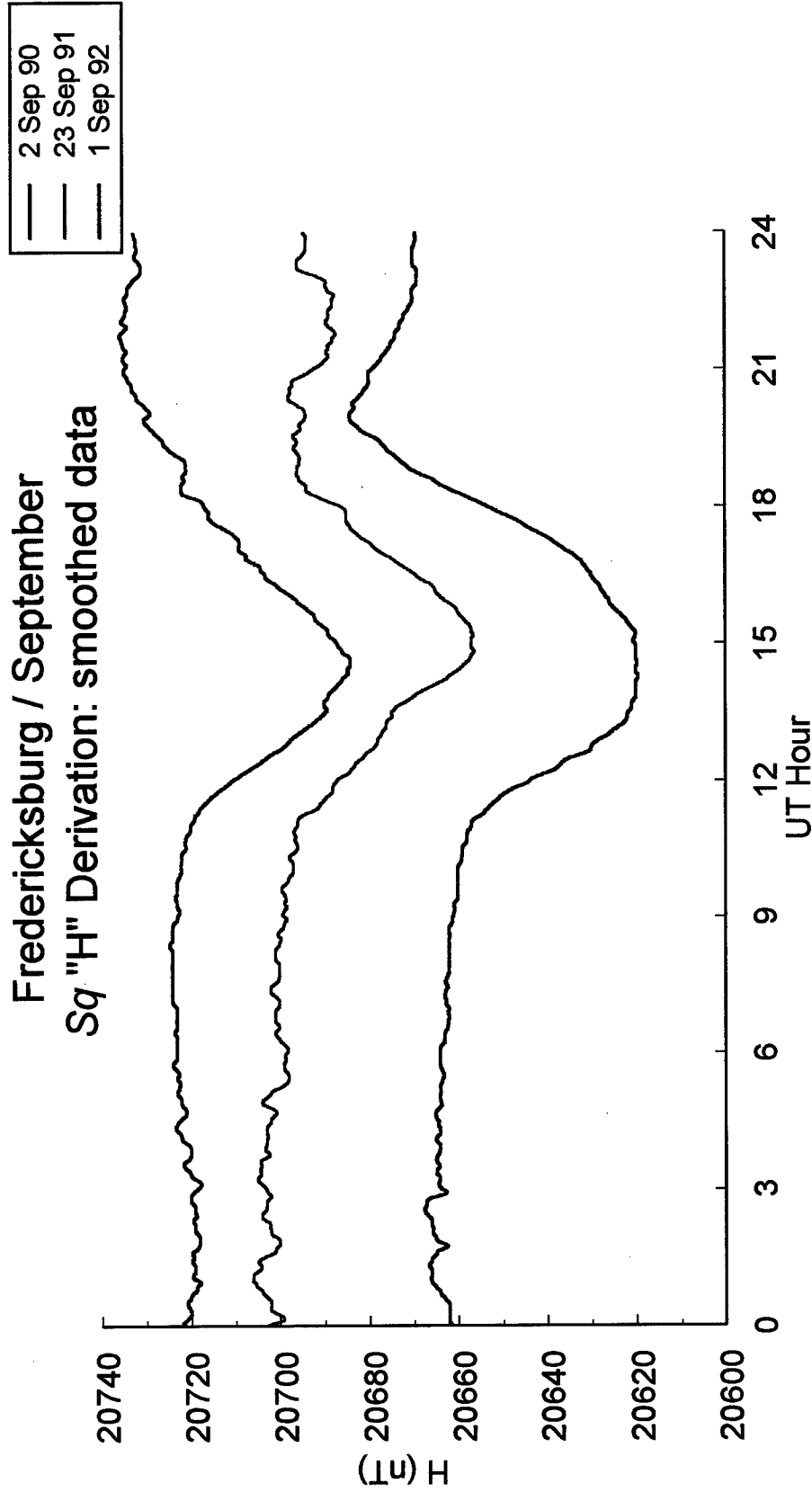
Fig. 19. Illustration of our *Sq* derivation for the September "H" component, showing the three quiet-day "H" curves from Figure 18 after smoothing.
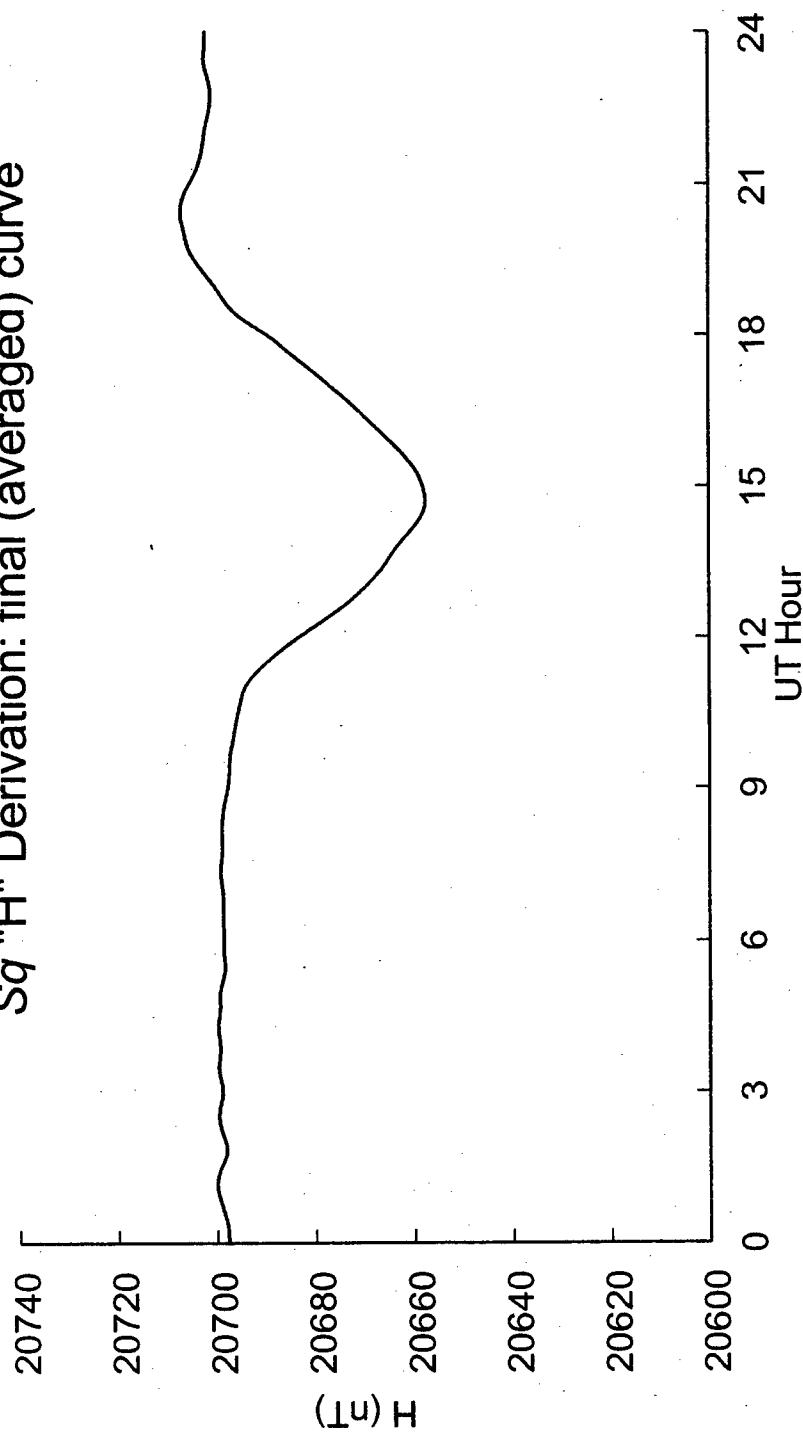
Fig. 20. Illustration of our *Sq* derivation for the September "H" component, showing the final "H" *Sq* curve resulting from the arithmetic average of the three curves shown in Figure 19 (plus smoothing of the averaged curve).

our *Sq* set as a whole. The *Sq* current system varies smoothly and continuously throughout the year, so we constructed 2-D contour plots of our 12-month "H" and "D" *Sq* sets to test for this "coherence." For each monthly *Sq* curve, we computed the average value (in nanoteslas) every 15 minutes of universal time. These average values were then plotted on a 2-D contour graph of UT "bin" value (96 values per UT day) versus month of the year. The resulting plots are shown in Figures 21 and 22. They show a high degree of continuity throughout the year, which helped convince us that our derived *Sq* was suitable for use to derive geomagnetic indices.

In addition, we compared our *Sq* set with a preexisting *Sq* algorithm described in Campbell et al. (1989). His computer program generates *Sq* curves for any location using extrapolations from global observatory records taken in 1965, an extremely "quiet" year (from a geomagnetic activity standpoint). The program will calculate values for any year in the range 1940 to 2005.

First we compared the Campbell algorithm with the Fredericksburg raw magnetometer data for 5 November 1990. This day recorded an A_K of zero, making it one of the quietest days in our data set. On such a day the magnetometer trace should almost exactly reflect the *Sq* current system. However, as you can see in Figures 23 and 24, the Campbell *Sq* curves are smaller in amplitude than the raw data—about 30 nT smaller in the "H" component, and about 20 nT smaller for "D". Similar differences were also observed on other very quiet days, such as 10 December 1990 (see Figures 25 and 26). Mr. Lyndon Odell from the Fredericksburg Observatory verified for me that the raw data on these two days matched the *Sq* used by the observatory during that period (private communication, June 1997).
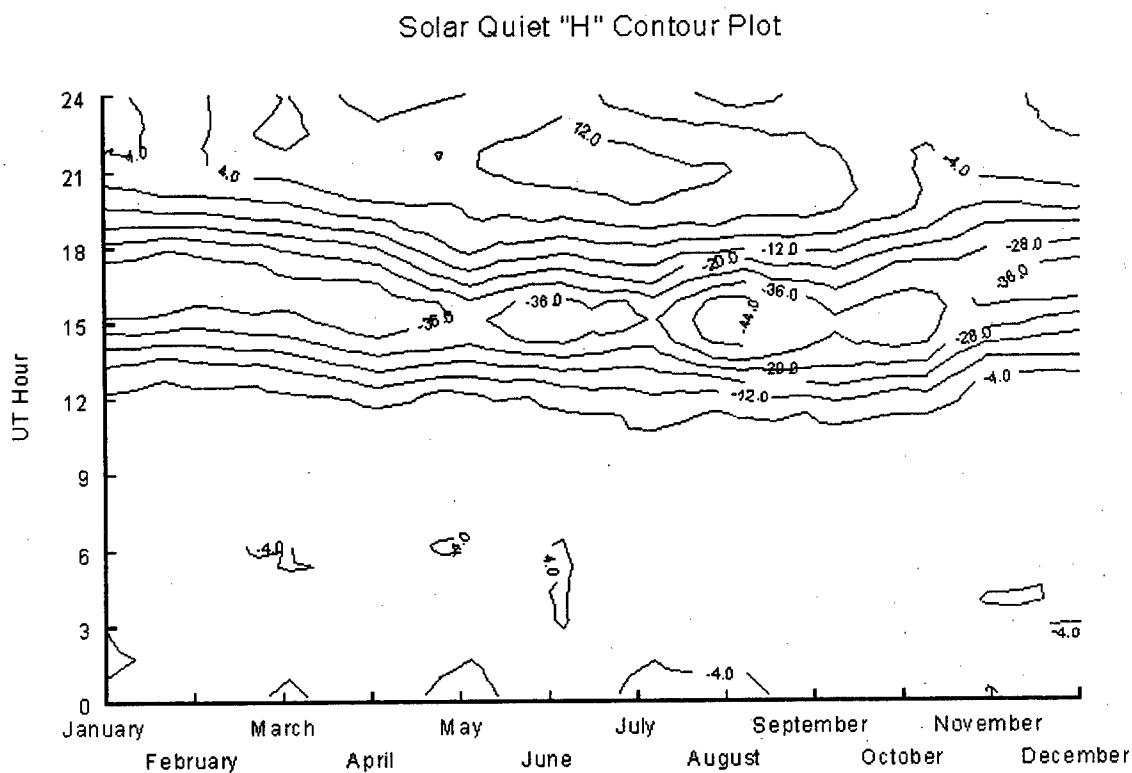
Fig. 21. Contour plot of our *Sq* "H" monthly curves derived from the 1990-1992 Fredericksburg raw data. For each monthly curve, the average *Sq* "H" value is computed for every 15 UT minutes (96 "bin" values per day). The contour interval is 8 nanoteslas. Diurnal and seasonal variations are clearly discernable, as is the "coherence" of the set as a whole.
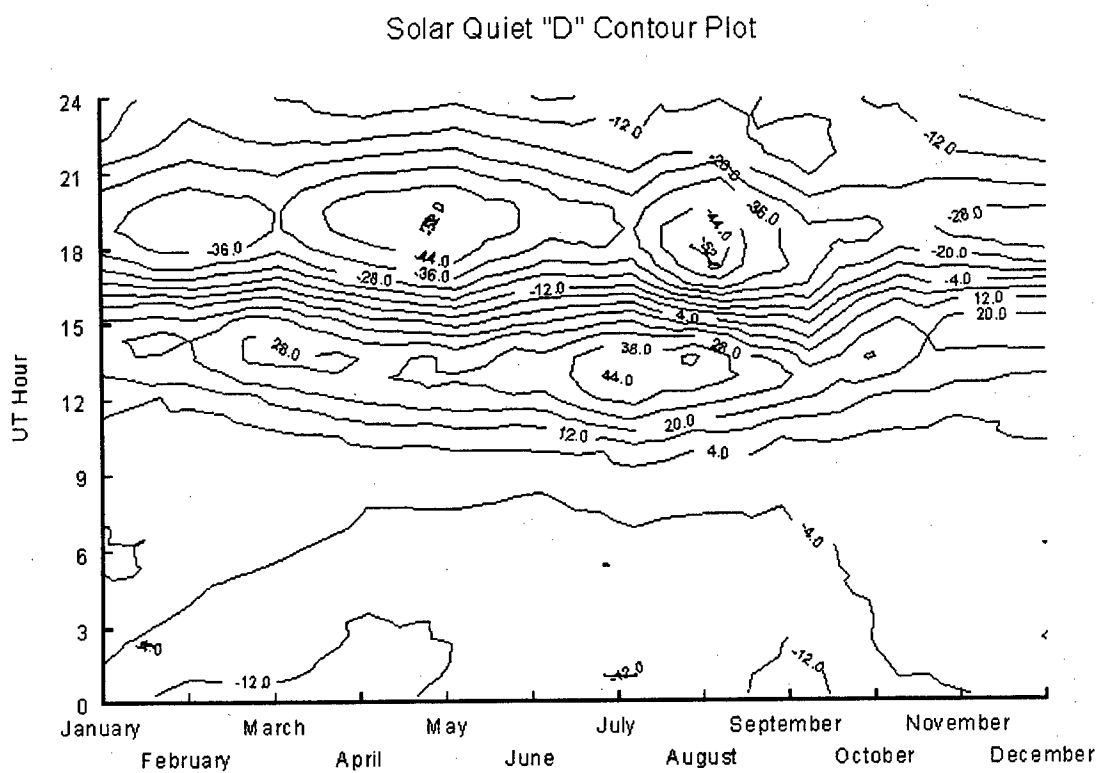
Fig. 22. Contour plot of our *Sq* "D" monthly curves derived from the 1990-1992 Fredericksburg raw data. For each monthly curve, the average *Sq* "D" value is computed for every 15 UT minutes (96 "bin" values per day). The contour interval is 8 nanoteslas. Diurnal and seasonal variations are clearly discernable, as is the "coherence" of the set as a whole.
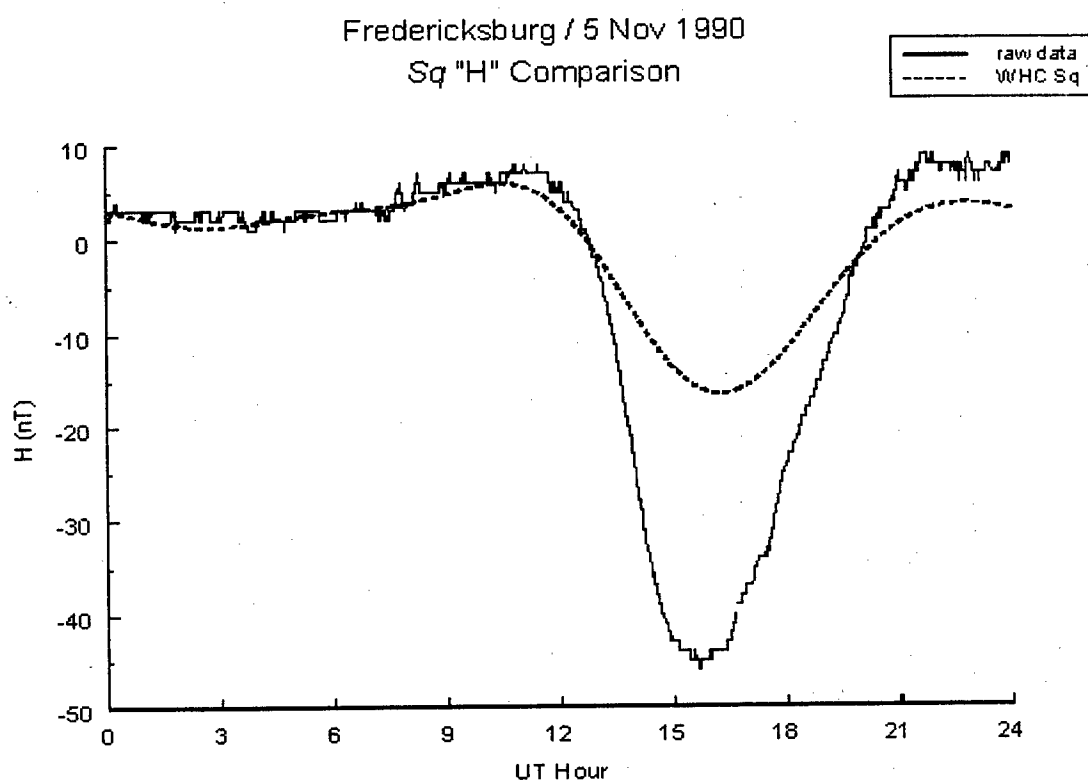
Fig. 23. Fredericksburg *Sq* "H" component comparison for 5 November 1990. The raw data is the solid line, and the dashed line is the Campbell *Sq* "H" curve for this date. This day was totally quiet (geomagnetically), with $K=0$ for all eight 3-hour periods. Thus the raw data is representative of the actual *Sq* "H" trace for this day. This reasoning also applies to the "D" component comparison in Figure 24.
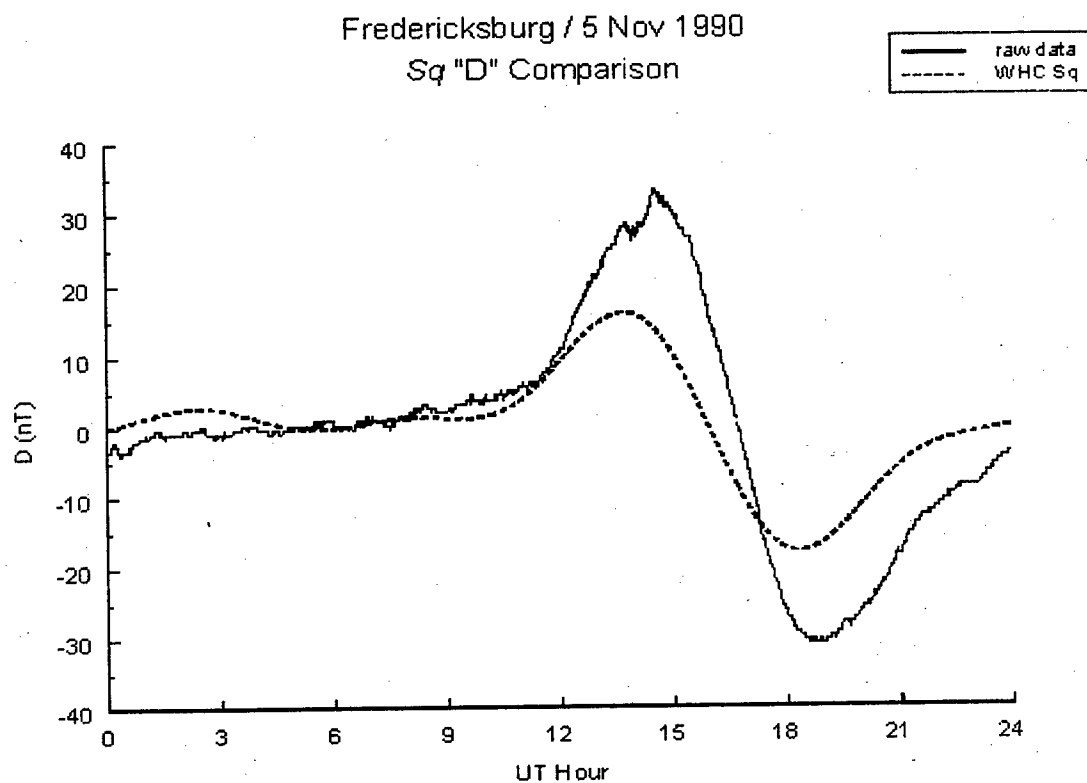
Fig. 24. Fredericksburg *Sq* "D" component comparison for 5 November 1990 (same format as Figure 23).
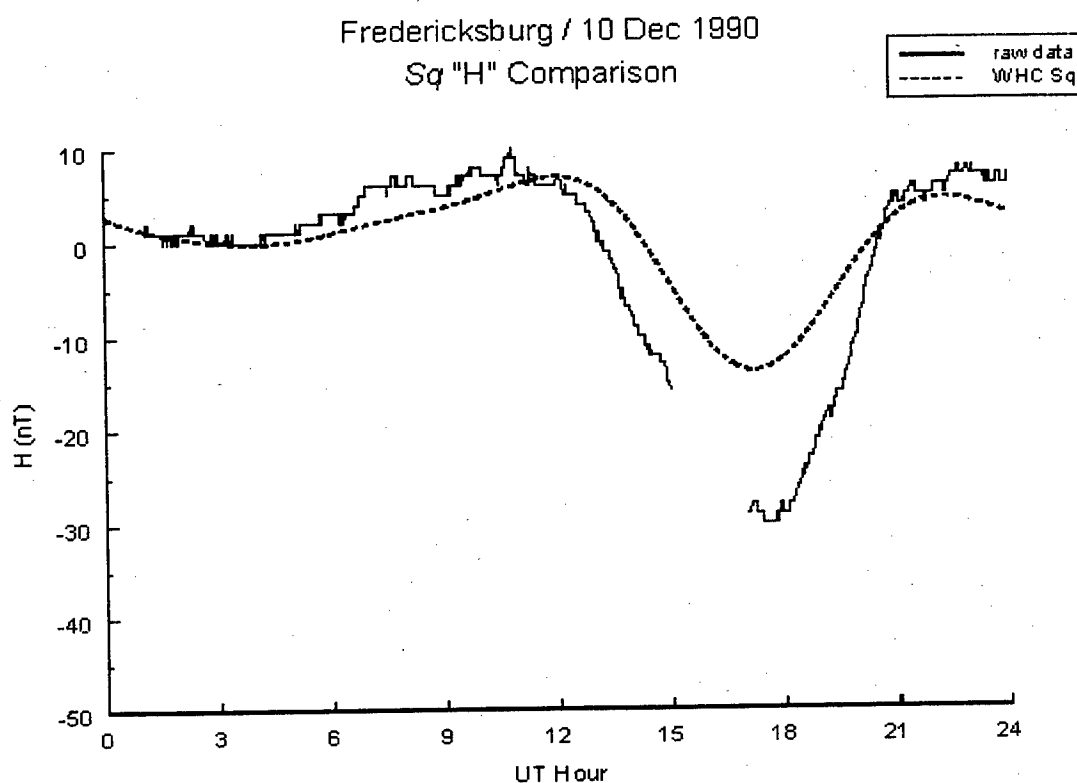
Fig. 25. Fredericksburg *Sq* "H" component comparison for 10 December 1990. The raw data is the solid line, and the dashed line is the Campbell *Sq* "H" curve for this date. This day was almost totally quiet (geomagnetically), with *K*=0 for seven of the eight 3-hour periods, and *K*=1 for the remaining period. Thus the raw data is representative of the actual *Sq* "H" trace for this day.). The gap in the raw curve indicates missing data, but the total amplitude of the trace is still evident. This reasoning also applies to the "D" component comparison in Figure 26.

Fredericksburg / 10 Dec 1990
Sq "D" Comparison
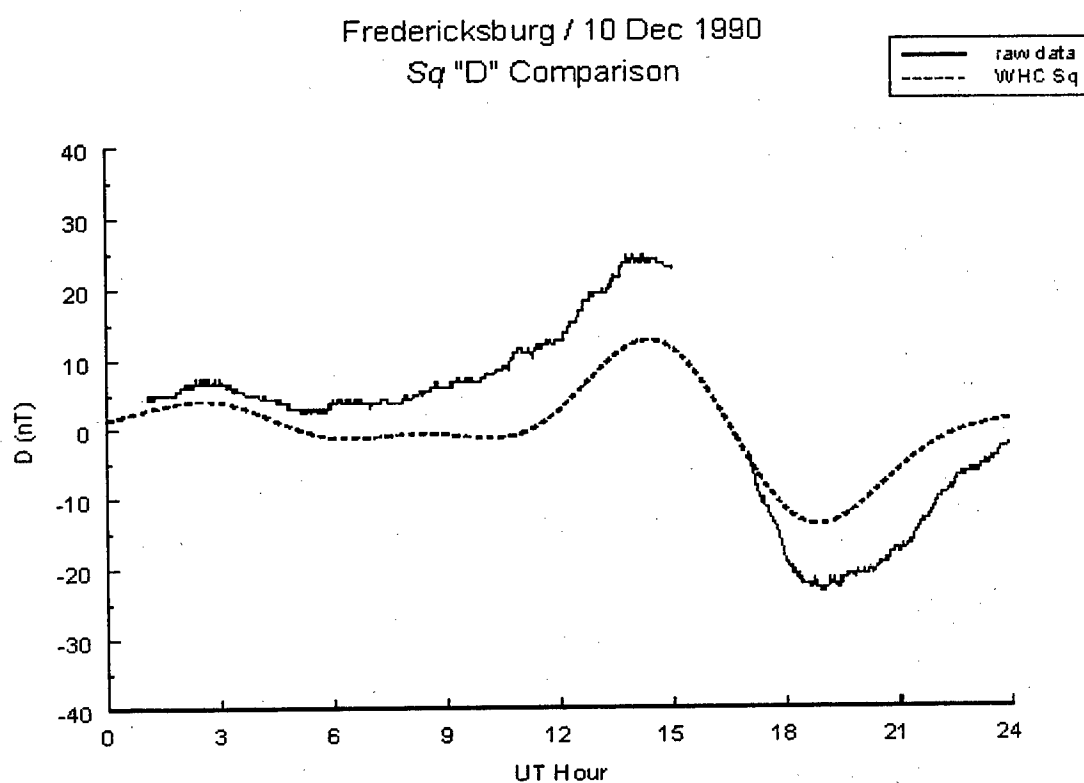
Fig. 26. Fredericksburg *Sq* "D" component comparison for 10 December 1990 (same format as Figure 25). Again, the gap in the raw curve indicates missing data, but the total amplitude of the trace is still evident.

These differences are due to the fact that our data set comes from an active portion of the solar cycle, whereas Campbell's algorithm is derived using data near solar cycle minimum. In fact, Campbell warns that the actual Sq curves during active years should be "somewhat different" from his set. Changes in peak electron density over the course of the solar cycle are easily as much as a factor of two to four—the same order-of-magnitude as the Sq differences observed for the two days discussed above. This correlation makes sense in that changes in density should be reflected linearly in conductivity changes, current changes, and thus magnetic field changes recorded at the surface. These remarks are consistent with Campbell and Matsushita (1982), as discussed in chapter 2.

These Sq differences also provided us a means to test the validity of one of our assumptions used to derive our Fredericksburg Sq—namely that, for a given month, the quiet days from any of the three years in our data set are basically equivalent. To accomplish this test, we created a complete Campbell Sq set corresponding to our raw magnetometer data set (details below). Then we used the Campbell Sq set in our index generating code to compute the 3-hour Fredericksburg "K-like" indices for 1990-1992. Next we repeated the index calculations using our derived Sq set. Finally, both sets of "K-like" indices were compared to the "official" '90-'92 K indices derived at Fredericksburg. These comparisons yielded only a 2% difference (see chapter 4, section 4.6) in accuracy between the Campbell Sq set and ours. Now recall that these two Sq sets represent the upper bound on solar cycle effects on Sq (solar minimum versus solar maximum), yet the difference in indices produced is minimal. Thus the difference in Sq

curves (for a given month) over only a 3-year portion of the solar cycle should produce an even smaller impact on index values, and our previous assumption is validated.

The results of our computation of the complete Campbell Sq set are as follows. We discovered that, for a given day of the year, the Campbell Sq amplitudes hardly changed as we varied the input year from 1990 to 1992. Furthermore, Sq amplitude changes across the days of a given month were found to be slow—as one would expect. Therefore we were able to create our Campbell Sq set by running the program for only one day in the middle of each month for the year 1991. We then had 12 "H" / "D" Campbell Sq sets, each one "valid" for a given month over all 3 years, 1990-1992.

4.4. The irregular variation

We now applied our Sq curves to the raw data to extract the irregular variation, or range, for a given integration period. The traditional integration time is three hours; however, we wrote our program to allow for any integration time. This flexibility would be necessary, of course, to create variations of the traditional 3-hour indices. The rest of this section describes the procedure to subtract Sq from the raw magnetometer data and determine the irregular variation for a given time period.

Recall from Figure 14 (chapter 3) as to how the Sq is subtracted from the raw data for both the "H" and "D" components. This subtraction gives us the irregular variations for "H" and "D" for a given period. The larger of these then determines the overall irregular variation, or range, for the period.

For the "H" component, our program subtracted Sq by forming the difference between the raw data value and the Sq value for each data point in the integration period (both the raw data and the Sq are at 1-minute resolution). The program searched for the largest

and smallest differences in the integration period, then subtracted the smallest

difference from the largest difference. This yielded the irregular variation in "H" for the

given integration period (recall that the index is "time-tagged" by the time at the *end* of

the period). Now of course the irregular variation must have the main-field contribution

subtracted out (the main-field "H" component was roughly 20,000 nT at Fredericksburg

during the time of our data set). However, in subtracting the smallest difference from the

largest difference, the main-field contribution is eliminated automatically.

Determining the "D" component irregular variation was more complicated. As

discussed in chapter 2, the "D" component is defined as the *angle* between "H" and the

X-axis (geographic north); the angle is positive when "H" is eastward of the X-axis.

However, to compare the "H" and "D" irregular variations for a given period, the "D"

variation must be expressed in dimensions of magnetic induction, not angular measure.

Again, chapter 2 explained the coordinate rotation to accomplish this transformation, and

equation 1 from that chapter gives D' (in nanoteslas) as a function of the total "H" (also

in nanoteslas), "D" (angular measure), and "D_{mean}" (angular measure). So unlike "H",

finding the declination component (D') of the irregular variation does involve

computation of the main-field baseline, namely, D_{mean}. To determine D_{mean}, we used the

International Geomagnetic Reference Field (IGRF) model located on the internet

webpage for the National Space Science Data Center (NSSDC). In running this program,

we discovered that D_{mean} only changes about 0.1 degree per year. We then decided it

would be accurate enough to use an average value of D_{mean} for each year in our data set.

Thus for 1990 we used a $\overline{D_{mean}} = -9.42°$, for 1991 we used $\overline{D_{mean}} = -9.51°$, and for 1992

we used $\overline{D_{mean}} = -9.60°$. The negative sign indicates that the Fredericksburg "H" baseline

vector points *west* of true north. Our *Sq* "D" curves were also derived using equation

· (1) along with the $\overline{D_{mean}}$ values listed above. The logic is that, on geomagnetically quiet

days, the only difference between *D* (the raw magnetometer values) and D_{mean} is due to

the *Sq* current system.

Now, for each data point in the integration period, equation (1) is used to compute the

total "D" value in nanoteslas. Then the corresponding *Sq* value is subtracted from this

total for each data point in the integration period. Finally, just as for "H", the smallest

"D" difference in the period is subtracted from the largest "D" difference, yielding the

"D" irregular variation for the period. This variation is then compared with the corres-

ponding largest "H" irregular variation. As stated at the beginning of this section, the

larger of these determines the overall irregular variation, or range, for the given

integration period.

Finally a note on missing data. We knew from our *Sq* derivation process that there

exist many missing data periods in our 3-year set. Obviously, we cannot calculate an

index when there are no data in a given period. However, occasionally there would be

missing data for only part of the integration period. To further complicate matters,

sometimes one component would be missing, but the other was present. In such cases

we tested to see if there were "enough" data points to compute an index. Our criterion

was that, if the total number of missing "H" *and* "D" data points in a period was equal to,

or greater than, the number of minutes in the integration period, then the index for that

period was not computed.

4.5. "Range-to-index" conversion

The final step in our index code was to convert the range values to the station K indices. The conversion procedure was described in chapter 3. As it turns out, Fredericksburg has the same $K=9$ lower limit (500 nT) as Niemegk, Germany. Thus we used the conversion chart shown in Table 1 from chapter 3. In addition, our code allows for a proportional scaling of this conversion table, a feature we used later in the research. In order not to confuse the indices produced by our code with the traditional K indices, we decided to call our index the n-hour (or n-minute, as the case may be) "JD" index, where n is the number of hours (or minutes) in the integration period. We adhered to this naming convention for the remainder of the research.

4.6. Program validation

To validate the code, we chose a 3-hour integration time (same as the traditional station K index), then ran the code for our 1990-1992 Fredericksburg raw magnetometer data set. There are 8,768 three-hour integration periods in this 3-year data set. Due to missing data, only 8,588 JD indices were computed—but this is still a statistically significant sample size. In addition, Figure 27 shows the frequency distribution of the official Fredericksburg K index during 1990-1992. As one can see, this period allowed us to test our JD index code under a wide variety of geomagnetic conditions. The code was run using five different Sq options:

1. Our manually derived set.

2. The "H" component of our derived set. Here we forced the code to use "H" only in determining the irregular variations.
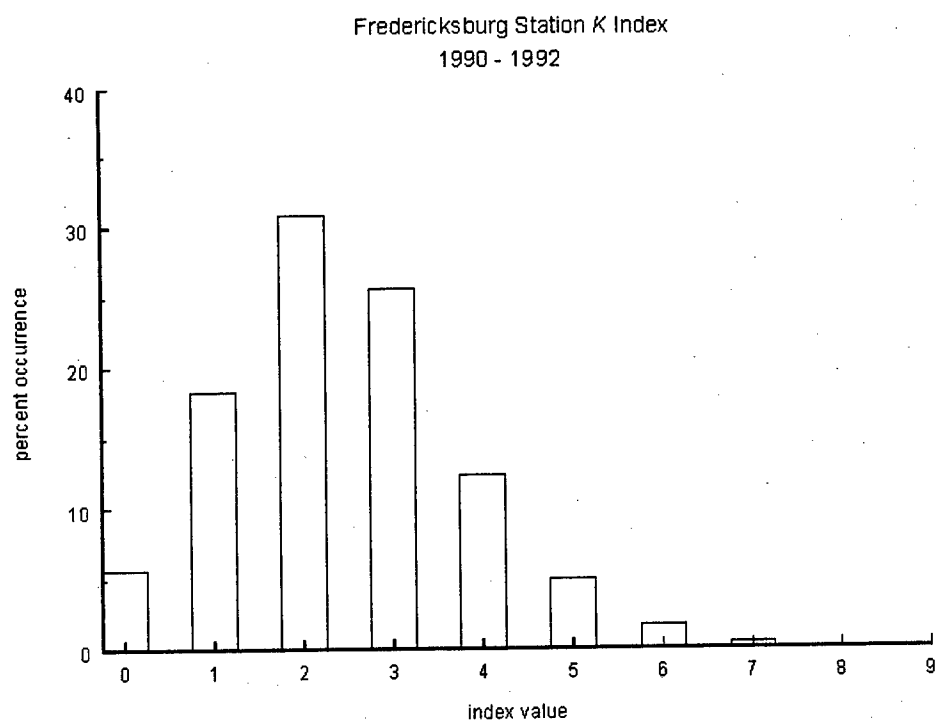
Fig. 27. Occurrence frequency of official 1990-1992 Fredericksburg 3-hour *K* indices.

3. The "D" component of our derived set. Here we forced the code to use "D" only in determining the irregular variations.

4. The *Campbell* [1989] set.

5. No *Sq*, i.e., *Sq* = 0.

For all five of these cases, the resulting 3-hour JD indices were compared to the corresponding official Fredericksburg station *K* indices; the results are shown in Table 7. In this table, the term "Data" refers to our *Sq* set derived from the magnetometer data. A "hit" means that the JD index was within ±1 index unit of the official Fredericksburg *K* index; a "miss" indicates the difference was larger than ±1 index unit. This criterion for comparison between official (hand-scaled) and computer-generated indices is standard in the literature. Using this criterion, our JD index code was 95% accurate when run with our derived *Sq* set. Now, of the 8,588 3-hour JD indices computed, the "H" irregular variation determined the JD index in 4,537 cases; "D" determined the index in the remaining 4,051 periods. This nearly even split in "H" versus "D" motivated us to repeat the run using two variations of our derived *Sq* set. First, we forced the code to use only the "H" component of our derived *Sq*; this run resulted in JD indices that were 93% accurate. For the "D" component only, we achieved 91% accuracy. If the "H"-only versus "D"-only accuracies had turned out quite different, it might have indicated a problem with our *Sq* set; however, the accuracies were similar. Next, we ran the code with the Campbell *Sq* set. The JD indices were 93% accurate when using the Campbell set—only a 2% difference from our derived *Sq* set. As mentioned earlier, this difference results from the fact that the Campbell *Sq* set is valid for solar minimum, and our data set is for solar maximum. Finally, in order to test the impact of using *some* form of *Sq* to

Table 7
"*JD*" code validation statistics

Sq Source	"Hits"	"Misses"	Accuracy (%)
Data	8143	445	95
Data (H only)	8016	572	93
Data (D only)	7809	779	91
Campbell *Sq*	7991	597	93
Sq = 0	7174	1414	84

compute these indices, we ran the code for *Sq* = 0, i.e., a "flat-line" *Sq*. As one would expect, the accuracy dropped significantly—down to 84%.

As a last validation item, we examined the 5% of "misses" resulting from the use of our derived *Sq* set. We did this primarily to ensure there were no undiscovered "bugs" in our code. Once we confirmed our code was working properly, we did not explore these cases further, except to note that, in all the cases, the official Fredericks-burg *K* indices were zero or one, whereas the JD indices indicated minor-to-moderate levels of activity. We concluded that these were "noise-level" deviations resulting from a variety of possible sources, such as minor imperfections in our method of deriving *Sq*, and maybe even some observer bias in computing the official indices at Fredericksburg. However, with a 95% accuracy rate, we concluded our JD index program was reproducing the official Fredericksburg *K* index well enough for us to use our code to produce variations of the traditional 3-hour index, analyze the physics, and have confidence in the results.

CHAPTER 5

COMPARISON OF *JD* AND *K* INDICES

5.1. Initial Work

Now that we had a reliable index-generating tool, our first goal was to compare the

traditional 3-hour index against *JD* indices with other integration times. To do this, we

used our *JD* index program to create "*K*-like" indices (from the 1990-1992

Fredericksburg data set) with the following integration times: 15 minutes, 30 minutes,

1 hour, 90 minutes, 2 hours, 3 hours, 4 hours, 6 hours, 8 hours, 12 hours, and 24 hours.

Then, as an initial comparison, we computed the arithmetic average *JD* index for each

integration time. One might question the validity of simple averaging of quasi-log index

values; however, such a practice occurs daily in the derivation of *Kp*. Therefore, we

considered this to be at least a "consistent" procedure in making a first comparison

among the different *JD* indices.

Our results, plotted in Figure 28, lead to the following observations. At the

conventional three hour time interval, the average *JD* index has a value of 2.68, which

compares reasonably with the 1990-1992 Fredericksburg station *K* average of 2.45.

However, at both shorter and longer time intervals, the average *JD* index changes

considerably. For shorter intervals the average index plummets, falling to an average

value of 1.7 for the 1-hour index, while at 15 minutes it is only 0.57. On the long side of

the spectrum, the increase is not quite as rapid, but still increases up to an average *JD* of

3.78 for a 12-hour interval. This immediately identifies one of the major problems in

altering the traditional 3-hour *K* index time interval. The quasi-log tables developed to

convert range-to-index are time interval sensitive. Within the scientific and space
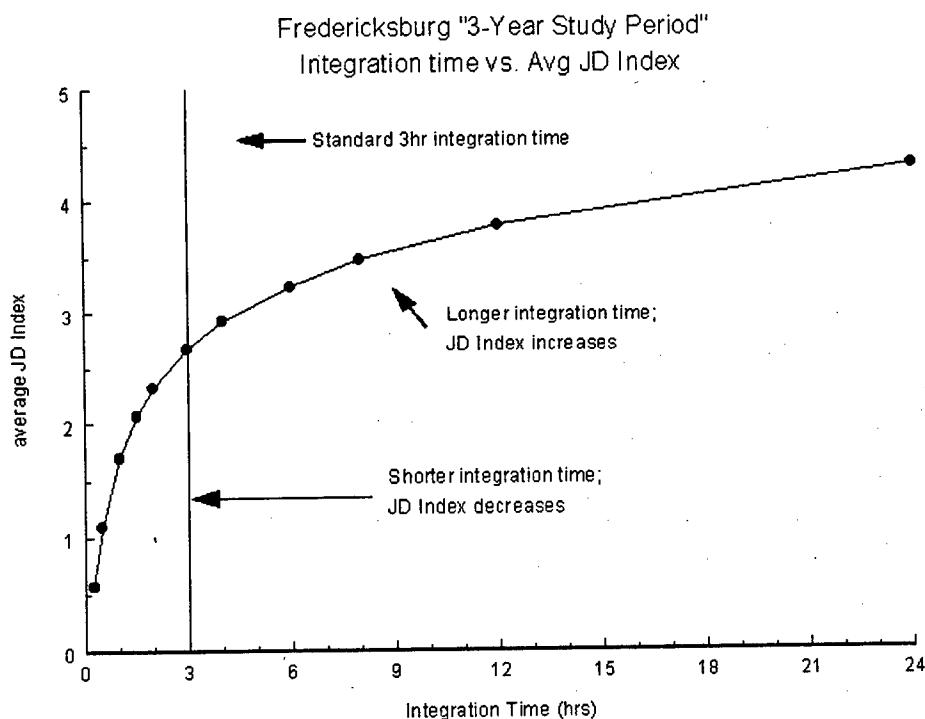
Fig. 28. Average JD index versus integration time. For each integration time, the average JD is the arithmetic mean of all indices computed from the 1990-1992 Fredericksburg data set. From this graph, one could estimate that most of the irregular magnetic variations in the 3-year sample have periods of about 6 hours or less.

weather forecast and application community there is an ongoing debate centered around the derivation and meaning of higher-time resolution "*K*-like" indices. For instance, ionospheric modelers are keenly interested in the development of such higher-time indices, since a 3-hour index can be rather coarse relative to ionospheric time constants. Thermospheric modelers, however, deal with slower time constants, and might be content with the traditional index. Figure 28 clearly shows one of the major hurdles that must be overcome in such a pursuit. For example, to create a 15-minute "*K*-like" station index where the frequency distribution is the same as the 3-hour index, one would have to revise the range-to-index conversion table. We further explore such a procedure in section 5.2.

The observed dependence of the average *JD* index on the time interval (as shown in Figure 28) can be better understood with the help of the following heuristic description. Consider a magnetic disturbance that exhibits its maximum variation over a period of three hours, say. Assume further that no disturbance exists outside this single "pulse". If the sampling window used to compute the index is much larger than the pulse width, and encompasses the pulse, then we get the same disturbance range value regardless of where we place the pulse within the window (recall that the maximum difference in "H" or "D" in the given time interval determines the disturbance range, and thus the index value). Now if we reduce the window size so it is too short to fully contain the pulse, then the disturbance range will depend on where we place the window relative to the pulse. However, in general, a decrease in window size (i.e., time interval) will result in a smaller range, and thus a lower index value. We can conclude that one (or both) of the following contributes to the observed behavior in Figure 28: (1) As the time interval

decreases, there are fewer disturbances with widths less than the given time interval;

(2) the mean disturbance amplitude decreases as the disturbance width decreases.

5.2. Index scale revision

As mentioned above, the concept of variable time interval "K-like" indices raises

many issues. One central question is whether our variable time JD indices are

"consistent" in some sense with the traditional 3-hour K index; such consistency would

be key if JD was ever to be used in place of K. To address this, we make use of Bartels'

assumption that we mentioned in chapter 3, namely, that K indices derived at different

magnetic latitudes have the same significance if the index frequency distributions are the

same (incidentally, Bartels also used this frequency distribution argument to eliminate

local time effects in the planetary index, Kp). In our study, we adapted this argument and

assumed that our Fredericksburg variable time indices would be "consistent" with the

Fredericksburg 3-hour K index if the frequency distributions are the same. We then

attempted to accomplish this in a very simple way: for a given time interval, we

multiplied the Niemegk range class limits (from chapter 3, Table 1) by a constant

proportionality factor until the average JD index (for the given time interval) equaled the

average 3-hour JD index (averages were computed for the entire 1990-1992 data set). We

applied this technique to the 15-minute, 1-hour, "sliding" 3-hour, and 12-hour JD

indices.

Figure 29 shows the resulting "normalized" JD index frequency distributions versus

the 3-hour K index distribution for Fredericksburg. Each panel also shows the

proportionality factor we applied to the Niemegk scale to produce the normalized
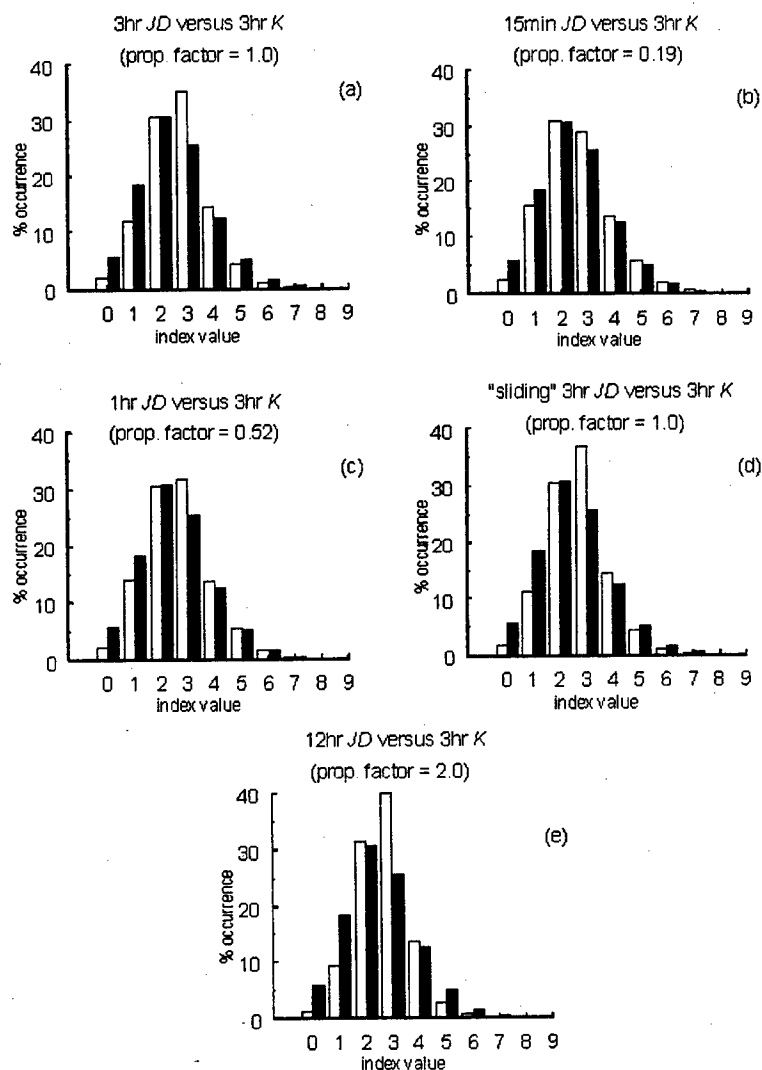
Fig. 29. Frequency distributions for the official Fredericksburg 3-hour K index (1990-1992) and the corresponding normalized variable time JD indices. Each panel compares the K distribution (black bars) with one of the JD distributions (white bars): panel (a) is the 3-hour JD distribution, panel (b) is the 15-minute JD distribution, panel (c) is the 1-hour JD distribution, panel (d) is the "sliding" 3-hour JD distribution, and panel (e) is the 12-hour JD distribution. The proportionality factor used to normalize the JD indices is shown in each panel. The K versus JD distribution agreement shown in panels (b)-(e) is at least as good as the 3-hour K versus JD agreement shown in panel (a); the normalized 15-minute JD distribution gives the best agreement with the K index.

distribution. Panel (a) of Figure 29 is for the 3-hour JD index, and reflects the differences already discussed (see chapter 4, section 4.6) between our code and the official station K index. In general, however, the agreement between the two distributions is quite good. Similar agreement is found between the K index distribution and the normalized variable time JD distributions as shown in panels (b) through (e) of Figure 29. In general, the differences in these panels are within the bounds of the recognized differences between our JD algorithm and the official K index (as seen in panel (a)). Notice that the "sliding" 3-hour distribution in panel (d) is almost identical to the "standard" 3-hour JD results, and the normalized 1-hour statistics in panel (c) are only slightly dissimilar to the 3-hour distributions. The normalized 15-minute JD index clearly produces the best match to the official K index distribution as shown in panel (b).

At this point, one might ask why we normalized the variable time JD indices to the 3-hour JD index instead of the 3-hour K index; after all, the comparisons in Figure 29 are all made against the 3-hour K index. We did this because, as Figure 29(a) shows, the JD distribution is not *identical* to the official K index distribution. Therefore, we felt it would be more consistent to normalize to the 3-hour JD index, then make comparisons with the K index distribution.

Finally, we wanted to verify that the good agreement of distribution functions shown in Figure 29 is not coincidental; i.e., we wanted to ensure the K and normalized JD time series follow each other (in time) reasonably well. To do this we simply computed the difference between the K index and the normalized variable time JD indices at each time step. Since the two series have different time intervals between data points, e.g., 3 hours versus 15 minutes, 1 hour, and 12 hours, we had to "fill in" the coarse series to provide

data points to the necessary resolution (so that differences could be computed at all those times). For example, consider differences between the 3-hour K index and the 15-minute JD index. If the 0300 UT K index is a 2, then all the 15-minute JD values between 0015 UT and 0300 UT are subtracted from the $K = 2$ value.

Now if the two time series are well correlated, one would expect the resulting difference histogram to be peaked at—and symmetric about—the zero difference. Figure 30 shows the difference histograms corresponding to the Figure 29 distributions. In all five Figure 30 panels, the differences are computed as K index minus normalized JD index. Panel (a) is the 3-hour JD difference histogram. Here, the peak does occur at zero difference, but the histogram is somewhat asymmetric. However, as stated earlier, this histogram represents a 95% "hit" rate, and thus the two indices are well correlated in time. The remaining four panels show the same zero difference peak and asymmetry pattern as panel (a), though the histograms get somewhat "flatter" when high-time resolution indices are compared with coarser indices. We conclude that the normalized variable time JD indices are well correlated in time with the 3-hour K index, and thus the distribution results in Figure 29 are not coincidence.

Thus, using a very simple technique, we succeeded in creating normalized Fredericks-burg variable time JD indices with frequency distributions quite similar to the official 3-hour Fredericksburg K index. Along with this, though, some cautions must be observed. For instance, the proportionality factor used to adjust the Niemegk scale certainly depends on the time interval used to compute it (3 years in our case). On the other hand, these same remarks apply to the derivation of the widely used Kp index. As mentioned earlier in this section, local time effects are eliminated from the different station K
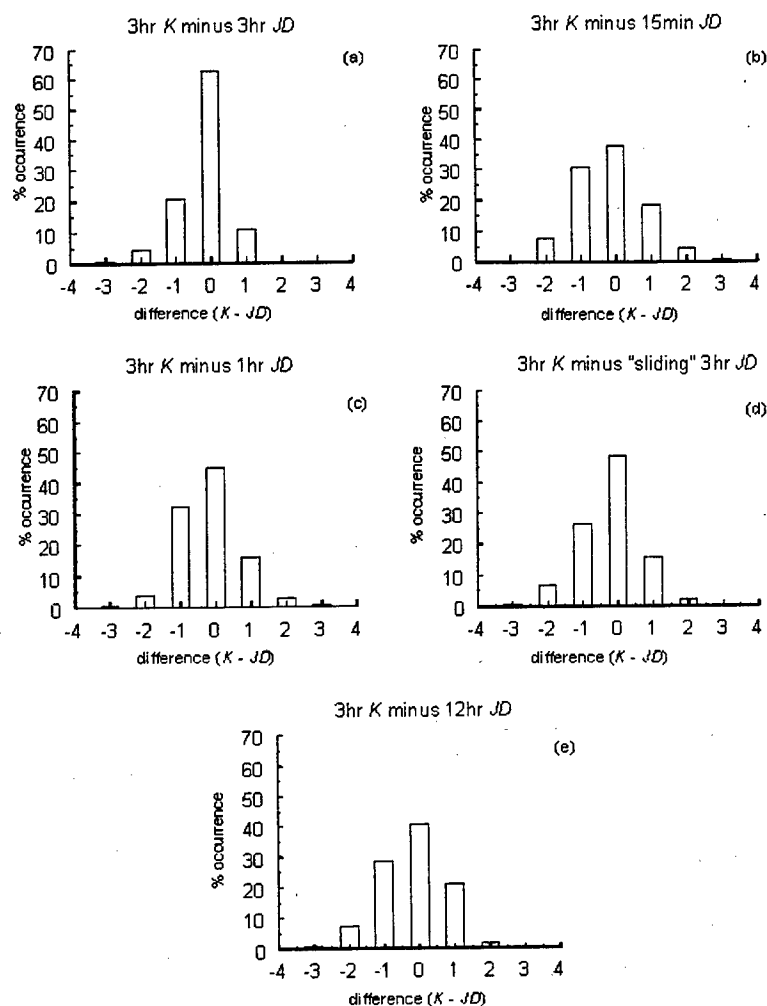
Fig. 30. The K index–JD (normalized) index difference histograms (computed from 1990-1992 data set). Each panel corresponds to the same panel from Figure 29. Panel (a), which shows the K minus normalized 3-hour JD index histogram, shows a peak at the zero difference, and has a somewhat asymmetric shape. We conclude that these two index time series are well correlated (see text). The remaining panels exhibit similar characteristics, and we conclude that the other normalized variable time JD indices are also well correlated in time with the 3-hour Fredericksburg K index. This means that the similar K versus JD distributions shown in Figure 29 is not coincidental.

indices by standardizing the frequency distributions (the resulting standardized index values are labeled *Ks*). The conversion tables used to convert *K* to *Ks* were derived using data from 1943-1948 (Menvielle and Berthelier, 1991), and would most likely be different if computed from a different data set. Also, as discussed in section 3.3, each *Kp* value is the result of an arithmetic average of station *Ks* values.

Finally, use of normalized, variable time indices would surely raise a focused discussion on whether the physics of geomagnetic disturbances is the same for time scales ranging from 15 minutes to several hours. Based on the very sensitive nature of the average *JD* index on the time interval (shown in Figure 28) and hence the sensitivity of proportionality (normalization) factors shown in Figure 29, it is critical that the community clearly understands and addresses this question before adopting variable time "*K*-like" indices.

5.3. Storm cases

Another method of comparing "*K*-like" indices with different integration periods is to examine how well they resolve the timing and duration of geomagnetic disturbances. We chose four Fredericksburg cases to analyze: 16 February 1990 (winter), 11 April 1990 (spring), 28 July 1990 (summer), and 28 October 1991 (fall). The comparison involved the behavior of the standard 3-hour index versus two other indices that have been discussed qualitatively within the Department of Defense space science community: the 15-minute index, and the "sliding" 3-hour index. The latter index has a 3-hour integration window which "slides" in 15-minute steps. Thus the index is calculated for the 3-hour intervals ending at 0000 UT, 0015 UT, 0030 UT, and so on. It has been

previously suggested that such an index might have advantages over the standard 3-hour index in identifying the timing of magnetic disturbances.

Figures 31-34 show the results of our storm-time analyses. Each figure has four panels. The top panel shows the Fredericksburg "irregular" magnetic variation (defined below) in nanoteslas. The component displayed (either "H" or "D") is the one that determined the storm-time 3-hour JD indices in each case. By "irregular" variation we mean the total component value less the contributions of both Sq and the main field. The bottom three panels in each figure show the 3-hour, 15-minute, and "sliding" 3-hour JD indices for the given UT day, respectively. All four panels share the same time axis, with tic marks shown every 3 hours. Again, we used the same range-to-index quasi-log scale for the variable time interval JD indices as is used for the conventional Fredericksburg 3-hour K index.

Figure 31 shows the 16 February 1990 magnetic disturbance, which extended from 0000 UT to approximately 0630 UT. The most significant activity begins with a prominent "spike" at about 0300 UT, and is followed by two "depression" features at 0430 UT and 0600 UT. Notice that the 3-hour JD index does not reflect the leading edge of this increased activity until 0600 UT—three hours late. This "lag," of course, is caused by the definition of the index. The "sliding" 3-hour JD index (bottom panel) identifies the onset 1.75 hours earlier. Neither index resolves individual features within the period; however, the 15-minute index *does* resolve the timing, duration, and relative magnitudes of the 0300 UT peak and the two depressions that follow.

Figure 32 shows the 11 April, 1990 disturbance; like Figure 31, this is basically a midnight-dawn disturbance. Notice the large storm features at 0100 UT and 0545 UT.
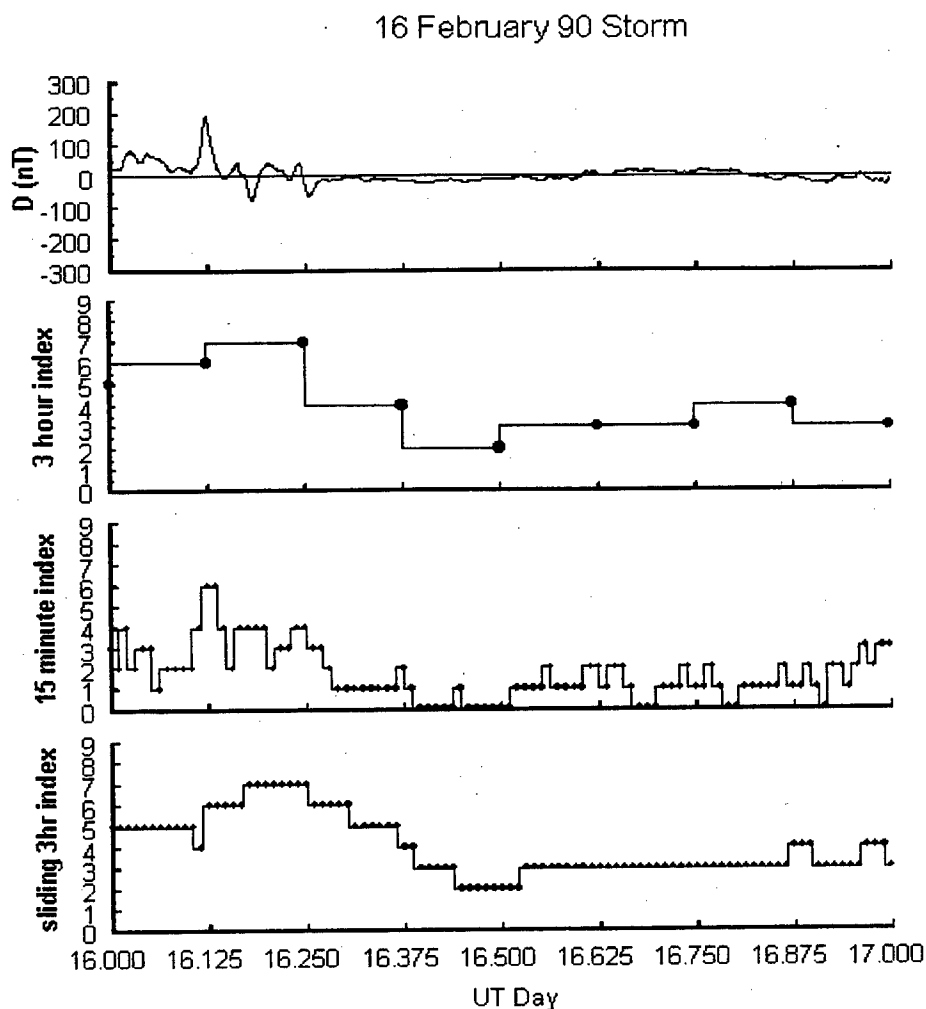
Fig. 31. JD index case study for the geomagnetic storm of 16 February 1990. The top panel shows the irregular "D" component trace for this UT day (see text for explanation). The other panels show the corresponding JD indices for three different integration times: 3 hours, 15 minutes, and "sliding" 3-hour window (computed every 15 minutes). All four plots share a common time axis, with tick marks every 3 hours. The 3-hour index is about 3 hours late in identifying the largest storm peak (located at about 0300 UT). The sliding 3-hour index is an hour late in identifying the same peak, but extends the storm several hours after activity levels have dropped. The 15-minute index gives the most accurate resolution of storm features.

The 3-hour *JD* index reflects the overall disturbance level, but as before does not resolve individual features within the period. In this case, the "sliding" 3-hour *JD* index does resolve both disturbance features, and accurately indicates the start times. However, this index extends the features too long—roughly 2 hours in each case. The 15-minute *JD* index, as in Figure 31, does the best job of resolving the features.

The storm period of 28 July 1990 is shown in Figure 33. There is a single "spike" of interest at about 0630 UT. The 3-hour index identifies this feature as one would expect. The "sliding" 3-hour index reflects the spike at 0845 UT—only 15 minutes earlier than the "normal" 3-hour index, and two hours after the spike occurs. Once again, the 15-minute *JD* index handles the spike well.

Figure 34 shows another single disturbance feature at about 1540 UT on 28 October 1991. Here, both the 15-minute and "sliding" 3-hour *JD* indices accurately indicate the start time of the spike, but the sliding index persists the feature about 1.5 hours too long.

Finally, we explored the possibility that some of these 3-hour index timing errors could be due to the fact that the index time is associated with the end of the integration window (as opposed to the midpoint). It is true that assigning the index time at the midpoint would reduce the maximum timing error by a factor of two (3 hours versus 1.5 hours), and improve the long-term statistics of 3-hour index timing errors. However, this would not eliminate timing problems on a case-by-case basis. For example, in Figure 31, use of the midpoint for index timing would still cause the 3-hour *JD* index to identify the disturbance period leading edge, and subsequent storm decay, 1.5 hours after-the-fact. Such an index time-tag change would also fail to correct the deficiencies we identified in the "sliding" 3-hour *JD* indices. Finally, from a practical point-of-view, the near real-
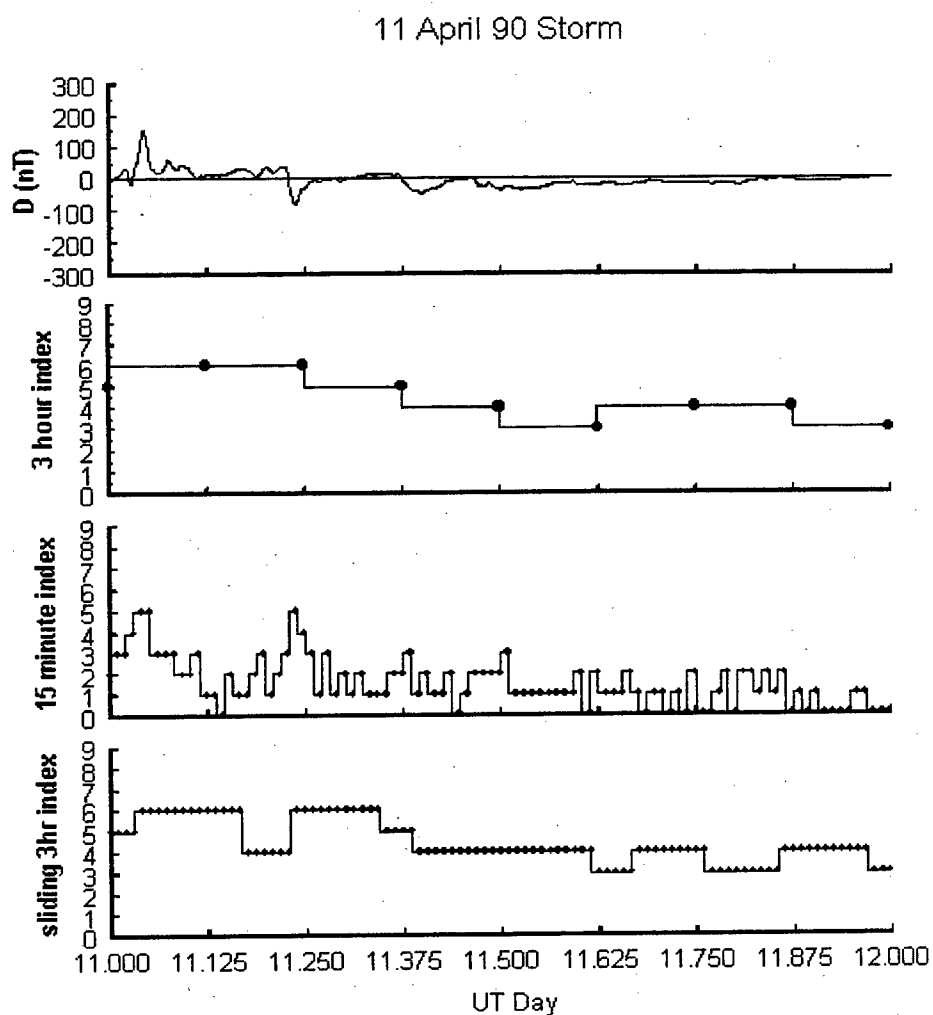
Fig. 32. JD index case study for the geomagnetic storm of 11 April 1990 (same format as Figure 31). Here, the 3-hour index reflects the "leading" (0100 UT) storm peak about two hours late, and remains at JD = 6 through the second major "tremor" at about 0530 UT. The 3-hour JD index decreases steadily thereafter. Both the 15-minute and sliding 3-hour indices resolve the start times of these two geomagnetic features adequately; however, as in Figure 31, the sliding JD index extends the features for 1-2 hours too long.

28 July 90 Storm
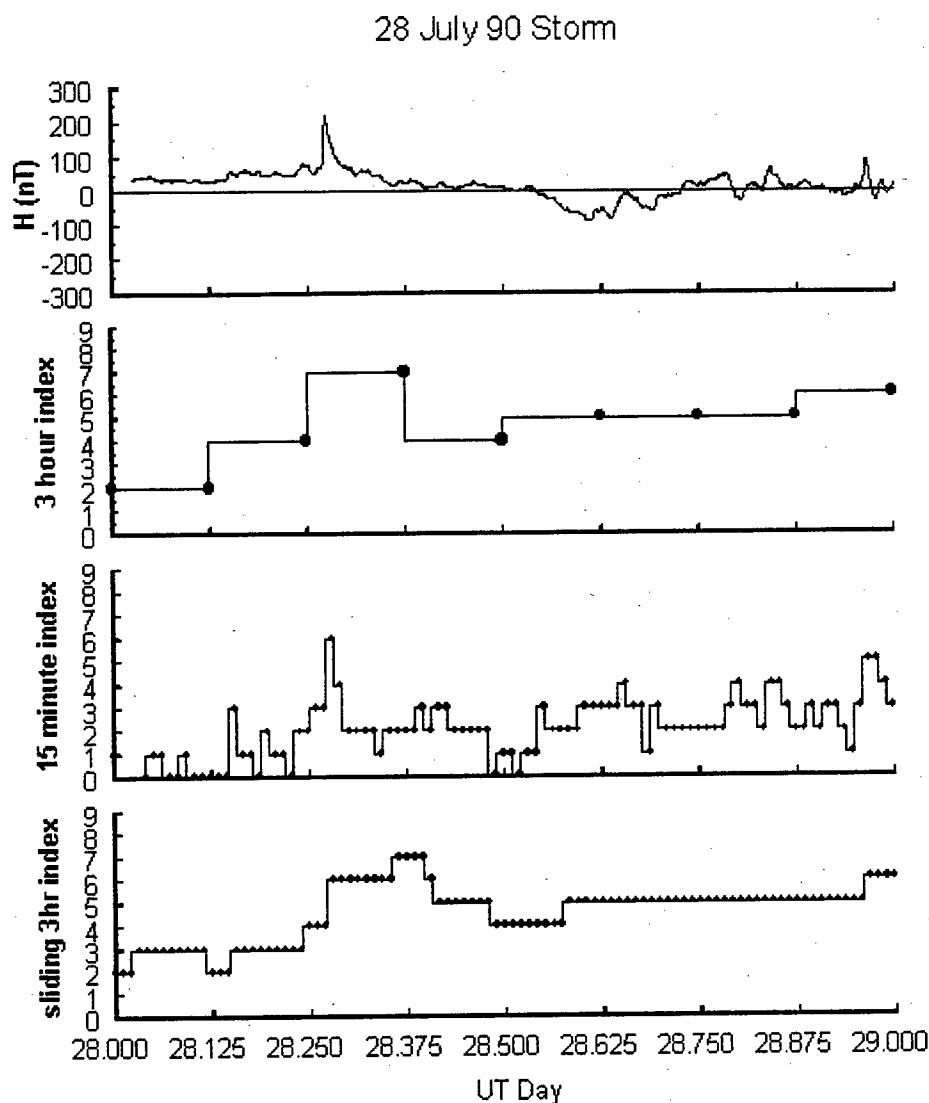
Fig. 33. JD index case study for the geomagnetic storm of 28 July 1990 (same format as previous two figures). In this case, the "H" irregular component determines the 3-hour JD index. As before, all three indices reflect the 0630 UT storm peak; the 3-hour index is about 2.5 hours late in identifying the feature, and the sliding 3-hour index resolves it only 15 minutes earlier. The 15-minute index is again best at both the timing and duration of the feature.
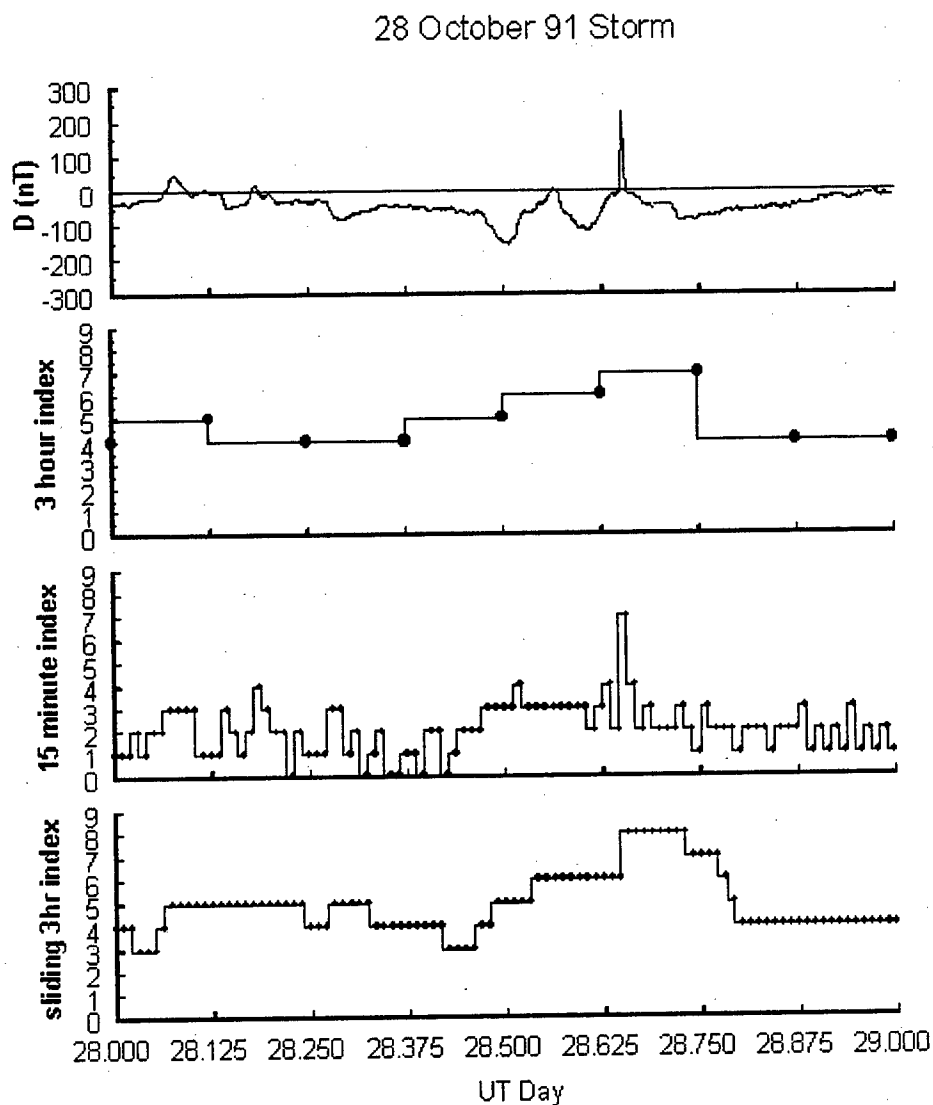
28 October 91 Storm

Fig. 34. JD index case study for the geomagnetic storm of 28 October 1991 (same format as previous three figures). The storm peak here is at about 1545 UT. Here again, both 15-minute and sliding 3-hour indices resolve the peak start time correctly, but the sliding JD index extends the feature over an hour too long.

time evaluation of an index can only be made after data acquisition, and hence for

operational purposes the end time of an interval is logical to use as the index time tag.

CHAPTER 6

TDIM SENSITIVITY STUDY USING OUR *JD* INDEX

6.1. Introduction

The scientific and space weather forecast and application communities have long

debated whether variable time interval "*K*-like" geomagnetic indices are appropriate to

drive today's state-of-the-art space weather models. Many ideas have been proposed, but

few, if any, have been thoroughly explored. However, based on the results of the

previous chapter, the stage was set for us to investigate the "suitability" of such high-

time resolution indices as proxies for the dynamics of ionospheric drivers. We decided

to use our *JD* indices to drive the auroral, convection, neutral atmosphere, and neutral

wind inputs to the Utah State University (USU) Time-Dependent Ionospheric Model

(TDIM). By then looking at the response of output fields such as electron density, we

could examine the correlation between high-latitude ionospheric dynamics and short-

term geomagnetic variations. In particular, such a study would determine the ionospheric

sensitivity to higher-time resolution indices and consequently assess the relevance of

such indices from an ionospheric perspective. However, before accomplishing such

work, we had to address the issue of range-to-index scaling of high-time resolution "*K*-

like" indices such that they are suitable for use in models designed for traditional 3-hour

indices.

In chapter 5 we used a simple adjustment to the Fredericksburg range-to-index

conversion scale (which is the same one used at Niemegk, Germany), and obtained

comparable frequency distributions between our "normalized" variable time indices and

the official 3-hour Fredericksburg *K* indices for 1990-1992. Again, the goal of

producing equivalent frequency distributions is the same strategy used to eliminate

latitude and local time / seasonal biases among the *Kp* network stations (Mayaud, 1980;

Menvielle and Berthelier, 1991). Thus, we decided it would be reasonable to consider

testing our variable time interval *JD* indices in applications where 3-hour "*K*-like"

indices have been used. The advantage of using higher-time resolution indices is clear,

since the ionosphere is oftentimes known to change on time scales significantly shorter

than the time resolution of the 3-hour *K* index (e.g., auroral electrojet variations during a

substorm).

6.2. TDIM sensitivity study

Ultimately, one would like to quantify the influence of short-term geomagnetic

variability on the ionosphere. Toward that goal, this chapter focuses on high-latitude *F*-

region peak electron density, or NmF2, values generated by the Utah State University

(USU) Time-Dependent Ionospheric Model (TDIM). The TDIM was initially developed

as a mid-latitude, multi-ion (NO^+, O_2^+, N_2^+, and O^+) model by Schunk and Walker

(1973). The time-dependent ion continuity and momentum equations were solved as a

function of altitude for a corotating plasma flux tube including diurnal variations and all

relevant *E*- and *F*-region processes. This model was extended to include high-latitude

effects due to convection electric fields and particle precipitation by Schunk et al. (1975,

1976). A simplified ion energy equation was also added, which was based on the

assumption that local heating and cooling processes dominate (valid below 500 km).

Flux tubes of plasma were followed as they moved in response to the convection electric

fields. The addition of plasma convection and particle precipitation models is described by Sojka et al. (1981a, b). Schunk and Sojka (1982) extended the ionospheric model to include ion thermal conduction and diffusion thermal heat flow. Also, the electron energy equation was included by Schunk et al. (1986), and consequently, the electron temperature is now rigorously calculated at all altitudes. The theoretical development of the TDIM is described by Schunk (1988), while comparisons with observations are discussed by Sojka (1989).

In addition to the physical processes built into the model, the TDIM requires several inputs. The magnetospheric inputs for the TDIM are the auroral precipitation and convection electric field. Typically, the auroral electron precipitation is obtained from the Hardy et al. (1987) model, and the convection is obtained from the Heppner and Maynard (1987) models. The MSIS-86 model is used to represent the neutral atmosphere (Hedin, 1987), while the neutral wind is represented by the Hedin et al. (1991) horizontal wind model (HWM) 90.

Each of these TDIM inputs, or "drivers," uses planetary "K-like" indices to help determine their output. The convection and auroral precipitation drivers use Kp directly, whereas MSIS and HWM use ap (the quasi anti-logarithm of Kp; see footnote on page 1). This flow of information through the TDIM, which finally results in an ionospheric simulation, is shown in Figure 35.

In section 6.2.2.1 we address the issue of how best to apply our variable time JD indices to these drivers. First we must discuss an issue regarding planetary versus single-station "K-like" indices. Our previous work has involved the development of a *single-*
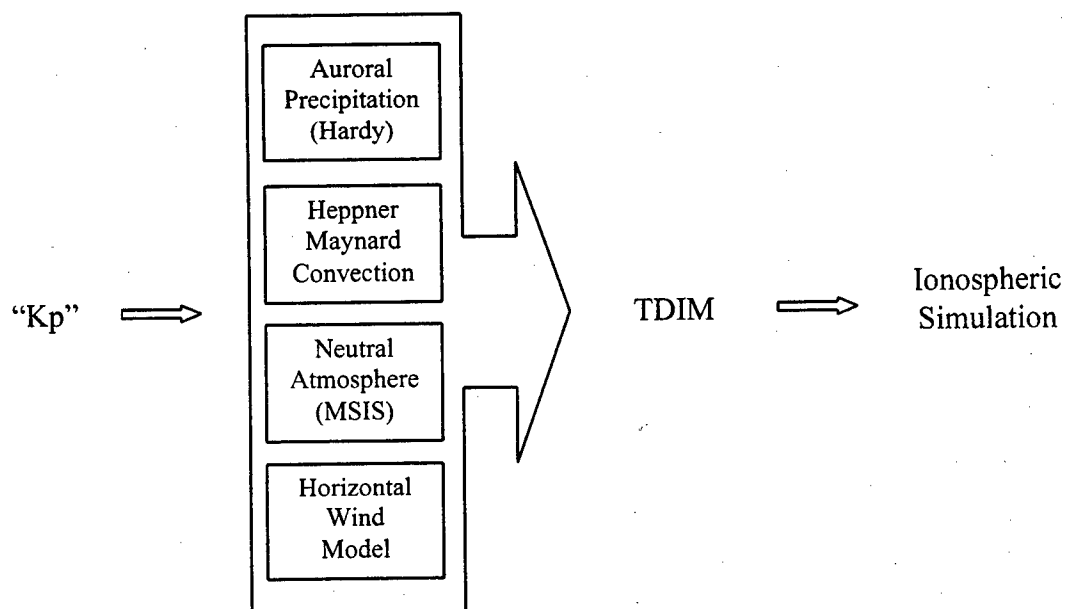
Fig. 35. *Kp* use in TDIM simulations. The index is input to the four models shown in boxes, the output of which helps drive the TDIM to produce an ionospheric simulation. In our sensitivity study, we used our Fredericksburg *JD* index (described in Della-Rose, et al., 1999) as a *Kp* "proxy" (see text for explanation).

station (Fredericksburg, Virginia) variable time interval *JD* index, and this is the index

used for our TDIM sensitivity study. However, as stated above, the TDIM drivers shown

in Figure 35 require a *planetary* index. This mismatch obviously requires justification.

The goal of our TDIM sensitivity study is *not* to produce "real" simulations that could be

compared with actual ionospheric observations. Instead, we wish to discover how the

high-latitude ionosphere would respond if the planetary *JD* index time series exhibited

the same behavior as our Fredericksburg *JD* time series. We make no claim that a

single-station index could replace a planetary index for "real-world" ionospheric

modeling.

The procedures and results for this study are described in subsequent sections.

6.2.1. Initial work

6.2.1.1. Description

Our first TDIM runs in this study centered on a large magnetic disturbance, shown in

Figure 36, that occurred at Fredericksburg on 28 July, 1990. It is important to keep in

mind we are using Fredericksburg "*K*-like" indices as a surrogate planetary index. The

idea was then to drive the TDIM with the 3-hour *JD* index, then repeat the run using the

variable time interval *JD* index, and finally compare the high-latitude NmF2 values

between the two runs (for a given location). We chose a magnetically disturbed period in

an attempt to maximize the density differences.

Next we had to select a time interval for the "normalized" *JD* index. Drawing on our

1999 paper, we chose 15 minutes as our time interval because the resulting index did an

excellent job of resolving the timing and duration of the 28 July 1990 Fredericksburg

Fredericksburg / 28 July 1990
3-hour JD vs. 15-min JD
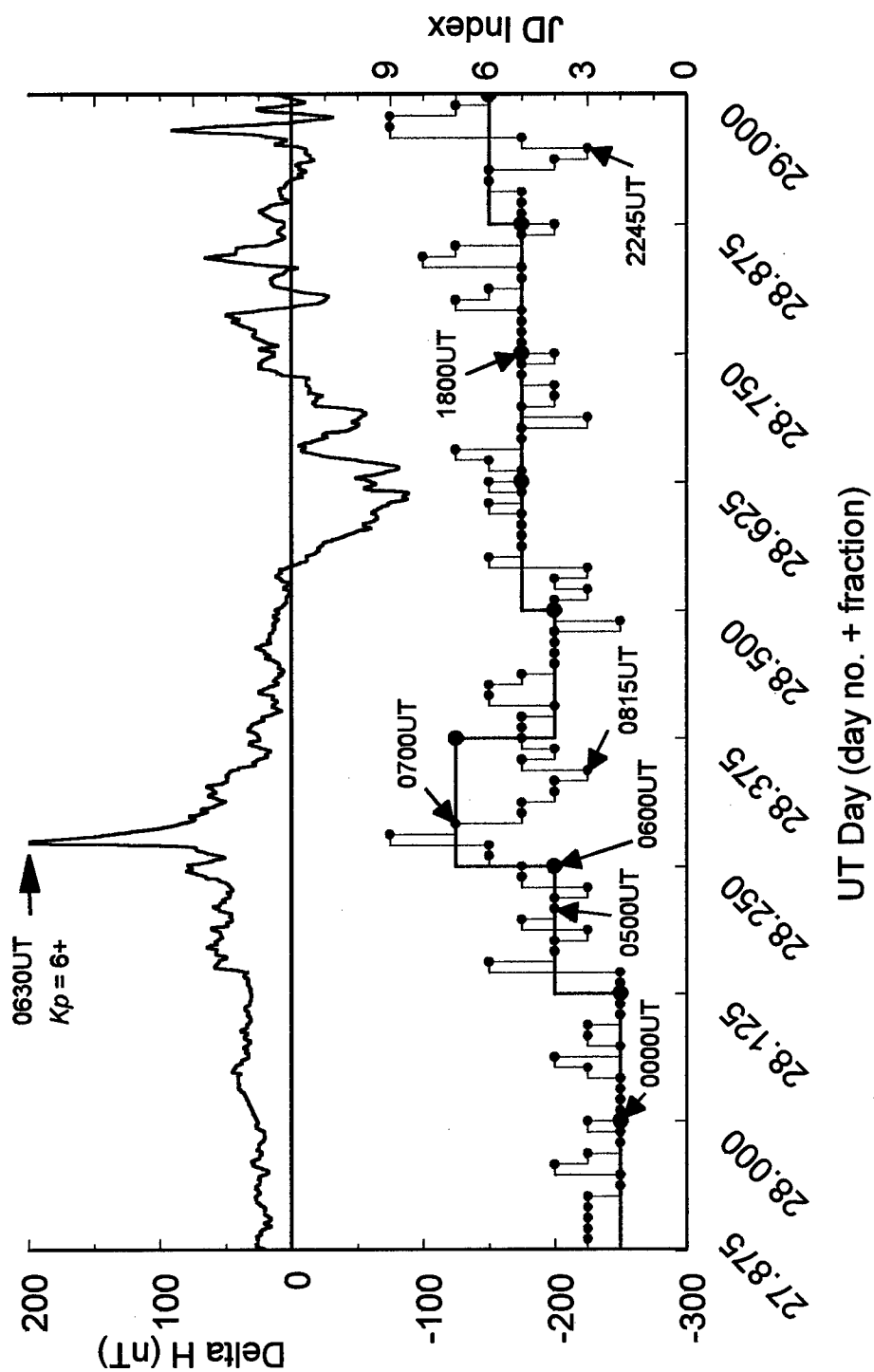
magnetic disturbance feature, as shown in Figure 36. In addition, 15 minutes is more in line with high-latitude ionospheric time constants than the traditional 3-hour interval.

Now the date of our chosen magnetic disturbance is only about one year after solar maximum, a fact we hoped would enhance the NmF2 differences in our study. In addition, as an artificial measure to encourage density differences, we adjusted the input date so the TDIM would use winter solstice solar production and terminator location.

We set the TDIM to compute densities at each grid point between 50 and 90 degrees magnetic latitude at a resolution of 1.8° × 1.8° (a total of 1,484 grid points). Initially, however, we did not analyze the results at every grid point. In fact, we chose just three locations we felt would be geomagnetically "active": a point near magnetic noon, one near dusk (1800 MLT), and a third near the Harang discontinuity. These locations are illustrated in Figure 37(a), superimposed on the Heppner-Maynard "A" convection pattern. Figure 37 also shows the "BC" and "DE" patterns; all three convection patterns were utilized in our study.

Now, referring back to Figure 36, notice the large magnetic "spike" at about 0630 UT on 28 July 1990. Using all the specifications described in this section, we ran the TDIM at two times prior to the spike—0500 UT and 0600 UT—and a third time just after the spike—0700 UT. The results from these runs are discussed in the next section.

6.2.1.2. Initial results

For a given location (noon, dusk, or Harang; see Figure 37a), UT (0500, 0600, and 0700), and convection pattern type ("A", "BC", or "DE"), we compared NmF2 values
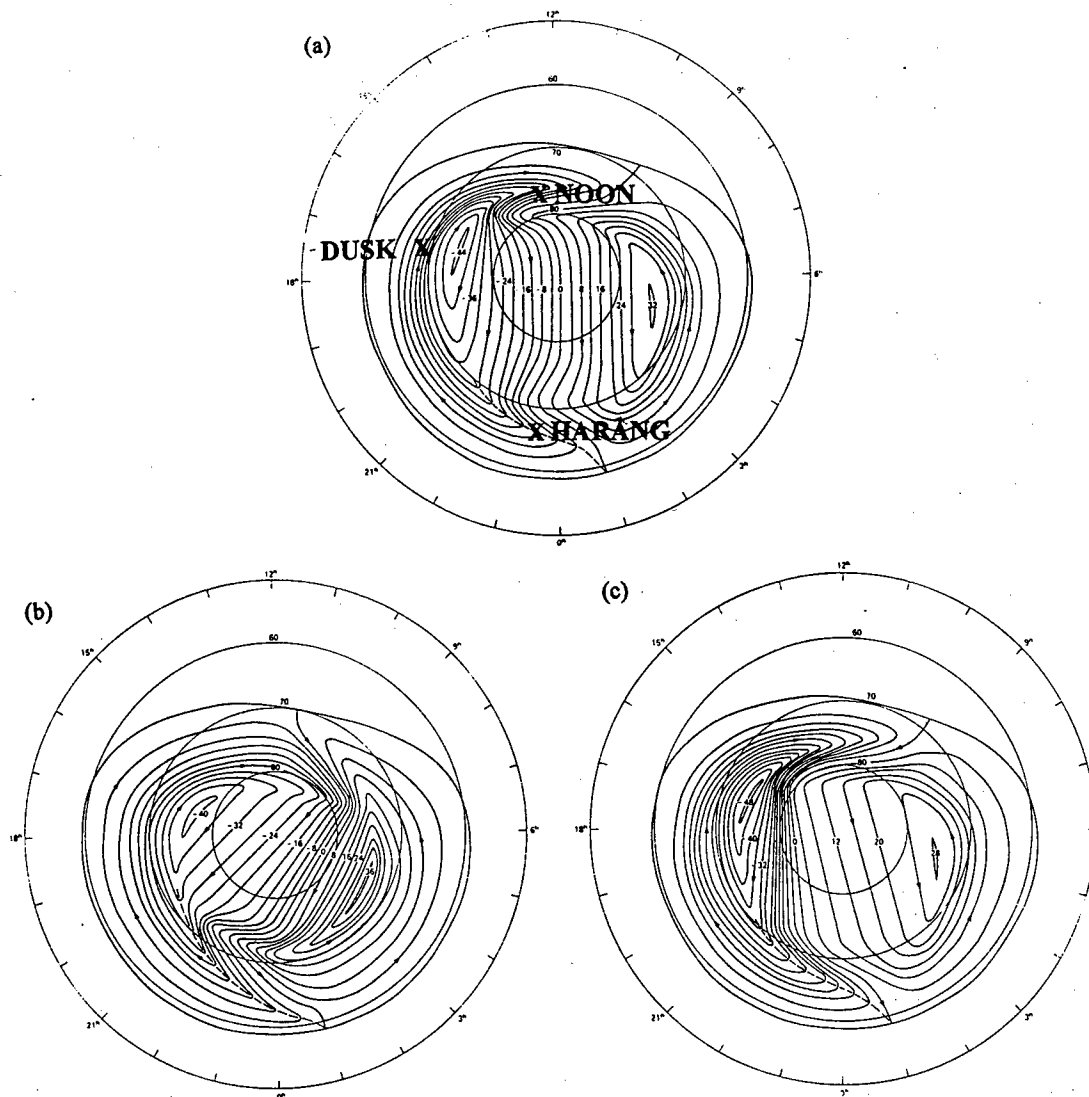
Fig. 37. The Heppner-Maynard convection patterns used in our TDIM simulations: (a) is the "A" pattern showing the three locations used in the initial part of our study, (b) is the "BC" pattern, and (c) is the "DE" pattern. The contours shown are at 4kV intervals (in the TDIM, pattern strengths are determined using an empirical relationship between Kp and cross-cap potential drop). These plots are taken from Heppner and Maynard (1987).

from the TDIM driven by the 3-hour *JD* index versus the TDIM driven by the 15-minute *JD* index. Most of the NmF2 differences had magnitudes of 10% or less; the maximum difference found among the 27 computed differences (27 = 3 locations × 3 convection patterns × 3 UT times) was 23%. Again, all these differences were computed within a given convection pattern type (i.e., holding the interplanetary magnetic field, or IMF, fixed).

Next we examined NmF2 differences due to IMF changes, holding the geomagnetic index "driver" fixed. We felt that such a comparison would help quantify the relative importance of using variable time interval "*K*-like" indices in ionospheric modeling. We limited our analysis to the noon location, since the average magnitude of the noon NmF2 differences computed in the first set of comparisons was comparable to the maximum difference found. Thus, using the TDIM driven by the 3-hour index, and for each of the three aforementioned UT times, we computed the magnitudes of the NmF2 differences for the "A" versus "BC" patterns, the "A" versus "DE" patterns, and finally the "BC" versus "DE" patterns. We then repeated the comparisons using the 15-minute index to drive the TDIM. The maximum difference magnitudes found in each case are shown in Table 8. Notice that, for the "A" versus "BC" and "BC" versus "DE" cases (and for both index time intervals), the high-latitude NmF2 differences resulting from varying the IMF are greater than a factor of two—over four times larger than the maximum difference found earlier when the IMF was fixed but the TDIM index "driver" was varied. Now the NmF2 differences decrease for the "A" versus "DE" case, but this is still consistent with the finding above, since both "A" and "DE" patterns correspond to IMF $B_y < 0$ ("A" is weakly negative, "DE" is strongly negative).

Table 8
Maximum NmF2 differences/noon location

	"A" vs. "BC"	"A" vs. "DE"	"BC" vs. "DE"
15 min JD	factor of 2.3	45%	factor of 2.2
3 hr JD	factor of 2.2	15%	factor of 2.1

These initial results were presented by Della-Rose et al. (1998) and suggest that, for accurate high-latitude F-region modeling in an operational environment, real-time IMF data are more important than the time resolution of the geomagnetic index "driver." However, even though this preliminary finding is interesting, the sample size was too small to be statistically significant. The required further study is the subject of the remainder of this article.

6.2.2. Main study

In the main phase of our sensitivity study, we continued with the high-latitude NmF2 comparisons for 28 July 1990 (using the same procedure as described in section 6.2.1.1). However, we modified the study in four ways. First, in order to establish statistical significance for our work, we would now compute NmF2 differences (for each type of comparison) for all 1,484 high-latitude grid points. Second, we would now keep track of the sign of the differences (earlier we only looked at magnitudes). Third, in addition to the comparisons for 0500 UT, 0600 UT, and 0700 UT, we ran comparisons for several UTs removed from the time of the magnetic "spike." Fourth, we refined the procedure for applying the normalized 15-minute JD index to the TDIM. This last change is

described more fully in next section, followed by the main study results in section

6.2.2.2.

6.2.2.1. TDIM drivers

6.2.2.1.1. Description. In our initial work, the normalized 15-minute JD index was

applied to every TDIM driver that requires a geomagnetic index (see Figure 35). It was

later argued that, because of the long time constants (tens of minutes or longer) of MSIS

and HWM, application of such a high-time resolution index to these models might

contribute to erratic and unphysical behavior in the TDIM's output. In view of this

concern, we wanted to assess the magnitude of such effects before proceeding further

with our main study.

To do this, we used the normalized 15-minute JD index to drive only the particle

precipitation and convection models. The other two index-dependent TDIM inputs,

MSIS and HWM, were driven by the 3-hour JD index. We called this the TDIM "keys"

run configuration, since we could "key in" any desired index/driver model combination.

The results of the "keys" TDIM runs were first compared against TDIM output obtained

by driving all four index-dependent models with the 3-hour JD index, i.e., a "pure" 3-

hour run configuration. This comparison highlighted TDIM sensitivity to the index time

interval used to drive the convection and precipitation models, since both the "keys" and

"pure" 3-hour configurations used the 3-hour index to drive MSIS and HWM. Second,

the "keys" results were compared with "pure" 15-minute TDIM output, i.e., all four

index-dependent models were driven with the 15-minute JD index. Using similar

reasoning as before, this second comparison type allowed us to focus on TDIM

sensitivity to variations in index time resolution used to drive MSIS and HWM.

Table 9
TDIM run scenarios

"driver" model	pure 3-hour TDIM run	"keys" TDIM run	pure 15-minute TDIM run
convection	3-hr *JD* index	15-min *JD* index	15-min *JD* index
precipitation	3-hr *JD* index	15-min *JD* index	15-min *JD* index
MSIS	3-hr *JD* index	3-hr *JD* index	15-min *JD* index
HWM	3-hr *JD* index	3-hr *JD* index	15-min *JD* index

All three TDIM run configurations are shown in Table 9. Finally, contrasting both comparison types would determine TDIM output sensitivity to the index time interval used to drive MSIS/HWM *relative* to the output sensitivity due to the index interval used to drive the convection/particle precipitation models.

The TDIM output parameters we used in these comparisons were both the high-latitude NmF2 and the high-latitude upper *E*-region (160 km) electron density (throughout the rest of this paper we will refer to this as Ne160). Even though our primary study involves only NmF2 values, we wanted to examine output sensitivities in both regions. Finally, we made comparisons for the following Universal Times: 0000 UT, 0500 UT, 0700 UT, 0815 UT, 1800 UT, and 0000 UT on the next day (29 July 1990). The times were chosen to give us a variety of geomagnetic conditions throughout the day of interest. The results of these comparisons follow.

6.2.2.1.2. Driver comparison results. The conclusions we obtained from these comparisons turned out basically the same for all six Universal Times analyzed; thus, we chose to use one case, 0500 UT, to illustrate our findings. Figure 38 shows the 0500 UT

"Driver" Difference Histograms
Fredericksburg / 28 July 90 / 0500UT
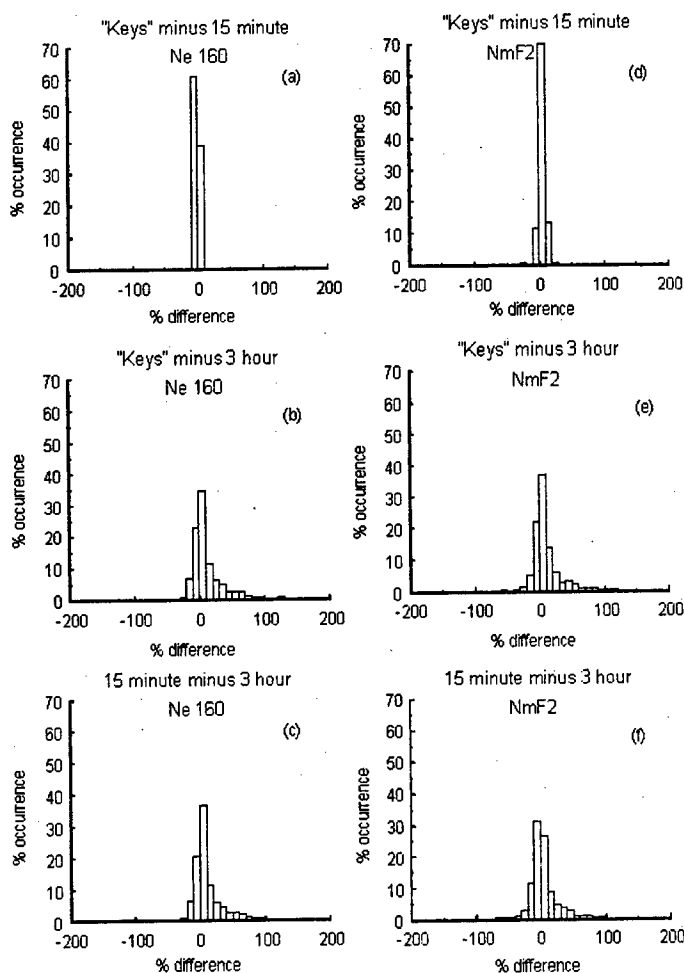
Fig. 38.. High-latitude electron density difference histograms for 0500 UT on 28 July 1990 (i.e., the Fredericksburg *JD* indices for this date were used to drive the TDIM simulations). Panels (a)-(c) are for upper *E*-region densities (at 160 km, which we label Ne160), and panels (d)-(f) are for NmF2. The density differences were computed (for each of the 1,484 grid points) from two TDIM simulations using different *JD* index configurations (see Table 9). The configurations used are at the top of each panel. Density differences are shown as a percent (plus or minus), and the distributions give percent occurrence of each density difference "bin" (bins are 10 percentage points wide). Notice that the "keys" minus 15-minute differences (for both Ne160 and NmF2), shown in panels (a) and (d), produce very narrow distributions relative to the remaining panels. This indicates that TDIM high-latitude densities are much more sensitive to the index used to drive the precipitation and convection models (as opposed to MSIS and HWM). Table 10 gives the statistics for these distributions.

difference histograms for the comparisons described in the previous section. Panels (a)-(c) are for the high-latitude Ne160 density differences; panels (d)-(f) are for the high-latitude NmF2 differences. In conjunction with this, we shall use Table 10, which gives the mean, standard deviation, and coefficient of skewness for the Figure 38 distributions. The skewness coefficient, a dimensionless quantity, is defined as:

$$\text{skewness} = m_3 \Big/ m_2 \sqrt{m_2} \qquad (2)$$

where m_2 is the variance (or second moment about the mean) and m_3 is the third moment about the mean. This coefficient measures the asymmetry of the distribution; a positive value indicates the right-hand distribution "tail" is more elongated than the left side, and vice versa for negative skewness. A skewness value of zero indicates a symmetric distribution.

First, we shall look qualitatively at the Figure 38 difference distributions. It is readily apparent that, for both Ne160 and NmF2, the "keys" minus 15-minute distributions are quite narrow. In the previous section we stated that the "keys" versus 15-minute distribution shows TDIM sensitivity resulting from the time interval used in the magnetic index that drives MSIS and HWM. Since the 0500 UT case shown is typical of the other five UT cases studied, this suggests that the TDIM high-latitude E- and F-region density values are relatively *insensitive* to whether MSIS and HWM are driven by a 3-hour or 15-minute "K-like" geomagnetic index. Continuing with our qualitative analysis, look at panels (b) and (e)—the "keys" minus 3-hour JD comparisons for Ne160 and NmF2, respectively. These distributions are much wider than panels (a) and (d), indicating that

the TDIM high-latitude electron densities are much more sensitive to the geomagnetic index time interval used to drive the precipitation and convection models.

These assertions are strengthened by looking at the statistics shown in Table 10. For Ne160, the "keys" minus 15-minute mean value is almost zero (percent), and the standard deviation is only 0.5%. The "keys" minus 3-hour mean value is 14%, with a standard deviation (centered about this mean) of about 28%. The NmF2 statistics follow this same trend, though the "keys" minus 15-minute distribution is wider and has a mean value farther from zero than in the Ne160 case. We attribute this to the fact that time constants are longer—and thus geomagnetic index "history" is more important—in the high-latitude F-region than in the E-region.

Next, notice the 15-minute minus 3-hour distribution and statistics shown in Figure 38 and Table 10. Both qualitatively and quantitatively, these distributions are quite similar

Table 10
Statistics for Fig. 38

	mean	standard deviation	skew
Ne160/0500 UT			
"keys" – 15 min JD	-0.2%	0.5%	-2.5
"keys" – 3 hr JD	14.0%	28.4%	2.3
15 min – 3 hr	14.2%	28.5%	2.3
NmF2/0500 UT			
"keys" – 15 min JD	4.5%	5.5%	0.3
"keys" – 3 hr JD	8.5%	21.0%	1.0
15 min – 3 hr	4.7%	26.3%	1.1

to the "keys" minus 3-hour distributions (the one exception is the NmF2 mean values; again, we believe this discrepancy is related to the longer *F*-region time constants). This indicates that the density differences encountered in the initial work (see section 6.2.1) were caused mainly by altering the *JD* time interval (3 hours versus 15 minutes) used to drive the *precipitation* and *convection* models.

Thus we have demonstrated that the *JD* index time interval used to drive MSIS and HWM plays a secondary role in influencing high-latitude *E*-region electron densities (compared to the *JD* time interval used to drive the precipitation and convection models). In the *F*-region, however, the longer time constants complicates the matter. Now, since the main part of our study involves high-latitude NmF2 comparisons, and since it is well-known that the thermosphere has time constants of tens of minutes or longer, we chose to apply our variable time *JD* indices to the TDIM using the "keys" configuration for the main study comparisons.

6.2.2.2. *Main study results*

With the "driver" results and section 6.2.2 introductory material in mind, we are now in a position to examine the main study results, starting with the high-latitude NmF2 comparisons at 0500 UT on 28 July 1990. Figure 39 and Table 11(b) show the results for this time. All four panels in Figure 39 depict NmF2 percent differences for each grid point north of 50 degrees magnetic latitude; differences within ±8% of zero were not assigned a color in order to highlight the larger differences. Figure 39(a) shows the NmF2 differences between driving the TDIM with the 3-hour *JD* versus driving TDIM with the "keys" *JD* index configuration. For this comparison, the IMF was held constant.

TDIM NmF2 Differences/28 July 90/0500UT
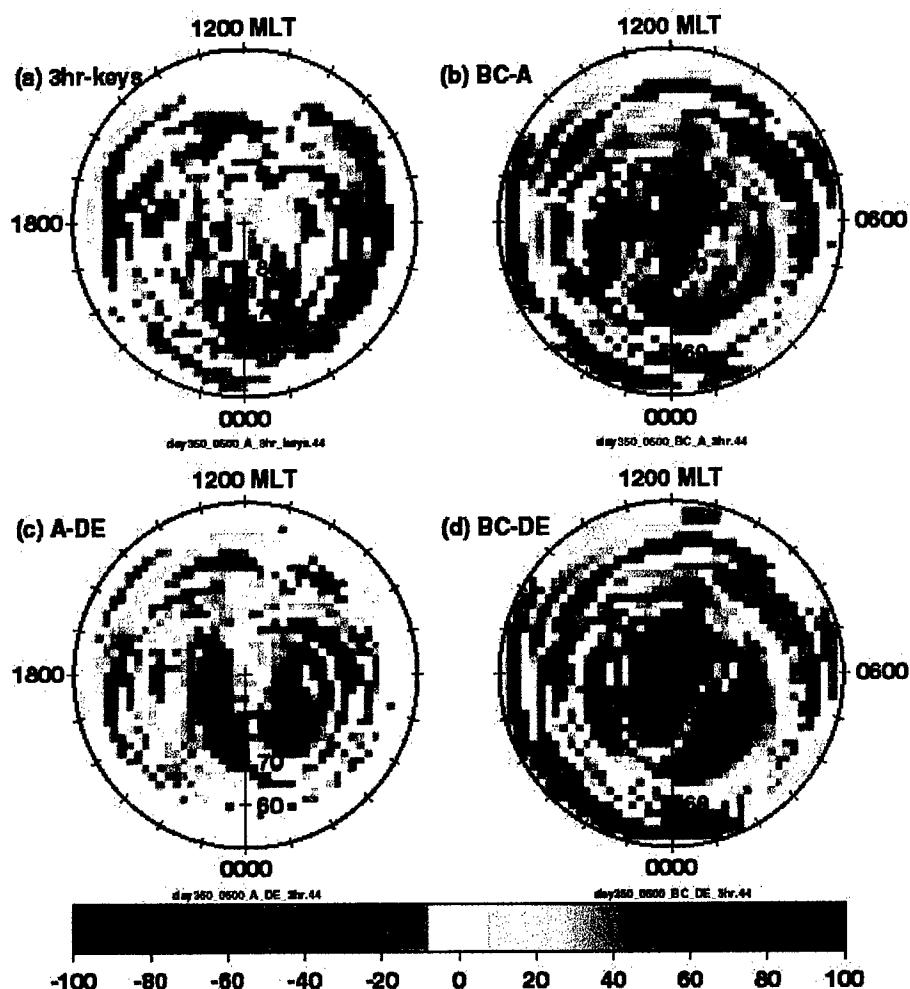
Fig. 39. High-latitude NmF2 percent difference plots for 0500 UT on 28 July 1990 (i.e., the Fredericksburg *JD* indices for this date were used to drive the TDIM simulations). Plots are in magnetic local time (MLT) versus magnetic latitude (50 to 90 degrees). NmF2 differences are computed at each grid point (1,484 points in each plot) from two TDIM simulations using different *JD* index configurations (see Table 9). Panel (a) shows the 3-hour *JD* configuration NmF2 value minus the "keys" configuration value (both run using the Heppner-Maynard "A" pattern). Panels (b)-(d) all use the 3-hour *JD* configuration, and compare NmF2 differences resulting from using different Heppner-Maynard convection patterns. Panel (b) shows the NmF2 differences for "BC" minus "A," panel (c) is for "A" minus "DE," and panel (d) is for "BC" minus "DE." Notice that the maximum NmF2 percent differences resulting from varying the *JD* index time interval (panel (a)) are not as large as those resulting from varying the convection pattern (panels (b) through (d)) with the index held constant.

Table 11
Main study high-latitude NmF2 difference statistics for
$|JD-K| \leq 1$

	mean	standard deviation	skew
(a) 0000 UT			
3-hour – "keys"	-3.9%	23.4%	-1.3
"BC" – "A"	-5.6%	38.9%	-0.4
"A" – "DE"	4.2%	29.0%	0.8
"BC" – "DE"	-0.3%	58.0%	0.6
(b) 0500 UT			
3-hour – "keys"	-8.5%	21.0%	-1.0
"BC" – "A"	-0.1%	44.2%	-0.1
"A" – "DE"	4.8%	35.9%	-0.05
"BC" – "DE"	-3.9%	66.3%	-0.3
(c) 0700 UT			
3-hour – "keys"	-2.9%	16.8%	0.7
"BC" – "A"	0.5%	48.9%	-0.3
"A" – "DE"	2.3%	38.4%	-0.3
"BC" – "DE"	0.5%	61.0%	-0.4
(d) 1800 UT			
3-hour – "keys"	5.4%	20.4%	0.8
"BC" – "A"	-7.4%	45.0%	-0.3
"A" – "DE"	9.1%	36.1%	1.6
"BC" – "DE"	1.3%	63.0%	1.0

We chose the Heppner-Maynard "A" convection pattern, since our initial work (section 6.2.1) indicated that any of the three pattern types should be equally suitable. Positive percent differences in Figure 39(a) indicate that the NmF2 value for the 3-hour driven run is higher than the NmF2 for the "keys" run, and vice versa for negative differences. Two features are noticeable in this figure. First, the NmF2 differences show some degree of structure. This indicates that our 15-minute "normalized" *JD* index did not introduce erratic, unphysical behavior into the TDIM. Second, the area of negative percent differences seems to outweigh the area of positive differences. This is confirmed in Table 11(b), since the mean of the distribution is about −8%. The distribution is not quite symmetric, having a skew of −1.0. The standard deviation of the Figure 39(a) percent differences is 21%. Ignoring the minor non-Gaussian quality of the distribution, this means that two-thirds of the 1,484 grid points have percent differences within 21% of the mean.

Next, as we did in the initial work, we wanted to compare these results against TDIM sensitivity to another critical parameter—IMF variability, which is provided by the three Heppner-Maynard patterns. Figures 39(b)-39(d) give the NmF2 percent differences between TDIM runs with two different convection pattern types. We used the 3-hour *JD* index to drive all runs shown in these three panels; we did not use the "keys" driving scheme because we wanted to concentrate only on the IMF influence. Figure 39(b) shows the "BC" versus "A" pattern comparison, 39(c) is for "A" versus "DE", and 39(d) is for "BC" versus "DE". In Figure 39(b), positive percent differences indicate that the "BC" pattern NmF2 value is greater than the "A" pattern value. In Figure 39(c), positive differences means that the "A" pattern NmF2 is greater than the "DE" pattern value.

Finally, in Figure 39(d), positive differences are for "BC" pattern NmF2 values greater than the "DE" pattern values. In each of the three panels, the opposite is true for negative percent differences.

Now, comparing Figure 39(a) versus the other three panels, it is plain that the high-latitude NmF2 percent differences are much larger when the IMF is changed and the geomagnetic index "driver" is held fixed than they are when the IMF is fixed and the index is altered. This is the same result we got in the initial study using only three grid points for comparison. The statistics in Table 11(b) also support this: "BC" versus "A" has a 44% standard deviation, "A" versus "DE" has about a 36% standard deviation, and "BC" versus "DE" has the largest standard deviation at 66%. The relative magnitudes of these deviations make physical sense, as discussed previously in section 6.2.1.2.

We obtained similar results for 0700 UT (just after the peak of the geomagnetic disturbance), as shown in Table 11(c). Next we ran the NmF2 comparisons for two times removed from the geomagnetic disturbance: 0000 UT and 1800 UT (see Figure 36). The statistics are shown in Tables 11(a) and 11(d), respectively. The results for these times are in good agreement with the 0500 UT comparisons; i.e., TDIM high-latitude NmF2 values are more sensitive to IMF changes than to changes in the time interval used for the geomagnetic index driver (for constant IMF conditions). This is the same result as we found in our initial work, and establishes some of the statistical significance lacking in our early efforts. It suggests that the space weather forecast community needs to pursue inclusion of real-time IMF data for their operational support models even more vigorously than they have examined use of variable time geomagnetic indices. However, this was not the end of the story.

In all four UT cases described above, the 3-hour and "normalized" 15-minute *JD* index values were within ±1 index unit of each other at the time of the analyses (see Figure 36). This prompted us to choose a UT case where the two indices had very different values; we picked 0815 UT, where the 3-hour *JD* had a value of 7, and the "normalized" 15-minute index had a value of 3. The results were quite different from the previous four cases (and the initial study results). Figure 40 shows the color difference polar plots for 0815 UT (same type of plots as Figure 39), and Table 12(b) gives the statistics. Figure 40(a) shows large NmF2 differences (pink areas) concentrated in two "lobes"—one in the morning sector, the other in the evening sector. It is also evident that the number of grid points with positive differences (i.e., the 3-hour "driven" NmF2 values are larger than the "keys" values) dominates the negative values. This is quantified in Table 12(b), where the mean value is shown to be about 25%—over five times larger than any of the IMF comparison mean values for 0815 UT. The standard deviation for Figure 40(a) is almost 60%, which was larger than any of the standard deviations in the 0815 UT IMF comparisons, and roughly three times larger than the 3-hour versus "keys" standard deviations in the other four cases. Thus we seem to have discovered a case in which altering the *JD* time interval affected high-latitude NmF2 values more than varying the IMF. To test the validity of this new result, we ran the comparisons for 0805 UT and 0825 UT. The results were comparable to the 0815 UT case, as shown in Tables 12(a) and 12(c). In addition, we tried to reproduce these results using a time far removed from 0815 UT. To do this, we searched for a time period in which the 3-hour and 15-minute *JD* indices exhibited similar trends to the 0815 UT case. We chose 2245 UT, as shown in Figure 36. However, the resulting statistics, shown in
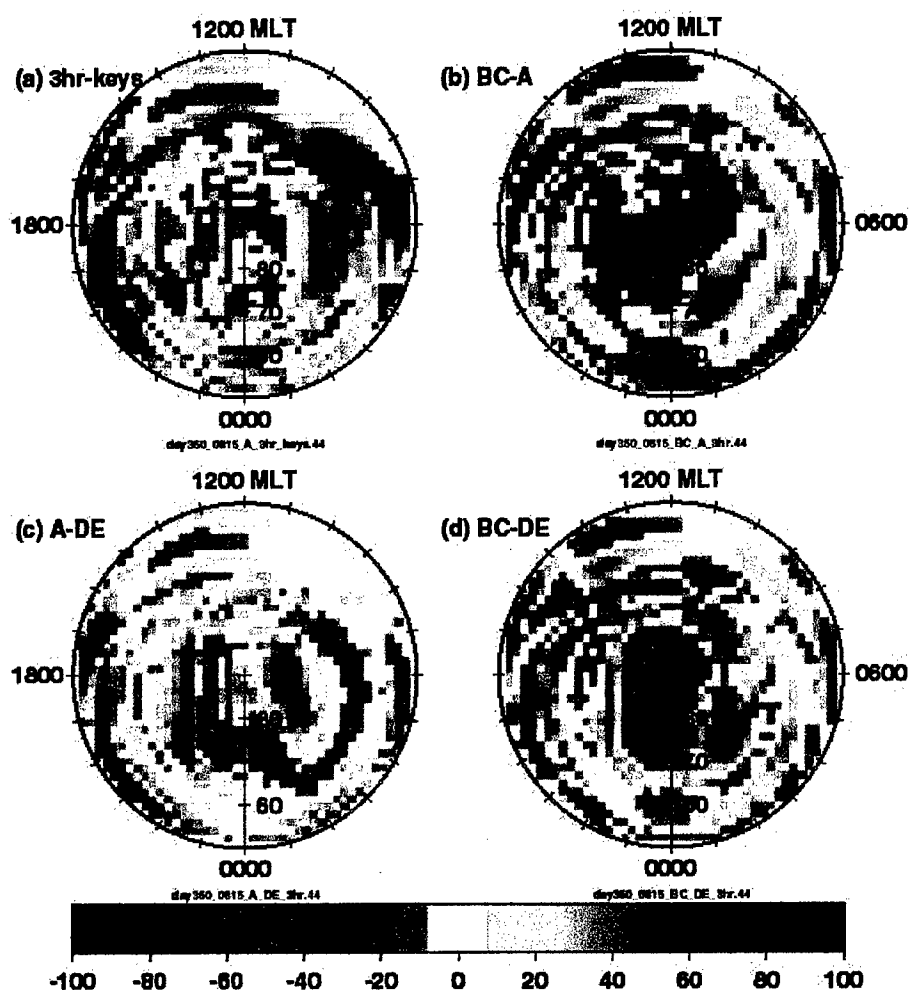
Fig. 40. High-latitude NmF2 percent difference plots for 0815 UT on 28 July 1990 (same format as Figure 39). In this case (as well as for 0805 UT and 0825 UT), varying the index time interval actually has a larger effect than varying the convection pattern. However, the convection pattern effect is still large. From our initial work and physical intuition, we feel the scenario in Figure 39 would occur much more often than the one shown here.

Table 12
Main study high-latitude NmF2 difference statistics for
$|JD{-}K| > 1$

	mean	standard deviation	skew
(a) 0805 UT			
3-hour – "keys"	20.4%	54.6%	1.2
"BC" – "A"	-4.8%	50.7%	-0.4
"A" – "DE"	3.6%	40.0%	0.8
"BC" – "DE"	-0.6%	49.3%	-0.2
(b) 0815 UT			
3-hour – "keys"	25.4%	59.5%	1.8
"BC" – "A"	-4.2%	46.9%	-0.2
"A" – "DE"	4.5%	32.6%	1.1
"BC" – "DE"	0.2%	47.9%	0.1
(c) 0825 UT			
3-hour – "keys"	30.0%	61.7%	1.3
"BC" – "A"	-4.8%	47.1%	-0.1
"A" – "DE"	5.1%	32.2%	1.2
"BC" – "DE"	0.8%	45.9%	0.3
(d) 2245 UT			
3-hour – "keys"	3.7%	35.0%	0.9
"BC" – "A"	-9.9%	64.6%	-0.8
"A" – "DE"	10.0%	43.9%	0.9
"BC" – "DE"	0.9%	68.3%	0.3

Table 12(d), revert back to the cases in which varying the IMF plays a dominant role in influencing high-latitude NmF2 values. One possible source of our failure to reproduce the 0805 UT→0825 UT behavior is that those cases occurred not long after the major magnetic "spike," whereas the magnetic activity just prior to the 2245 UT is not nearly so large. Another possible source is that the dependence could be a UT effect.

The 0805 UT→0825 UT behavior does not alter our thoughts about the importance of IMF data; rather, it indicates that, for some cases, varying the index time interval can cause greater high-latitude NmF2 fluctuations than varying the IMF values. We feel that such cases would not happen nearly as often as ones in which IMF effects dominate; however, this obviously needs to be addressed further.

6.2.2.3. TDIM "noise level"

As a final test of the significance of our results, we wanted to make sure that the computational "noise" generated by the TDIM is small compared to the percent differences we observed in our study. We ran NmF2 comparisons for 0500 UT using the Heppner-Maynard "A" convection pattern and the 3-hour JD index to drive the model. The test was then conducted in two parts. First, we decreased the typical 100- second time step to 40 seconds, ran the model, then compared the NmF2 values at each grid point against the typical time step run. Second, we increased the time step to 200 seconds, ran the model, and again compared NmF2 point by point against the typical run. For the former test, the mean value of the percent difference distribution was about one-tenth of a percent. The standard deviation was 2.2%, and the distribution was near symmetric with a skew of 0.4. For the latter test, the mean was again about 0.1%, the

standard deviation was 3.6, and the skew was only 0.2. We considered this proof enough that the TDIM noise level is far below the level of significance of the NmF2 differences we saw in our study.

These results should be of great interest to the space weather forecast and applications community, who have often discussed use of high-time resolution geomagnetic indices for use in space weather models. We have demonstrated that, even though the effect of using such indices can be significant, the introduction of real-time IMF data to such models can have a much larger impact on operational space weather support.

CHAPTER 7

CONCLUSIONS AND FURTHER STUDY

We have produced a computer program to explore "K-like" geomagnetic indices of variable integration times. Statistically, our code is 95% accurate when compared against the official 1990-1992 Fredericksburg 3-hour K indices. Analyses performed with this index-generating tool led to the following conclusions. First, varying the index time interval causes the average index to be significantly changed; shortening the time interval decreases the average JD index, and lengthening the time interval increases the average index value. This presents problems regarding the derivation, concept, and use of variable time interval "K-like" indices. Our pursuit of these issues led to our second key finding. Using a very simple normalization scheme to revise the Niemegk range-to-index quasi-log table, we succeeded in producing variable time Fredericksburg JD indices having frequency distributions comparable to the official 3-hour Fredericksburg K index. The significance of this result is tied to our assumption that our variable time JD indices would be "consistent" with the 3-hour K index if the frequency distributions of the two indices are the same. Our analysis further revealed that the normalized 15-minute JD frequency distribution gave the best agreement with the official K distribution. We also noted some cautions regarding the fact that such a scaling is a function of the time period used to compute the averages. However, these same comments are applicable to the $K \rightarrow Ks$ conversion tables and arithmetic averaging of Ks values used in deriving the official Kp index. In addition, even though "consistency" is a must for JD to function in place of the K index, we are still left with the concerns regarding the physical

processes represented by variable time "K-like" indices. Such concerns are nontrivial and must be understood and addressed by the space weather forecast and application community before any such indices could be adopted.

Our third conclusion is that, even though the physical processes represented by the shorter-time interval indices are probably different from that of the 3-hour index, the higher-time indices do provide more accurate information about magnetic variations that occur in the vicinity of a specific station. This was demonstrated by using the JD 3-hour, "sliding" 3-hour, and 15-minute indices to resolve several Fredericksburg magnetic disturbance features. For the cases studied, the 15-minute JD index accurately resolved the timing, duration, and relative magnitudes of each disturbance feature. The "sliding" 3-hour index mishandled these same disturbances with regard to timing, duration, or failure to resolve individual features. Thus the "sliding" 3-hour index does not improve upon the traditional 3-hour index without introducing additional problems.

We explored the possibility that some of these 3-hour index timing errors could be due to the fact that the index time is associated with the end of the integration window (as opposed to the midpoint). It is true that assigning the index time at the midpoint would reduce the maximum timing error by a factor of two (3 hours versus 1.5 hours), and improve the long-term statistics of 3-hour index timing errors. However, this would not eliminate timing problems on a case-by-case basis. Also, the near real-time evaluation of an index can only be made after data acquisition, and hence operationally the end time of an interval should be used as the index time tag.

Having created variable time interval "K-like" station indices, the next step was to investigate the "suitability" of such high-time resolution indices as proxies for the

dynamics of ionospheric drivers. We used our *JD* indices to drive the auroral, convection, neutral atmosphere, and neutral wind inputs to the Utah State University (USU) Time-Dependent Ionospheric Model (TDIM). We then examined the sensitivity of high-latitude TDIM NmF2 values to the time interval (3 hours versus 15 minutes) of the geomagnetic "*K*-like" index used to drive the model. In other words, the NmF2 response was measured by first driving the TDIM with the traditional 3-hour index, then comparing the resulting NmF2 field with the one produced by driving the TDIM with the normalized 15-minute *JD* index.

We focused our study on Fredericksburg data from 28 July 1990, a day containing a large magnetic disturbance. In our initial work we made a limited study of three selected locations, and found that variation of the geomagnetic index time interval resulted in NmF2 variations of about 20%. However, this was small compared to the NmF2 variations found (over a factor of two) when we varied the IMF and kept the index fixed. The desire to increase the sample size of grid points analyzed led to our main study, in which we computed differences for all 1,484 high-latitude grid points, refined the method of applying the 15-minute *JD* index to the TDIM, and made comparisons for several times throughout the day of interest. In five of the eight cases studied, we found that the TDIM high-latitude NmF2 variations due to IMF variations exhibited a standard deviation 2-3 times larger than the standard deviation due to variation in the *JD* index time interval. However, in three cases spaced closely together in time, we found that varying the index time interval from 3 hours to 15 minutes had a larger effect (about 60% standard deviation) on high-latitude NmF2 values than IMF variations, although the IMF effect remained very significant. As mentioned earlier, further study is warranted to

address the circumstances in which either IMF effects, or variation of the index time interval, dominates. Our intuition—based on the results of this study—is that the former effect should dominate most of the time. The TDIM study results suggest that the space weather forecast and application community should pursue the incorporation of near real-time IMF data into their models as being even a higher priority than adjustment of the geomagnetic index time interval.

Our sensitivity study has also provided the space weather community with its first quantitative estimates of the effects of driving the ionosphere with a variable time index. The variations we found in the high-latitude NmF2 (20% or more) are quite significant to space weather forecasters, some of whom regularly use a computationally fast version of the TDIM. Further, with regard to choosing NmF2 as the parameter of study, it has been noted by R.W. Schunk (private communication, 1999) that other ionospheric parameters, such as the height of the F-region peak (hmF2), would respond even more readily to changes in the index time interval.

Our ability to conduct this sensitivity study rested on two findings. First, our earlier work (Della-Rose et al., 1999) demonstrated that variable time "K-like" geomagnetic indices could be normalized in such a way to make them "consistent" with the traditional 3-hour station K index. The normalization was most effective for the 15-minute time interval, and since space weather forecasters have expressed interest in high-time resolution indices, 15 minutes was the ideal choice for our sensitivity study. Second, the goal of our sensitivity study was not to produce "real" ionospheric simulations that could be compared to observed data. Rather, we used the Fredericksburg 3-hour and 15-minute (normalized) *JD* indices as surrogate planetary indices to learn how high-latitude NmF2

values would respond if we had a planetary JD time series with the same behavior as our single station time series.

Even though our results are encouraging, much work remains to be done before our JD indices could be considered for operational use. Our method should be applied to data from the remaining 12 Kp network magnetic observatories to produce JD indices for those stations. Each station JD index could be "normalized" as we did for Fredericksburg. From the 13 normalized station JD indices, a planetary JD index, or "JDp", could be derived. This is a critical step, since models that use "K-like" indices are designed for use with *planetary* "K-like" indices; our study has only dealt with a single station. With a planetary JD index in hand, we could re-run the TDIM sensitivity study with a legitimate planetary index; the resulting high-latitude ionospheric simulations could also be compared against actual ionospheric observations. Another area to explore in such a study would be to allow the IMF to vary continuously, then determine the sensitivity of TDIM output to the choice of geomagnetic index—Kp or JDp—used to drive the model.

Finally, and perhaps most important, we have not yet addressed the physical significance and appropriateness of using "K-like" indices (of any time interval) in such ionospheric models. Research in this area might involve statistical studies such as correlations between our station JD indices and auroral zone energetics in the "vicinity" of the observatory. Hopefully this would help determine whether our variable time interval JD indices accurately represent the temporal behavior of ionospheric drivers. Additionally, one would want to examine whether the variable time JD index could be applied directly to existing models, or whether new empirical models—binned for the

new time interval—would have to be developed. In either case, the hope is that

ionospheric specification would be improved.

REFERENCES

Ballatore, P., Lanzerotti, L. J., 1998. Relationships of polar cap indices with interplanetary parameters. Ann. Geophys. (in press).

Bartels, J., Heck, N. H., Johnston, H. F., 1939. The three-hour-range index measuring geomagnetic activity. J. Geophys. Res. 44, 411-454.

Bartels, J., 1940. Report on the numerical characterization of days. International Association of Terrestrial Magnetism and Electricity Bulletin (11), 27-28.

Bartels, J., 1949. The standardized index, Ks, and the planetary index, Kp. International Association of Terrestrial Magnetism and Electricity Bulletin (12b), 97.

Bartels, J., 1951. An attempt to standardize the daily international magnetic character figure. International Association of Terrestrial Magnetism and Electricity Bulletin (12e), 109.

Bartels, J., 1957. The technique of scaling indices K and Q of geomagnetic activity. Ann. Int. Geophys. Year 4, 215-226.

Campbell, W. H., Matsushita, S., 1982. Sq currents: A comparison of quiet and active year behavior. J. Geophys. Res. 87, 5305-5308.

Campbell, W. H., Schiffmacher, E. R., Kroehl, H. W., 1989. Global quiet day field variation model. WDCA/SQ1, Eos Trans. AGU 70 (5), 66-74.

Campbell, W. H., 1997. Introduction to Geomagnetic Fields. Cambridge University Press, New York, NY.

Cliffswallow, W., 1993. Evaluation of AFSFC geomagnetic indices (final report). Air Force Space Forecast Center (OL-A) Report.

Davis, T. N., Sugiura, M., 1966. Auroral electrojet activity index AE and its universal time variations. J. Geophys. Res. 71, 785-801.

Della-Rose, D. J., Sojka, J. J., Zhu, L., Schunk, R. W., 1998. Ionospheric sensitivity to geomagnetic temporal variability on time scales less than that of the Kp (Ap) geomagnetic indices. EOS Trans. Amer. Geophys. Union 79 (45), Fall Meet. Suppl., 677.

Della-Rose, D. J., Sojka, J. J., Zhu, L., 1999. Resolving geomagnetic disturbances using "K-like" geomagnetic indices with variable time intervals. J. Atmos. Solar Terr. Phys. (in press).

Fuller-Rowell, T. J., Codrescu, M. V., Moffett, R. J., Quegan, S., 1994. Response of the thermosphere and ionosphere to geomagnetic storms. J. Geophys. Res. 99, 3893-3914.

Fuller-Rowell, T. J., Codrescu, M. V., Rishbeth, H., Moffett, R. J., Quegan, S., 1996. On the seasonal response of the thermosphere and ionosphere to geomagnetic storms. J. Geophys. Res. 101, 2343-2353.

Hardy, D. A., Gussenhoven, M. S., Raistrick, R., McNeil, W. J., 1987. Statistical and functional representations of the pattern of auroral energy flux, number flux, and conductivity. J. Geophys. Res. 92, 12275-12294.

Hargreaves, J. K., 1992. The Solar-Terrestrial Environment. Cambridge University Press, New York, NY.

Hedin, A. E., 1987. MSIS-86 thermospheric model. J. Geophys. Res. 92, 4649-4662.

Hedin, A. E., Spencer, N. W., Biondi, M. A., Burnside, R. G., Harnandez, G., Johnson, R. M., 1991. Revised global model of thermospheric winds using satellite and ground-based observations. J. Geophys. Res. 96, 7657-7688.

Heppner, J. P., Maynard, N. C., 1987. Empirical high-latitude electric field models. J. Geophys. Res. 92, 4467-4489.

Jacobs, J. A. (Ed.), 1989. Geomagnetism. Academic Press, New York, NY.

Kamide, Y., Akasofu, S. I., 1981. Global distribution of the Pedersen and Hall currents and the electric potential during a moderately disturbed period. J. Geophys. Res. 86, 3665-3680.

Kelley, M. C., 1989. The Earth's Ionosphere: Plasma Physics and Electrodynamics. Academic Press, San Diego, CA.

Kivelson, M. G., Russell, C. T. (Eds.), 1995. Introduction to Space Physics. Cambridge University Press, New York, NY.

Knecht, D. J., Shuman, B. M., 1985. The geomagnetic field. In: Jursa, A. S., (Ed.). Handbook of Geophysics and the Space Environment, Air Force Geophysics Laboratory, p. 4-2.

Mayaud, P. N., 1967. Atlas des indices K. International Association of Geomagnetism and Aeronomy Bulletin (21), 113 pp.

Mayaud, P. N., 1980. Derivation, Meaning, and Use of Geomagnetic Indices. Geophysical Monograph Series (22), AGU, Washington, DC.

McPherron, R. L., 1991. Physical processes producing magnetospheric substorms and magnetic storms. In: Jacobs, J. A. (Ed.). Geomagnetism, Volume 4. Academic Press, pp. 593-739.

Menvielle, M., Berthelier, A., 1991. The K-derived planetary indices: Description and availability. Rev. Geophys. 29, 415-432.

Rastogi, R. G., 1989. The equatorial electrojet: Magnetic and ionospheric effects. In: Jacobs, J. A. (Ed.). Geomagnetism, Volume 3. Academic Press, pp. 461-525.

Rostoker, G., 1972. Geomagnetic indices. Rev. Geophys. Space Phys. 10, 935-950.

Schroeder, J. D. III, and Cliffswallow, W., 1992. The geomagnetic analysis program. Space Environment Laboratory Report.

Schunk, R. W., Walker, J. C. G., 1973. Theoretical ion densities in the lower ionosphere. Planet. Space Sci. 21, 1875-1896.

Schunk, R. W., Raitt, W. J., Banks, P. M., 1975. Effects of electric fields on the daytime high-latitude E and F regions. J. Geophys. Res. 80, 3121-3130.

Schunk, R. W., Banks, P. M., Raitt, W. J., 1976. Effects of electric fields and other processes upon the nighttime high-latitude F layer. J. Geophys. Res. 81, 3271-3282.

Schunk, R. W., Sojka, J. J., 1982. Ion temperature variations in the daytime high-latitude F region. J. Geophys. Res. 87, 5169-5183.

Schunk, R. W., Sojka, J. J., Bowline, M. D., 1986. Theoretical study of the electron temperature in the high-latitude ionosphere for solar maximum and winter conditions. J. Geophys. Res. 91, 12041-12054.

Schunk, R. W., 1988. A mathematical model of the middle and high-latitude ionosphere. Pure Appl. Geophys. 127, 255-303.

Schunk, R. W., Zhu, L., Sojka, J. J., Bowline, M. D., 1997. Ionospheric response to an auroral substorm. Geophys. Res Lett. 24, 1979-1982.

Sojka, J. J., Raitt, W. J., Schunk, R. W., 1981a. A theoretical study of the high-latitude winter F region at solar minimum for low magnetic activity. J. Geophys. Res. 86, 609-621.

Sojka, J. J., Raitt, W. J., Schunk, R. W., 1981b. Theoretical predictions for ion composition in the high-latitude winter F region for solar minimum and low magnetic activity. J. Geophys. Res. 86, 2206-2216.

Sojka, J. J., Schunk, R. W., 1983. A theoretical study of the high latitude *F* region's response to magnetospheric storm inputs. J. Geophys. Res. 88, 2112-2122.

Sojka, J. J., 1989. Global scale, physical models of the *F* region ionosphere. Rev. Geophys. 27, 371-403.

Sojka, J. J., Schunk, R. W., 1997. Simulations of the high latitude ionospheric climatology. J. Atmos. Terr. Phys. 59, 207-229.

Sojka, J. J., Schunk, R. W., Bowline, M. D., Chen, J., Slinker, S., Fedder, J., Sultran, P. J., 1998. Ionospheric storm simulations driven by magnetohydrodynamic MHD and by empirical models; with data comparisons. J. Geophys. Res. 103, 20669-20684.

Sugiura, M., 1964. Hourly values of equatorial *Dst* for the IGY. Ann. Int. Geophys. Year 35, 9-45.

Thompson, D. C., 1993. Smoothing data by convoluting with Gaussians. Center for Atmospheric and Space Sciences Report.

Volland, H., 1984. Atmospheric Electrodynamics. Springer-Verlag, Berlin.

Vennerstrøm, S., 1991. The geomagnetic activity index PC. Ph.D. Thesis, Danish Meteorological Institute, Copenhagen, Scientific report 91-3.

CURRICULUM VITAE

Devin J. Della-Rose
(September 1999)

Maj Devin J. Della-Rose, U. S. Air Force, obtained his Bachelor of Science Degree in 1985 from Texas Christian University, majoring in Astronomy and Physics (math minor). He then obtained a second B.S. in Meteorology in 1987 from Penn State University. This was followed by an M.S. in Upper Atmospheric Physics from Utah State University, awarded in 1993. The research involved coupling of incoherent-scatter radar data with the Utah State Time-Dependent Ionospheric Model (TDIM) to derive topside electron heat fluxes (a critical boundary condition for ionospheric modeling). Maj Della-Rose is currently pursuing a Ph.D. in Physics from Utah State University (expected graduation date is November 1999). His dissertation research involves a critical feasibility & variability study of planetary geomagnetic indices used extensively in DOD space environmental support.

In addition, Maj Della-Rose has over five years' operational experience in the space environment field in support of Air Force Space Command (AFSPC), United States Space Command (USSPACECOM), and the North American Aerospace Defense Command (NORAD). He developed space environmental effects training and briefing packages for all headquarters personnel, as well as operators in the field. He served as technical liaison in the development and operational transition of two Defense Meteorological Satellite Program (DMSP) instrument packages to monitor space environmental activity. He also served as technical advisor in the validation, testing, and operational transition of a multimillion-dollar suite of space environment computer models referred

to as SETT (Space Environmental Technology Transition). Finally, Maj Della-Rose

has served as space environment team chief in an operations center, providing forecasts,

alerts, warnings, and impact assessments to a wide variety of DOD customers, including

multibillion-dollar National Programs controlled by the Secretary of Defense (SECDEF).